MICROCOPY RESOLUTION TEST CHART
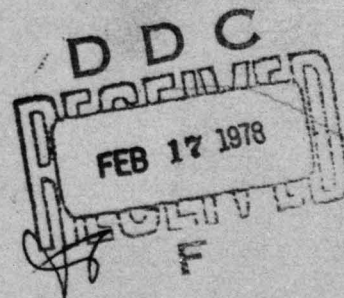NATIONAL BUREAU OF STANDARDS-1963-A

104

Report No. AFOSR-76-3025-2

SMALL APERTURE ON A MULTICONDUCTOR TRANSMISSION

LINE FILLED WITH INHOMOGENEOUS DIELECTRICS

by

Darko Kajfez and Donald R. Wilton

Department of Electrical Engineering
University of Mississippi
University, MS   38677

D D C

FEB 17 1978

F

November, 1977

REPORT DOCUMENTATION PAGE	READ INSTRUCTIONS BEFORE COMPLETING FORM

1. REPORT NUMBER AFOSR-TR 78-0104	2. GOVT ACCESSION NO.	3. RECIPIENT'S CATALOG NUMBER Rept. no. 2

4. TITLE (and Subtitle)
Small Aperture on a Multiconductor Transmission Line Filled with Inhomogeneous Dielectrics.

5. TYPE OF REPORT & PERIOD COVERED
Final, 1 MAY 76 - 30 Sep 77
May 1, 1976 - Sept 30, 1977

6. PERFORMING ORG. REPORT NUMBER

7. AUTHOR(s)
Darko Kajfez and Donald R. Wilton

8. CONTRACT OR GRANT NUMBER(s)
AFOSR-76-3025

9. PERFORMING ORGANIZATION NAME AND ADDRESS
Department of Electrical Engineering
University of Mississippi
University, MS 38677

10. PROGRAM ELEMENT, PROJECT, TASK AREA & WORK UNIT NUMBERS
2301-A3
61102 F

11. CONTROLLING OFFICE NAME AND ADDRESS
AFOSR, Building 410, Bolling AFB, DC 20332/NP

12. REPORT DATE 1 NOV 77
November 1, 1977

13. NUMBER OF PAGES
117 120 p.

14. MONITORING AGENCY NAME & ADDRESS(if different from Controlling Office)

15. SECURITY CLASS. (of this report)
Unclassified

15a. DECLASSIFICATION/DOWNGRADING SCHEDULE

16. DISTRIBUTION STATEMENT (of this Report)

Approved for public release;
distribution unlimited.

17. DISTRIBUTION STATEMENT (of the abstract entered in Block 20, if different from Report)

18. SUPPLEMENTARY NOTES

19. KEY WORDS (Continue on reverse side if necessary and identify by block number)

9E. Subsystems
20C. Electricity and Magnetism
20N. Wave Propagation

20. ABSTRACT (Continue on reverse side if necessary and identify by block number)
The penetration of the electromagnetic pulse through a small aperture in the conducting plane is studied, when a multiconductor transmission line is located behind the aperture. The multiconductor transmission line is filled with inhomogeneous dielectric material, so that the propagating modes have different velocities. The aperture is replaced by a pair of electric and magnetic current moments, and the equivalent multiport for the aperture junction is developed. The accuracy of the dipole moment approach is checked by the continuous spectrum approach, and the limits of validity are established.

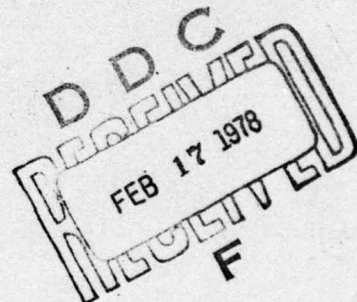DD FORM 1473 EDITION OF 1 NOV 65 IS OBSOLETE

UNCLASSIFIED

Report No. AFOSR-76-3025-2

SMALL APERTURE ON A MULTICONDUCTOR TRANSMISSION
LINE FILLED WITH INHOMOGENEOUS DIELECTRICS

·

by

Darko Kajfez and Donald R. Wilton

AFOSR-76-3025

Department of Electrical Engineering
University of Mississippi
University, MS 38677

November, 1977

CONTENTS

1

ILLUSTRATIONS

3

4

SECTION I

APERTURE REPRESENTATION BY A PAIR OF DIPOLES

A convenient approximation of the electromagnetic field in the presence of a small aperture is in terms of a pair of dipoles, as originated by Bethe [1]. Assume that the local distribution of the total electric field $\vec{E}_t(x,z)$ over an aperture in x-z plane, such as in Fig.1.(a), has been determined by an analytical or a numerical solution of the boundary-value problem. Then, the electromagnetic field in the "internal" region y>0 remains unchanged if the aperture is closed by a metal lid on top of which there is a magnetic surface current

$$\vec{J}_s^{\,m}(x,z) = \vec{E}_t(x,z) \times \vec{a}_y \tag{1}$$

where $\vec{a}_y$ is the unit vector in y direction.

The coupling to the TEM wave on the system of conductors can be then computed by replacing the aperture with a conducting lid on top of which there are two dipoles, $\vec{c}_e$ and $\vec{c}_m$ as shown in Fig. 1.(b). Electric dipole moment $\vec{c}_e$ is oriented in y direction:

$$c_{ey} = \iint J_{sx}^{m}(x,z)\,dxdz, \tag{2}$$

and the magnetic dipole moment of interest here is oriented in x direction:

$$c_{mx} = j\omega\epsilon \iint z J_{sx}^{m}(x,z)\,dxdz. \tag{3}$$

5
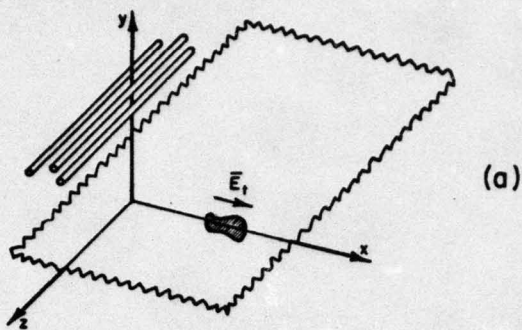
Fig. 1(a) Multiconductor transmission line with a small aperture.
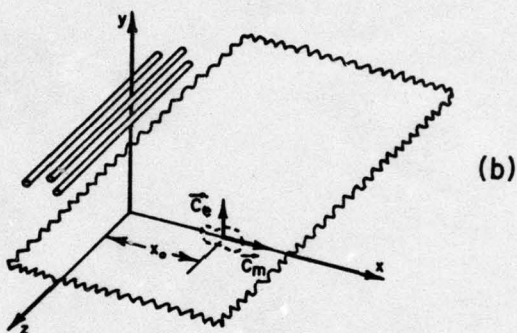
Fig. 1(b) The aperture is replaced by a pair of dipoles.
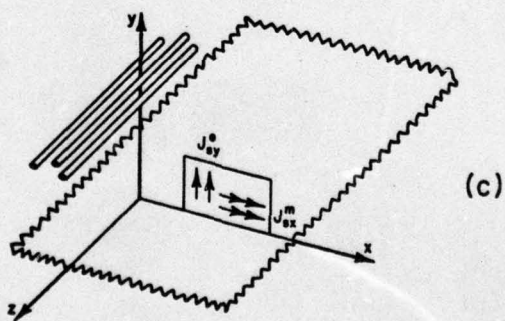
Fig. 1(c) Magnetic and electric surface currents which are equivalent to the pair of dipoles.

6

The magnetic dipole moment may also have the z-component, but the present report is devoted solely to a coupling of quasi-TEM waves guided along z direction by a system of conductors as indicated in Fig. 1.(b). Therefore, the z component of the magnetic dipole is of no importance, because it does not interact with these quasi-TEM waves.

In this report, the electric dipole moment $\vec{c}_e$ (in Ampere·meters) has a meaning of the moment of an electric current element, similarly as in references [2]-[4]. This current moment should not be confused with the electric charge moment $\vec{p}$ (in Coulomb·meters) such as used for example in references [5]-[7]. The relationship between these two moments, for exp(jωt) variation, is as follows:

$$\vec{c}_e = j\omega\vec{p} .$$ (4)

Similarly, the magnetic dipole moment $\vec{c}_m$ (in Volt·meters) in this report denotes the moment of the magnetic current element, in the sense as used by references [8]-[10]. The magnetic charge moment $\vec{m}$ (in Ampere·square-meters), such as used for instance in references [5]-[7] is related to $\vec{c}_m$ as follows:

$$\vec{c}_m = j\omega\mu\vec{m}.$$ (5)

Figure 1.(b) is a first-order equivalent of the original configuration from Fig.1.(a). Sometimes, it is convenient to further change Fig. 1.(b) into an equivalent configuration in Fig. 1.(c) in which there is a distribution of the surface magnetic current $\vec{J}_s^m$ and of the surface electric current $\vec{J}_s^e$ over the x-y plane. Figures 1.(b) and 1.(c) are equivalent if the surface currents become delta functions as follows:

7

$$\vec{J}_s^{\,e} = \vec{c}_e \delta(x-x_0)\delta(y) \,, \tag{6}$$

$$\vec{J}_s^{\,m} = \vec{c}_m \delta(x-x_0)\delta(y) \,. \tag{7}$$

For an aperture of general shape, integrations (2) and (3) are to be performed numerically. For several characteristic shapes (circle, ellipse, narrow slit, square, etc.), the dipole moments have been computed or determined experimentally. It is customary to express the moments in terms of the excitation fields $\vec{E}_s$, $\vec{H}_s$ and in terms of the polarizabilities α_e, α_m. Consider the aperture in Fig. 2 which is to be replaced by the dipole moments so that the field in the "internal" region $y > 0$ is maintained. The excitation fields (so-called short circuit fields) produced by the sources located in the internal region will be denoted $\vec{E}_s^{\,int}$ and $\vec{H}_s^{\,int}$. When the excitation comes from the side $y < 0$, the short circuit fields will be denoted by $\vec{E}_s^{\,ext}$ and $\vec{H}_s^{\,ext}$. For the purpose of coupling to the quasi-TEM waves in the internal region, only the components E_{ys} and H_{xs} are of interest. Instead of performing the numerical integrations from (2) and (3), the dipole moments of small apertures of characteristic shapes may be computed as follows:

$$c_{mx} = -j\omega\mu\alpha_m \, (H_{xs}^{ext} - H_{xs}^{int}) \,, \tag{8}$$

$$c_{ey} = j\omega\varepsilon\alpha_e \, (E_{ys}^{ext} - E_{ys}^{int}) \,. \tag{9}$$

The electric polarizability α_e and the magnetic polarizability α_m of a circular aperture of diameter d are:

8

y

internal
region

E_{ys}^{int}

H_{xs}^{int}

x

E_{ys}^{ext}

H_{xs}^{ext}

external
region
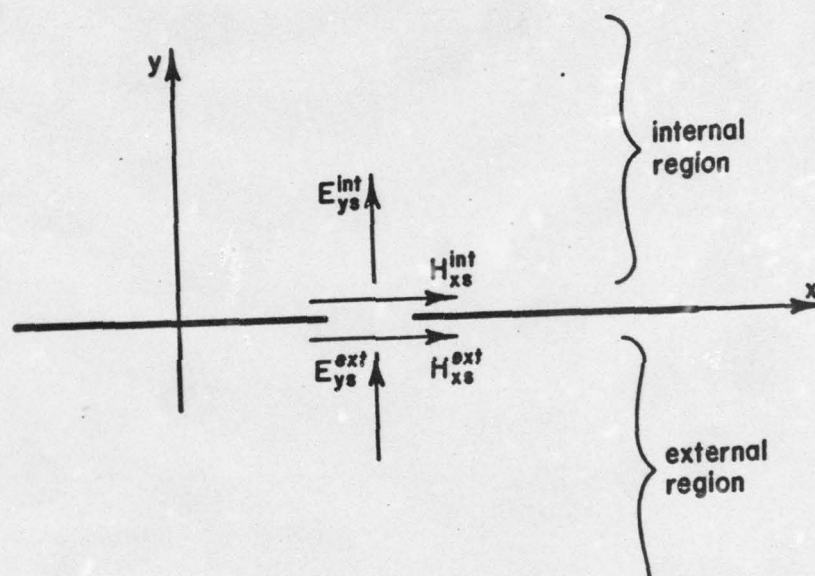
Fig. 2. Excitation fields.

9

$$\alpha_e = \frac{1}{12} d^3 , \quad \alpha_m = \frac{1}{6} d^3 . \tag{10}$$

For a square aperture of side ℓ, Cohn [11], [12] has measured the following polarizabilities:

$$\alpha_e = 0.1137\ell^3 , \quad \alpha_m = 0.2590\ell^3 .$$

The last two references also contain the measured polarizabilities for rectangular and other shapes of apertures.

In Fig. 3, a plane wave is shown incident from the $y < 0$ region. The two possible polarizations of the plane wave are denoted TE and TM. The corresponding dipole moments are computed from (8) and (9) by substituting the following excitation fields:

$$\text{TM:} \quad E_{ys}^{ext} = 2E_0 \sin\theta, \quad H_{xs}^{ext} = -\frac{2E_0}{\eta} \sin\alpha , \tag{11}$$

$$\text{TE:} \quad E_{ys}^{ext} = 0 \quad , \quad H_{xs}^{ext} = \frac{2E_0}{\eta} \cos\theta \cos\alpha. \tag{12}$$

For this excitation, take $E_{ys}^{int} = 0$ and $H_{xs}^{int} = 0$.

When electromagnetic fields in the presence of a ground plane are considered, sometimes it is convenient to remove the plane and replace it by appropriate images. In the present report the ground plane has not been removed and the images have not been invoked.
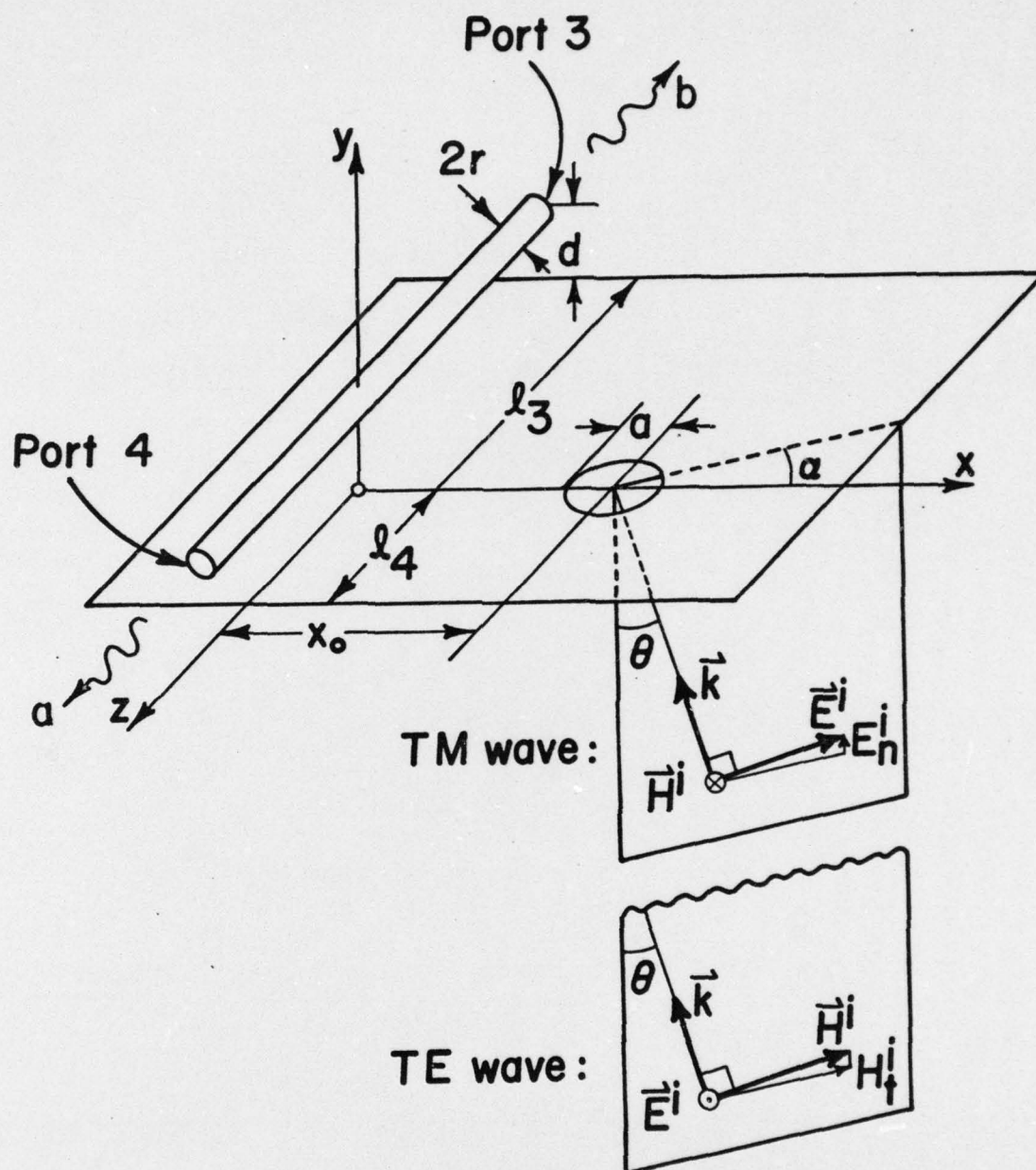
Fig. 3. Orientation of coordinates.

11

When dipole moments c_{mx} and c_{ey} have been determined, it is possible to compute the amplitudes of the outgoing guided waves created by these dipole moments. In Fig. 3, the scattering amplitudes of the TEM guided waves traveling in the positive and negative z direction are denoted by a_s and b_s. Using the appropriate boundary conditions in the xy plane, the following scattering amplitudes a_s and b_s are obtained [13]:

$$a_s = \frac{1}{2} \left[-c_{mx} h_{xTEM}(x_0, 0) - c_{ey} e_{yTEM}(x_0, 0) \right], \tag{13}$$

$$b_s = \frac{1}{2} \left[c_{mx} h_{xTEM}(x_0, 0) - c_{ey} e_{yTEM}(x_0, 0) \right]. \tag{14}$$

The scattering amplitudes are complex numbers, normalized in such a way that $|a_s|^2/2$ and $|b_s|^2/2$ are powers of the outgoing waves traveling in positive and in negative z directions [14].

It should be noted that Collin [14] uses superscripts (+) or (-) to denote the direction of the wave propagation. In the present report, letter a denotes the complex amplitude of the wave traveling in the positive z direction, and letter b is used for propagation in negative z direction. These are the familiar scattering parameters [15].

SECTION II

TRAVELING WAVE FORMULATION

Lossless multiconductor transmission lines (MTL) with unequal conductors and inhomogeneous dielectrics give rise to multivelocity quasi-TEM waves. As shown in the Appendix C, the voltages and currents on a MTL are described by

$$|V(z)\rangle = \sum_{n=1}^{N} (a_i e^{-j\beta_i z} + b_i e^{j\beta_i z})|\phi_i\rangle \quad , \tag{15}$$

$$|I(z)\rangle = \sum_{n=1}^{N} (a_i e^{-j\beta_i z} - b_i e^{j\beta_i z})|\psi_i\rangle \quad . \tag{16}$$

$|\phi_i\rangle$ and $|\psi_i\rangle$ are normalized voltage and current eigenvectors, and a_i's and b_i's are scattering amplitudes of the waves traveling in positive and negative z direction, respectively. It is assumed that on an N conductor MTL there are N normal modes, each of them having a distinct propagation constant β_i.

The notation from (15) and (16) may be made more compact by introducing the vectors of incident and reflected normal-mode amplitudes

$$|a\rangle = \begin{pmatrix} a_1 \\ \vdots \\ a_N \end{pmatrix} \quad , \qquad |b\rangle = \begin{pmatrix} b_1 \\ \vdots \\ b_N \end{pmatrix} \tag{17}$$

and by introducing the diagonal matrix $\underline{E}(z)$ containing the exponential functions

$$\underline{E}(z) = \text{diag.} (e^{j\beta_1 z}, \ldots, e^{j\beta_N z}) \quad . \tag{18}$$

13

In the new notation, (15) and (16) become:

$$|V(z)> = \underline{M}_V(\underline{E}^*(z)|a> + \underline{E}(z)|b>) \quad , \tag{19}$$

$$|I(z)> = \underline{M}_I(\underline{E}^*(z)|a> - \underline{E}(z)|b>) \quad , \tag{20}$$

where * denotes a complex conjugate number, and $\underline{M}_V$ and $\underline{M}_I$ are matrices consisting of voltage and current eigenvectors, as defined by (C-42) and (C-43). (19) and (20) may be now solved for $|a>$ and $|b>$:

$$\underline{E}^*(z)|a> = \frac{1}{2}(\underline{M}_I^+|V(z)> + \underline{M}_V^+|I(z)>) \quad , \tag{21}$$

$$\underline{E}(z)|b> = \frac{1}{2}(\underline{M}_I^+|V(z)> - \underline{M}_V^+|I(z)>) \quad . \tag{22}$$

$|a>$ is a constant vector containing the amplitudes of the individual modes as its components. For instance, a_i is the complex amplitude such that the total power of the i-th mode transmitted in positive z direction is

$$P_i^+ = \frac{1}{2}|a_i|^2 \quad .$$

The entire power of all the modes traveling in the positive z direction is

$$P^+ = \frac{1}{2}<a|a> \tag{23}$$

where $<a|$ denotes a transpose conjugate of $|a>$. Similarly, the entire negative-traveling power is

$$P^- = \frac{1}{2}<b|b> \quad . \tag{24}$$

The net power is the difference of the two. On a uniform MTL there is no exchange of power between different modes. Each mode travels with

14

constant magnitude, while its phase grows linearly with distance.

The z dependence of scattering amplitudes may be expressed as

$$|a(z)> = \underline{E}^*(z)|a> \tag{25}$$

and

$$|b(z)> = \underline{E}(z)|b> \tag{26}$$

where $|a>$ and $|b>$ are vectors consisting of complex constants. Thus, the i-th component of the vector equation (25) is

$$a_i(z) = e^{-j\beta_i z} a_i ,$$

and the corresponding i-th component of (26) is

$$b_i(z) = e^{j\beta_i z} b_i .$$

The signal flow graph [16] of the MTL section of length ℓ is shown in Fig. 4. The i-th mode has two variables $a_i(0)$ and $b_i(0)$ at z=0. Similarly, at z=ℓ the two variables of the i-th mode are $a_i(\ell)$ and $b_i(\ell)$. The coefficients of matrix $\underline{E}^*(\ell)$ equal to $e^{-j\beta_i \ell}$. Thus, $a_i(\ell)$ is obtained by multiplying $a_i(0)$ by the coefficient $e^{-j\beta_i \ell}$. The signal flow graph in Fig. 4 is extremely simple, since along the transmission line there is no cross coupling between different modes.

Figure 5 shows a MTL section with 3 conductors above the ground plane. At z=0, a source is coupled to the MTL, inducing the waves traveling toward +z and -z directions. The amplitudes of the i-th mode produced by the source are a_{is} and b_{is}. The direction of propagation of these waves is indicated by a wavy arrow. The wave traveling in +z direction arrives at z=ℓ_4 shifted in phase for $e^{-j\beta_i \ell_4}$. There, a three-port network terminates the MTL. The impedance matrix of this network is $\underline{Z}_4$.

15
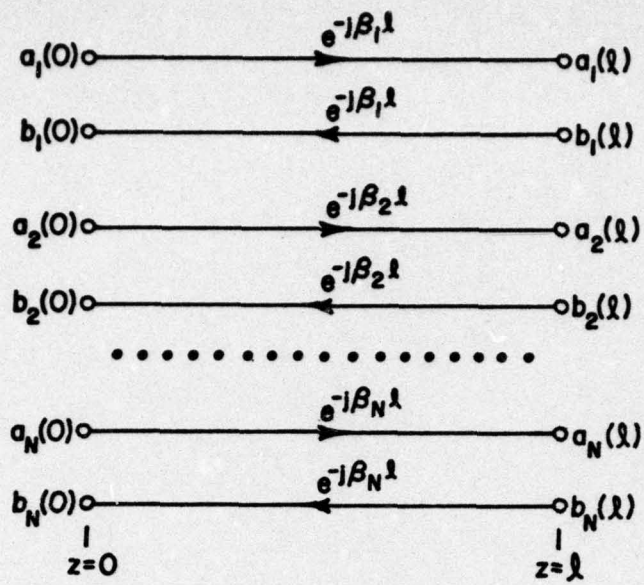
Fig. 4. Signal Flow graph of a MTL section.
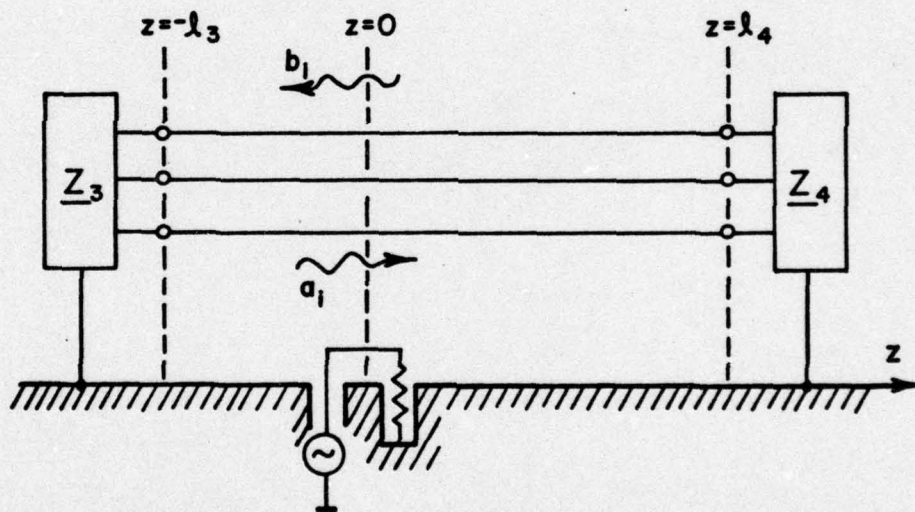
Fig. 5. Terminated MTL with a source of outgoing waves located at z = 0.

16

The amount of reflection on the MTL can be computed from $\underline{Z}_4$ as follows.

At z=0, the total amplitude a_i of the i-th mode traveling in the positive z direction consists of two parts: the source part a_{is} and the part which arrives reflected from the left-hand termination at $z=-\ell_3$. The total amplitudes of all waves at z=0 are arranged in vector $|a>$. Then, the vector of all waves arriving at $z=\ell_4$ is

$$|a(\ell_4)> = \underline{E}^*(\ell_4)|a>$$

From (21), this is furthermore equal to

$$|a(\ell_4)> = \frac{1}{2}(\underline{M}_I^+|V(\ell_4)> + \underline{M}_V^+|I(\ell_4)>). \tag{27}$$

From (22), the reflected mode vector at the end of line is

$$|b(\ell_4) = \frac{1}{2}(\underline{M}_I^+|V(\ell_4)>- \underline{M}_V^+|I(\ell_4)>), \tag{28}$$

The currents and voltages at the load network terminals are related through $\underline{Z}_4$

$$|V(\ell_4)> = \underline{Z}_4|I(\ell_4)> . \tag{29}$$

By eliminating $|V(\ell_4)>$ and $|I(\ell_4)>$ from the last three equations one obtains

$$|b(\ell_4)> = \underline{S}_4|a(\ell_4)> \tag{30}$$

where the reflection matrix at port 4 is

$$\underline{S}_4 = (\underline{M}_I^+ \ \underline{Z}_{L4}\underline{M}_I - \underline{U}) \ (\underline{M}_I^+ \ \underline{Z}_{L4}\underline{M}_I + \underline{U})^{-1} \tag{31}$$

17

When the load impedance matrix is equal to the characteristic impedance $\underline{Z}_L = \underline{Z}_0$, one has a reflectionless termination, as can be verified by (C-46) and (C-50). Otherwise, $\underline{S}_4$ is a matrix which has usually non-vanishing off-diagonal elements. This means that a single incoming mode a_i produces a multitude of reflected modes $b_j (j=1,2,3,$ etc.$)$. Thus, energy transfers from any one mode into all other modes.

This fact is illustrated in the signal-flow diagram on Fig. 6. On top of the figure, a_{1s} represents the amount of energy coupled from an external source to mode 1, traveling in $+z$ direction. The total wave amplitude a_1 at the origin, consists of a_{1s} plus the wave which was reflected from the termination at $z = -\ell_3$:

$$a_1 = a_{1s} + a_1(-\ell_3) e^{-j\beta\ell_3} .$$

This wave arrives at port 4 as

$$a_1(\ell_4) = a_1 e^{-j\beta_1\ell_4} .$$

A portion of this wave goes back as a reflected wave of the mode 1:

$$S_{4,11} a_1(\ell_4)$$

where $S_{4,11}$ is the coefficient $(1,1)$ of the matrix $\underline{S}_4$.

Another portion of the wave $a_1(\ell_4)$ goes to the enhancement of the reflected mode 2:

$$S_{4,21} a_1(\ell_4)$$

and so on, as shown in Fig. 6. For example, the total reflected wave of the mode 2 is

$$b_2(\ell_4) = S_{4,21} a_1(\ell_4) + S_{4,22} a_2(\ell_4) + S_{4,23} a_3(\ell_4) .$$

Similar situation occurs at port 3, where the load network $\underline{Z}_{L3}$ is attached. There, the reflected wave is

$$|a(-\ell_3)\rangle = \underline{S}_3 |b(-\ell_3)\rangle , \tag{32}$$

18
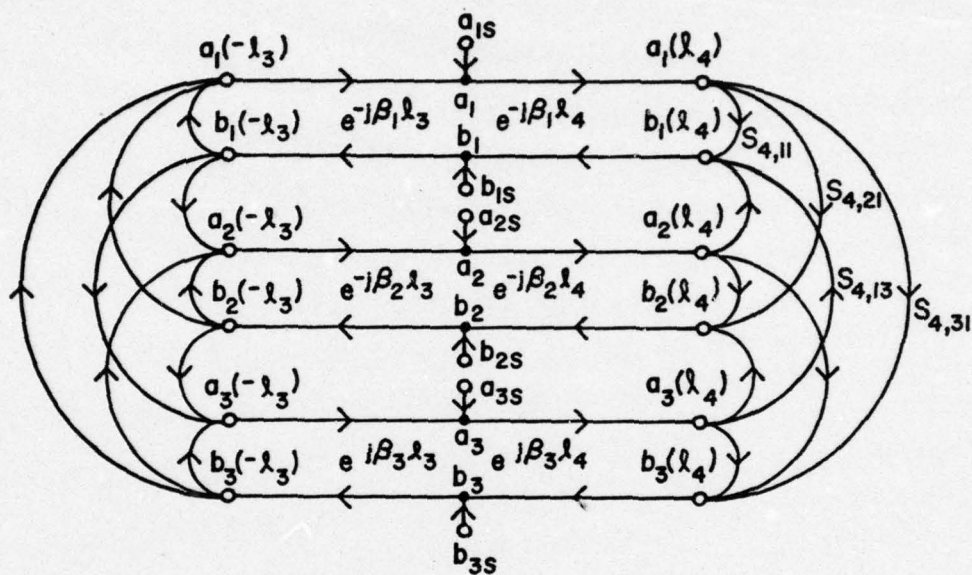
Fig. 6. Signal flow graph of the MTL from Fig. 5.

with

$$\underline{S}_3 = (\underline{M}_I^+ \, \underline{Z}_{L3} \, \underline{M}_I - \underline{U})(\underline{M}_I^+ \, \underline{Z}_{L3} \, \underline{M}_I + \underline{U})^{-1} \tag{33}$$

The above discussion was based entirely on the frequency-domain considerations, where each mode was a steady-state sinusoidal function of time. Assuming the quasi-TEM waves are non-dispersive, an arbitrary waveform is transmitted by each mode without a distortion. Therefore, for mode i, the wave $a_{i4}(t)$ traveling in the +z direction at the port 4 is just a delayed waveform which started at the origin as $a_{i0}(t)$:

$$a_{i4}(t) = a_{i0}(t - \frac{\ell_4}{v_i}) \tag{34}$$

Since the waves are now functions of both time and position, the second subscript is used to specify the position: 0 for origin , 4 for $z=\ell_4$ etc.

The time-table of the outgoing and reflected waves on a 3 conductor line is presented in Fig. 7. At z=0, the three waves start to travel to the right:

$$a_{10}(t) \ , \quad a_{20}(t) \ , \quad a_{30}(t)$$

and similarly the three waves start to travel to the left

$$b_{10}(t) \ , \quad b_{20}(t) \ , \quad b_{30}(t) \ .$$

Each wave travels with its mode velocity v_i. At $t=t_1$, the first wave arrives at port 4:

$$t_1 = \frac{\ell_4}{v_1} \ .$$

20
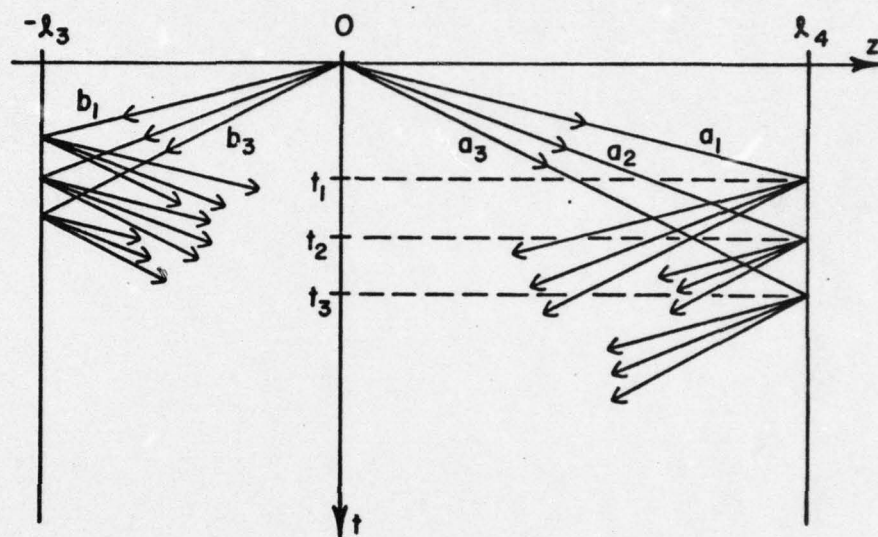
Fig. 7. Time-table representation of multiple reflections on the terminated MTL.

Its shape is a shifted shape of the wave which started from the origin, according to (34). This wave produces three reflected waves, which then travel with their corresponding velocities back in the negative z direction. When the load network contains inductances and capacitances, the shape of the reflected waves will be different from the incoming waveshape. For simplicity, consider the case when the load network is purely re-sistive. In that case, the reflected waves will be of the same shape as the incoming waves. The amount of reflection is specified by (30) and (31), where $\underline{Z}_{L4}$ is a purely resistive network, thus $\underline{S}_4$ has also purely real elements. The reflections from the left-hand termination are handled in an analogous manner.

22

As demonstrated above the scattering representation in terms of vectors $|a(z)>$ and $|b(z)>$ is very convenient for the treatment of propagation and reflection of waves on a MTL. Nevertheless, often it is necessary to compute explicitly the voltages and currents on individual conductors. They are specified by vectors $|V(z)>$ and $|I(z)>$. The transformation from scattering variables to the currents and voltages is obtained from (19), (20), (25), and (26) as follows

$$|V(z)> = \underline{M}_V(|a(z)> + |b(z)>) , \tag{35}$$

$$|I(z)> = \underline{M}_I(|a(z)> - |b(z)>) . \tag{36}$$

The inverse transformation is obtained from (21), (22), (25), and (26):

$$|a(z)> = \frac{1}{2} (\underline{M}_I^+|V(z)> + \underline{M}_V^+|I(z)>) , \tag{37}$$

$$|b(z)> = \frac{1}{2} (\underline{M}_I^+|V(z)> - \underline{M}_V^+|I(z)>) . \tag{38}$$

Note that the components of scattering vectors $|a(z)>$ and $|b(z)>$ correspond to the individual normal modes, while the components of the voltage and current vectors $|V(z)>$ and $|I(z)>$ correspond to the individual conductors. As an example, a_i is the complex amplitude of the i-th mode. On the other hand, V_i is the voltage of the i-th conductor w.r. to ground.

23

Fig. 8.(a) shows a section of MTL of the length ℓ. The voltages $V_i(z)$ are specified between each conductor and the ground, where the conductor side is considered as positive. The currents $I_i(z)$ on the individual conductors are specified positive when flowing in (+z) direction. This apparently trivial fact is pointed out because by using this convention, the current at $z=\ell$ points out of the MTL section, which is not customary in the network theory. However, the present convention is found to be more natural for the matrix manipulations which follow. The consequence of this convention is that the total power

$$P = \frac{1}{2} \, \text{Re} <V|I>$$

is not always pointed into the network, as customary in network theory, but here P represents the power flow in the positive z direction. Thus, at $z=0$, P is into the MTL, at $z=\ell$, P is out of the MTL.

The use of $|a>$ and $|b>$ variables in place of $|V>$ and $|I>$ variables is indicated in Fig. 8.(b). At each end of the MTL there is a transforming network N_T, which transforms the variables according to (35)-(38). At $z=0$, the left-hand terminals of N_T are the actual MTL conductors. Here, the variables are $|V(0)>$ and $|I(0)>$. The other side of N_T network has the mode variables $|a(0)>$ and $|b(0)>$. Each mode is represented by a fictitious single transmission line, shielded from all the other lines. Each single transmission line passes the wave through by simply adding the phase shift $(-\beta_i \ell)$ as follows

$$a_i(\ell) = a_i(0)e^{-j\beta_i \ell}$$

At the other end of the MTL, at $z=\ell$, variables $|a(\ell)>$ and $|b(\ell)>$ are transformed back to variables $|V(\ell)>$ and $|I(\ell)>$ in another identical transforming network N_T.

24

Terminals   Terminals

1   1
2   2
$I_3(0)$ → 3 $I_3(z)$ →   3 → $I_3(\ell)$
        +   +   +

$V_3(0)$ $V_3(z)$ $V_3(\ell)$

                    −   z
        −   −
    z=0   z=ℓ

                    (a)

Fig. 8(a). MTL section of length ℓ.

Terminals   Modes   Modes   Terminals

1   1   1   1

2   N_T 2   2 N_T 2

$I_3(0)$ 3   3   3   3 $I_3(\ell)$
        + $a_3(0)$ $a_3(\ell)$ +
$V_3(0)$ $V_3(\ell)$
                $b_3(0)$ $b_3(\ell)$
        −   −

                    (b)
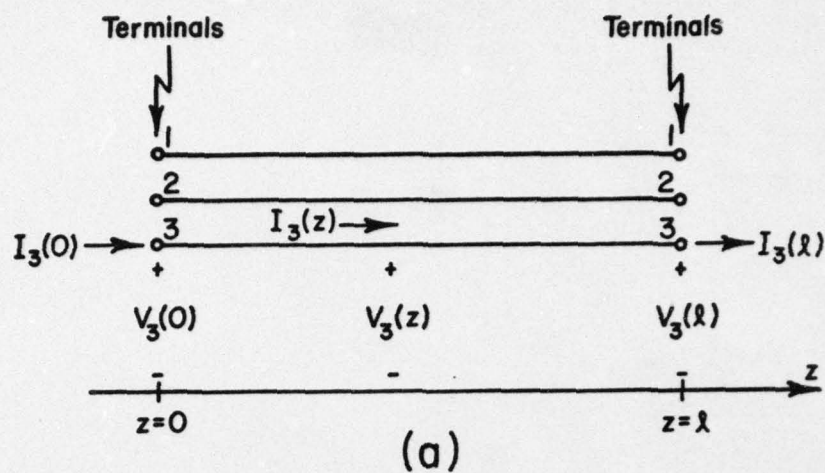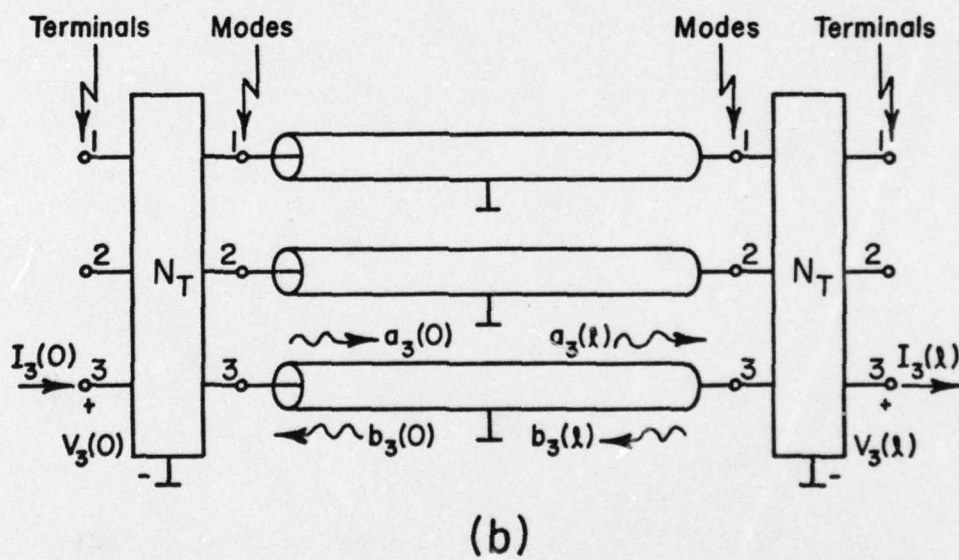
Fig. 8(b). Equivalent circuit for normal modes.

25

SECTION III

EQUIVALENT SOURCES FOR APERTURE EXCITATION

Each normal mode is described by its scattering amplitude a_i (waves traveling in +z direction) or b_i (waves traveling in -z direction). The detailed distribution of the electric and magnetic field, for the i-th mode traveling in +z direction, is

$$\vec{E}_i(x,y,z) = a_i e^{-j\beta_i z} \vec{e}_i(x,y) \quad , \tag{39}$$

$$\vec{H}_i(x,y,z) = a_i e^{-j\beta_i z} \vec{h}_i(x,y) \quad . \tag{40}$$

$\vec{e}_i$ and $\vec{h}_i$ are the normalized modal field distributions over the cross section of the MTL. The total power transmitted by the i-th mode traveling in +z direction is obtained by integrating the Poynting vector over the cross section:

$$P_i^+ = \frac{1}{2} \operatorname{Re} \iint_{\text{cross section}} [\vec{E}_i(x,y) \times \vec{H}_i(x,y)] \cdot d\vec{s} \quad .$$

For normalized modal field distributions

$$\iint_{\text{cross section}} [\vec{e}_i(x,y) \times \vec{h}_j^*(x,y)] \cdot d\vec{s} = \delta_{ij} \quad , \tag{41}$$

and the power transmitted by the i-th mode is

$$P_i^+ = \frac{1}{2}|a_i|^2$$

in accordance with circuit theory.

Fig. 9.(a) shows the junction representing an aperture on a MTL. The aperture is excited by an external field from below the ground plane.

26
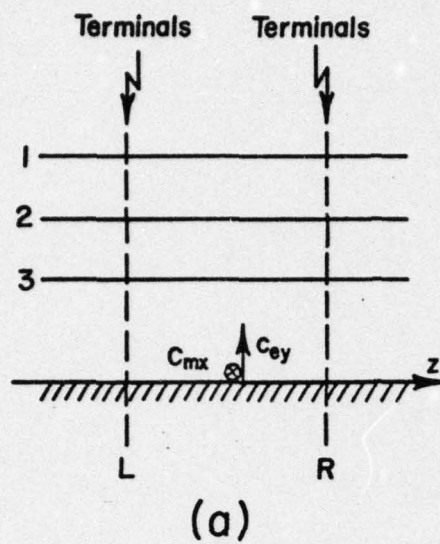
Fig. 9(a). A junction with an aperture.
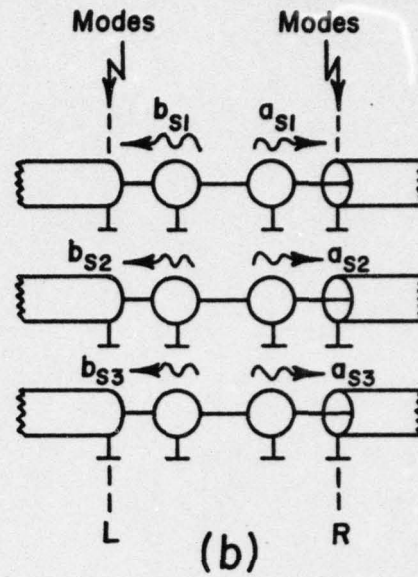
Fig. 9(b). Normal-mode sources.
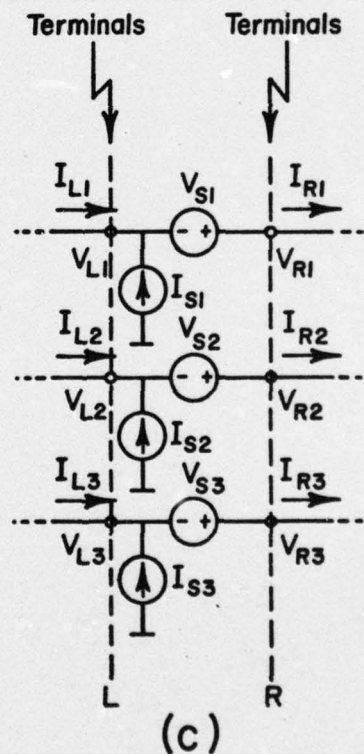
Fig. 9(c). Voltage and current sources.

27

This excitation is replaced by an equivalent pair of dipoles c_{mx} and c_{ey}. In what follows, an equivalent circuit will be established for the junction between the two infinitely close planes, denoted by L and R (letters stand for "left" and "right").

According to (13), the dipole pair c_{mx} and c_{ey} excites the i-th mode traveling in +z direction as follows

$$a_{si} = \frac{1}{2} [c_{mx} h_{xi}(x_0,0) - c_{ey} e_{yi}(x_0,0)] . \qquad (42)$$

As indicated previously, a convention in the present report is that the waves traveling in +z direction are denoted by a_i, while the waves traveling in -z direction are denoted by b_i. Therefore, (42) gives a source of the traveling mode in +z direction, and is denoted by a_{si}. A traveling wave source is a three-terminal device, as explained in Appendix B.

Another word about the notation in (42): $h_{xi}(x_0,0)$ is the x-component of the magnetic-field modal distribution of the i-th mode, evaluated at the point $x=x_0$ and $y=0$. Similarly $e_{yi}(x_0,0)$ is the y-component of the normalized electric modal field.

For the traveling-wave source of the i-th mode propagating in -z direction, the following is obtained from (9):

$$b_{si} = \frac{1}{2} [-c_{mx} h_{xi}(x_0,0) - c_{ey} e_{yi}(x_0,0)] . \qquad (43)$$

Fig. 9.(b) shows the modal sources between the left and right reference planes. This equivalent circuit is appropriate for an analysis in terms of scattering coefficients. The equivalent circuit in terms

28

of voltages and currents can be now obtained by a simple matrix manipulation. First, define the vectors containing the scattering sources as follows:

$$|a_s> = \begin{pmatrix} a_{s1} \\ \vdots \\ a_{sN} \end{pmatrix} \quad , \qquad |b_s> = \begin{pmatrix} b_{s1} \\ \vdots \\ b_{sN} \end{pmatrix} \quad . \tag{44}$$

The traveling wave vector, $|a_R>$ traveling in +z direction out of the right-hand reference plane is a sum of the source vector $|a_s>$ and the wave vector $|a_L>$ incoming from the left upon the left-hand reference plane:

$$|a_R> = |a_L> + |a_s> \quad . \tag{45}$$

Similarly, the waves traveling in the -z direction are related as

$$|b_L> = |b_R> + |b_s> \quad . \tag{46}$$

The voltage and current variables of the source junction are shown in Fig. 9.(c). The voltages and currents at the left-hand plane are defined by $|V_L>$ and $|I_L>$, while the right-hand variables are $|V_R>$ and $|I_R>$. The current sources from Fig. 9.(c). constitute vector $|I_s>$ while the voltage sources make $|V_s>$. The Kirchhoff laws require

$$|V_L> + |V_s> = |V_R> \quad , \tag{47}$$

and

$$|I_L> + |I_s> = |I_R> \quad . \tag{48}$$

To change from scattering representation to voltage representation, use (35)

$$|V_s> = |V_R>-|V_L> = \underline{M}_V(|a_R>-|a_L> + |b_R>-|b_L>) \quad .$$

29

By virtue of (45) and (46):

$$|V_s> = \underline{M}_V(|a_s> - |b_s>) \, . \tag{50}$$

The components of $|a_s>$ and $|b_s>$ are given by (28) and (29). The difference term is

$$a_{si} - b_{si} = c_{mx}h_{xi} \, (x_0, 0) \tag{51}$$

and it depends only on the magnetic dipole excitation. Thus, the voltage sources in Fig. 9(c) are to be computed as follows:

$$|V_s> = \underline{M}_V \begin{pmatrix} c_{mx}h_{x1}(x_0,0) \\ \cdots\cdots\cdots \\ c_{mx}h_{xN}(x_0,0) \end{pmatrix} \, . \tag{52}$$

The current sources are similarly found as follows

$$|I_s> = \underline{M}_I \, (|a_s> + |b_s>) \, . \tag{53}$$

The sum term depends entirely on the electric dipole moment

$$a_{si} + b_{si} = c_{ey}e_{yi}(x_0,0) \, , \tag{54}$$

so that the formula for computation of the current sources becomes

$$|I_s> = \underline{M}_I \begin{pmatrix} c_{ey} \, e_{y1}(x_0,0) \\ \cdots\cdots\cdots \\ c_{ey} \, e_{yN}(x_0,0) \end{pmatrix} \, . \tag{55}$$

In the above derivation, the energy storage at the junction was not taken in the account. The circuits from Fig. 9.(b) and (c) are thus the zeroth-order equivalents, such as the zeroth-order equivalent of a single transmission line from reference [13].

30

SECTION IV
EXAMPLES OF VOLTAGE WAVEFORMS

The voltages induced on a 2-conductor transmission line
filled with inhomogeneous dielectric will be now computed in order
to illustrate the use of the theory developed thus far. The system
is shown in Fig. 10. A small circular aperture of diameter $d = 2$ cm
is located at $z = 0$. The two-conductor transmission line is located
between $z = -\ell_3 = -7m$ and $z = \ell_4 = 5$ m.

The cross section of the transmission line is shown in Fig. 11:
it consists of two strip conductors of width w, placed between the
three layers of dielectrics denoted ε_1, ε_2, and ε_3. The dielectric
thicknesses are denoted by h_1, h_2, and h_3. This parallel-plate
model of the transmission line is selected because of its simplicity,
and it will be used to illustrate the procedure of computing
voltages induced by an EMP wave. The electrostatic field within the
transmission line from Fig. 11 may be produced in two independent
ways. In the excitation A, a potential V_a is applied to conductor
a, while conductor b and the shield are held at zero potential. Then,
the fields in the three regions are

$$\vec{E}_{1A} = \vec{a}_y \frac{V_a}{h_1} \quad ; \quad \vec{E}_{2A} = \vec{0} \quad ; \quad \vec{E}_{3A} = -\vec{a}_y \frac{V_a}{h_2} \; .$$

In the excitation B, a potential V_b is applied to conductor b, while
conductor a and the shield are held at zero potential. The corresponding
fields are

31
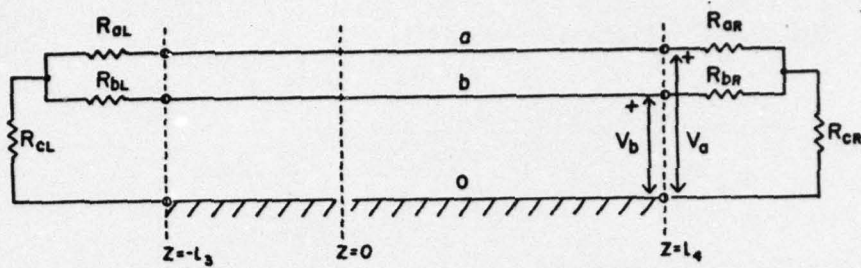
Fig. 10. Terminated 2-conductor transmission line with an aperture.
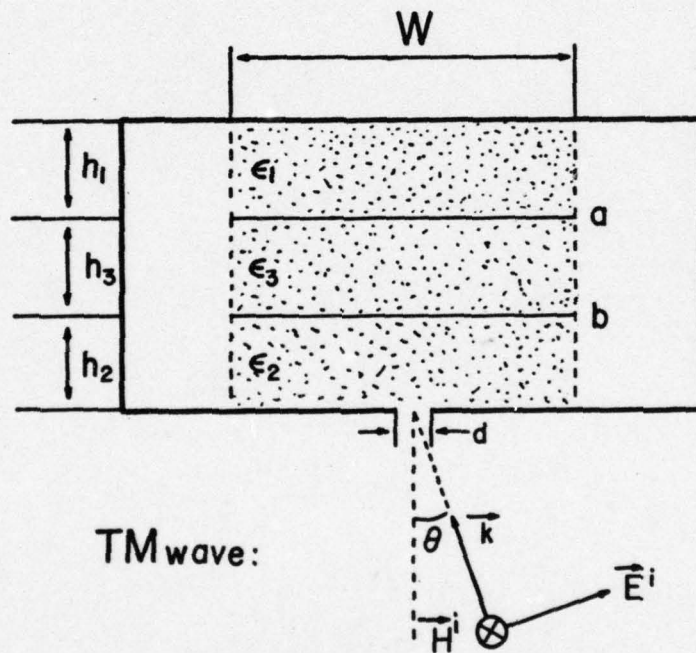
Fig. 11. Parallel-plate 2-conductor transmission line.

$$\vec{E}_{1B} = \vec{0} \quad ; \quad \vec{E}_{2B} = -\vec{a}_y \frac{V_b}{h_2} \quad ; \quad \vec{E}_{3B} = \vec{a}_y \frac{V_b}{h_3} \quad .$$

Under arbitrary excitation the fields in the individual regions (i = 1, 2, 3) are obtained by superposition:

$$. \vec{E}_i = V_a \vec{E}_{ia} + V_b \vec{E}_{ib} \quad . \tag{56}$$

In order to compute the coefficients of electric induction matrix, one must find the charge per unit length of the conductor a. This is accomplished by integrating the electric flux through the closed surface S_a around the conductor a:

$$Q_a = \int_{S_a} \varepsilon \vec{E} \cdot d\vec{S}$$

where ε and $\vec{E}$ depend on the point of integration. Using (56), the charge Q_a is found to consist of two parts, one proportional to V_a and the other proportional to V_b.

$$Q_a = V_a \int_{S_a} \varepsilon \vec{E}_A \cdot d\vec{S} + V_b \int_{S_a} \varepsilon \vec{E}_B \cdot d\vec{S}$$

$$\tag{57}$$

$$Q_a = V_a K_{aa} + V_b K_{ab}$$

The constants of proportionality are called induction coefficients, denoted K_{aa} and K_{ab}. They depend only on the geometry of the system. For example, K_{aa} is computed as follows:

33

$$K_{aa} = \varepsilon_1 \int_{x=-w/2}^{w/2} \vec{E}_{1A} \cdot \vec{a}_y dx - \varepsilon_3 \int_{x=-w/2}^{w/2} \vec{E}_{3A} \cdot \vec{a}_y dx$$

$$K_{aa} = w\left(\frac{\varepsilon_1}{h_1} + \frac{\varepsilon_3}{h_3}\right) \tag{58}$$

Similarly, the other induction coefficients are found as follows:

$$K_{ab} = K_{ba} = -w\frac{\varepsilon_3}{h_3} \tag{59}$$

$$K_{bb} = w\left(\frac{\varepsilon_3}{h_3} + \frac{\varepsilon_2}{h_2}\right) \tag{60}$$

These coefficients form induction coefficient matrix $\underline{K}$

$$\underline{K} = \begin{pmatrix} K_{aa} & K_{ab} \\ K_{ab} & K_{bb} \end{pmatrix} \tag{61}$$

As an example of a symmetric system, the following dimensions have been selected:

$h_1 = 2$ cm, $h_2 = 2$ cm, $h_3 = 1$ cm, $w = 10$ cm, $\varepsilon_{1r} = 1.0$,

$\varepsilon_{2r} = 1.0$, $\varepsilon_{3r} = 2.0$, $d = 2$ cm.

The corresponding matrix $\underline{K}$ is

34

$$\underline{K} = \varepsilon_0 \begin{pmatrix} 25 & -20 \\ -20 & 25 \end{pmatrix}$$

The induction coefficient matrix with only air as dielectric will be denoted $\underline{K}'$:

$$\underline{K}' = \varepsilon_0 \begin{pmatrix} 15 & -10 \\ -10 & 15 \end{pmatrix}$$

By using matrices $\underline{K}$ and $\underline{K}'$ one can find the modal velocities, voltage and current eigenvectors, and the impedance matrix by the procedure described in Appendix C. The inverse of the induction matrix $\underline{L}$ is directly proportional to $\underline{K}'$ as follows

$$\underline{L}^{-1} = c^2 \, \underline{K}' \tag{62}$$

where c is the velocity of the light in vacuum. Next, the eigenvectors and eigenvalues of $\underline{L}^{-1}$ are found, and an auxiliary matrix $\underline{B}$ is formed according to (C-15). When the eigenvalues of $\underline{B}$ are computed, the modal velocities v_i are found as their inverse square roots, according to (C-16). The eigenvectors of $\underline{B}$ are then used to form the modal matrices $\underline{M}_V$ and $\underline{M}_I$, according to (C-42) and (C-43):

$$\underline{M}_V = \begin{pmatrix} \phi_{a1} & \phi_{a2} \\ \phi_{b1} & \phi_{b2} \end{pmatrix} = \begin{pmatrix} -6.136 & -2.369 \\ -6.136 & 2.369 \end{pmatrix} \tag{63}$$

$$\underline{M}_I = \begin{pmatrix} \psi_{a1} & \psi_{a2} \\ \psi_{b1} & \psi_{b2} \end{pmatrix} = \begin{pmatrix} -0.081489 & -0.21106 \\ -0.081489 & 0.21106 \end{pmatrix} \tag{64}$$

35

Subscripts a and b denote the conductors, and subscripts 1 and 2 denote the modes.

Next, modal functions e_y and h_x will be evaluated. The aperture is placed at the center of the bottom shield conductor, as shown in Fig. 11. By definition, the electric field of the nth mode traveling in positive z direction is

$$\vec{E}_n(x,y,z) = a_n \vec{e}_n(x,y) e^{-j\beta_n z} \tag{65}$$

By selecting $a_n = 1$, the electric field at $z = 0$ becomes

$$\vec{E}_n(x,y,0) = \vec{e}_n(x,y) \tag{66}$$

When $a_n = 1$ and $b_n = 0$, the voltage vector is obtained from (35) as follows

$$| V_n > = | \phi_n > = \begin{pmatrix} \phi_{an} \\ \phi_{bn} \end{pmatrix} \tag{67}$$

Thus, in order to find the modal function $\vec{e}_n$ of the mode n (here, n = 1 or 2), the potentials on the two conductors must be selected equal to ϕ_{an} and ϕ_{bn} as shown in Fig. 12. Then the modal function is equal to the electric field, according to (66). Since the field has only the y component, the result is

$$e_{yn} = \phi_{an} E_{y2A} + \phi_{bn} E_{y2B} = - \frac{\phi_{bn}}{h_3} \tag{68}$$

The modal function $\vec{h}_n(x,y)$ is equal to the magnetic field $\vec{H}_n(x,y,0)$ inside the transmission line, when conductor a carries a current $I_a = \psi_{an}$

36

and conductor b carries current $I_b = \psi_{bn}$. The situation is shown in Fig. 13. The currents are assumed to be uniformly distributed over the conductor surfaces. An elementary computation gives the following value for the magnetic field modal function:

$$h_{xn} = \frac{\psi_{an}h_1 + \psi_{bn}(h_1 + h_3)}{w(h_1 + h_2 + h_3)} \tag{69}$$

In the example treated here, a time domain response will be evaluated, while most of the theory presented until now has been formulated in the frequency domain. In order to use formulas (8) and (9) for a general time variation, they are rewritten as follows:

$$c_{mx} = -\mu\alpha_m \frac{\partial}{\partial t}\left(H_{xs}^{ext} - H_{xs}^{int} \right) \tag{70}$$

$$c_{ey} = \varepsilon\alpha_e \frac{\partial}{\partial t}\left(E_{ys}^{ext} - E_{ys}^{int} \right) \tag{71}$$

The polarizabilities α_m and α_e are given by (10).

The incident wave orientation is specified by angles α and θ as shown in Fig. 3. Then for a TM polarization, the field components of importance are

$$E_{ys}^{ext} = 2E_0 F(t)\sin\theta \quad , \quad H_{xs}^{ext} = -\frac{2E_0}{\eta} F(t)\sin\alpha \tag{72}$$

An arbitrary time variation of the incident plane wave is described by function $F(t)$. For EMP wave, a simple function is selected as follows

$$F(t) = e^{-\alpha_1 t} - e^{-\beta_1 t} \tag{73}$$

37
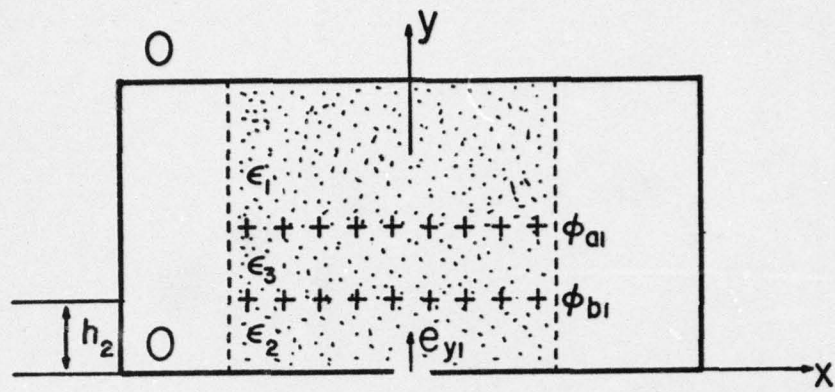
Fig. 12. Evaluation of the electric field on the line from Fig. 11.
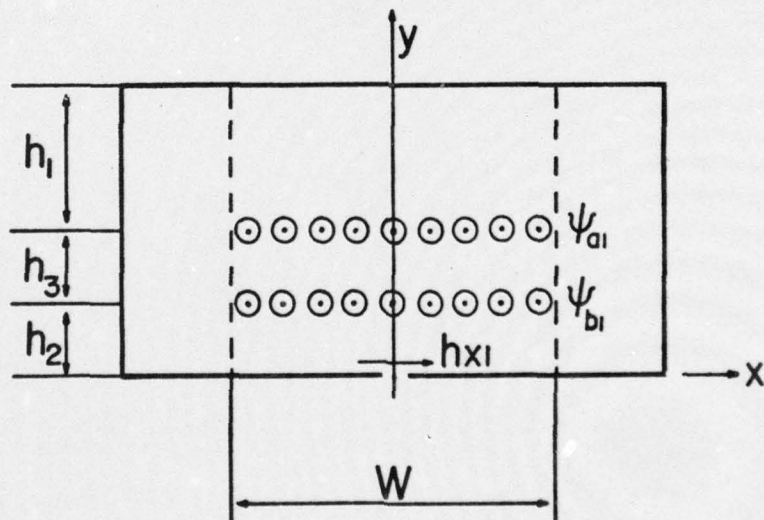
Fig. 13. Evaluation of the magnetic field on the line from Fig. 11.

having the following derivative

$$F'(t) = -\alpha_1 e^{-\alpha_1 t} + \beta_1 e^{-\beta_1 t} . \qquad (74)$$

The following parameters of the incident plane wave have been selected for the present example:

$E_0 = 100 kV/m$, $\alpha = 30°$, $\theta = 45°$, $\alpha_1 = 3.10^6 s^{-1}$, $\beta_1 = 10^8 s^{-1}$.

The electric and magnetic current moments are now computed by (70) and (71):

$$c_{mx} = 2 \frac{\mu}{\eta} \frac{d^3}{6} E_0 F'(t) \sin\alpha, \qquad (75)$$

$$c_{ey} = 2 \varepsilon \frac{d^3}{12} E_0 F'(t) \sin\theta \qquad (76)$$

These values are to be substituted in (42) and (43) in order to compute the traveling wave sources for different modes on the multiconductor line. For the present example, the modal functions e_{yi} and h_{xi} which are needed in (42) and (43) are determined by (68) and (69). The initial amplitudes of the traveling wave sources can be now computed and the multipole reflection traced down in a manner indicated in Fig. 7. As long as the loading at each end of the multiconductor line consists of pure resistances, such as in Fig. 10, the wave shape remains unchanged after each reflection, and is specified by the function $F'(t)$ from (74).

39

In the first example to be computed, the following loading resistances have been selected:

$$R_{aL} = R_{aR} = 1k\Omega, \ R_{bL} = R_{bR} = 100\Omega, \ R_{cL} = R_{cR} = 1\Omega$$

The load impedance matrix of a T network is then obtained as

$$Z_{L11} = R_{aL} + R_{cL} = 1.001k\Omega$$

$$Z_{L12} = R_{cL} = 1\Omega$$

$$Z_{L22} = R_{bL} + R_{cL} = 1.001k\Omega$$

The corresponding scattering matrix is obtained from (33)

$$\underline{S}_3 = \begin{pmatrix} 0.43488 & 0.17495 \\ 0.17495 & 0.90584 \end{pmatrix}$$

Since the load resistances on the right-hand side are the same as on the left-hand side, $\underline{S}_4 = \underline{S}_3$. For each incident wave a_i at the port 4, the reflected waves are computed by

$$b_j = S_{ji} a_i \qquad \text{for } j = 1,2$$

Then, the voltages are obtained from (35)

$$|V\rangle = \underline{M}_V \ (|a\rangle + |b\rangle)$$

40

The velocities of the two waves are $v_1 = 3 \cdot 10^8$ m/s and $v_2 = 2.236 \cdot 10^8$ m/s. Fig. 14 shows the voltages on the right-hand end of the transmission line. V_1 is the voltage on the conductor a , while V_2 is the voltage on the conductor b. First pulse arrives at $t_1 = \ell_4/v_1 = 16.6$ ns. Note that this is even mode, since the polarity of the pulse is the same on both conductors. Shortly afterwards, at $t_2 = \ell_4/v_2 = 22.4$ ns, the odd mode arrives producing a positive pulse of V_1 and a negative pulse of V_2. The next arrival is the group of four waves which are reflected from the left-hand end of the line, and the process is continued through multiple reflections bouncing back and forth on the line.

At each of the bounces, some of the energy is lost in resistances terminating the line, so the process gradually dies off as seen in Figure 14. If one end of the line is terminated in a resistance matrix equal to the characteristic impedance matrix $\underline{Z}_0$, there are no reflections from that end. In the next example, we terminate the right-hand end of the MTL by a matched impedance. The necessary resistances are obtained from $\underline{Z}_0$ as follows. First $\underline{Z}_0$ is computed by (C50)

$$\underline{Z}_0 = \begin{pmatrix} 43.260 & 32.036 \\ \\ 32.036 & 43.260 \end{pmatrix}$$

Then, the resistances of the T-network are obtained as

$R_{aR} = Z_{011} - Z_{012} = 11.224\Omega$

$R_{bR} = Z_{022} - Z_{012} = 11.224\Omega$

$R_{cR} = Z_{012} = 32.036\Omega$

41
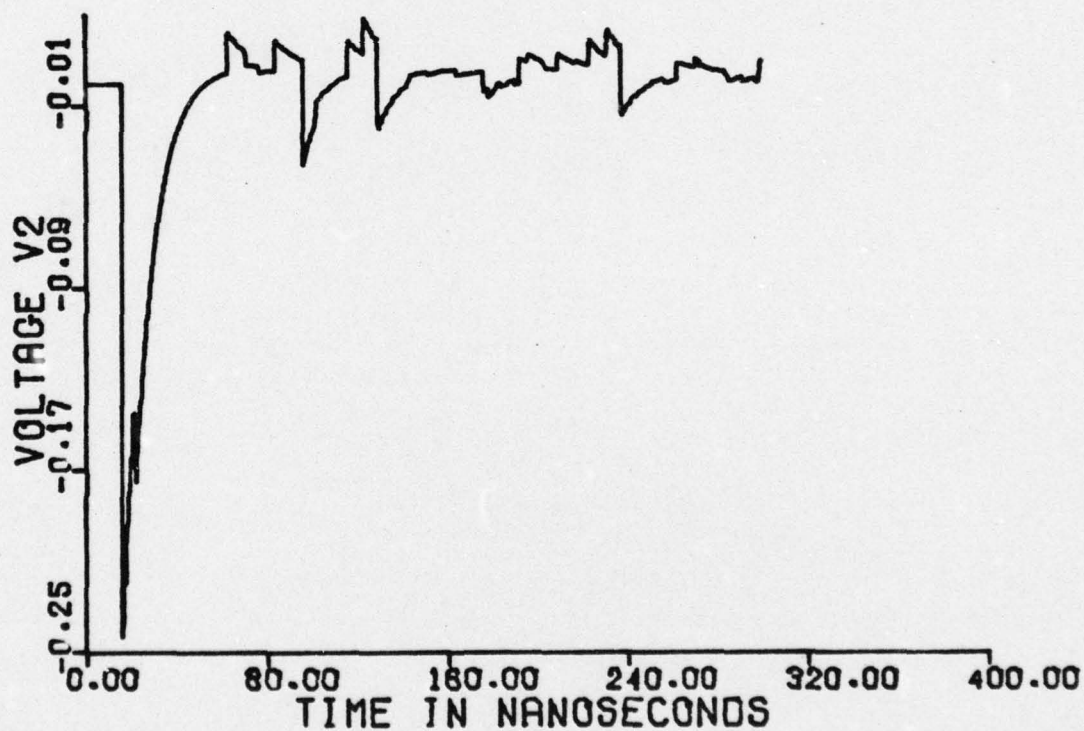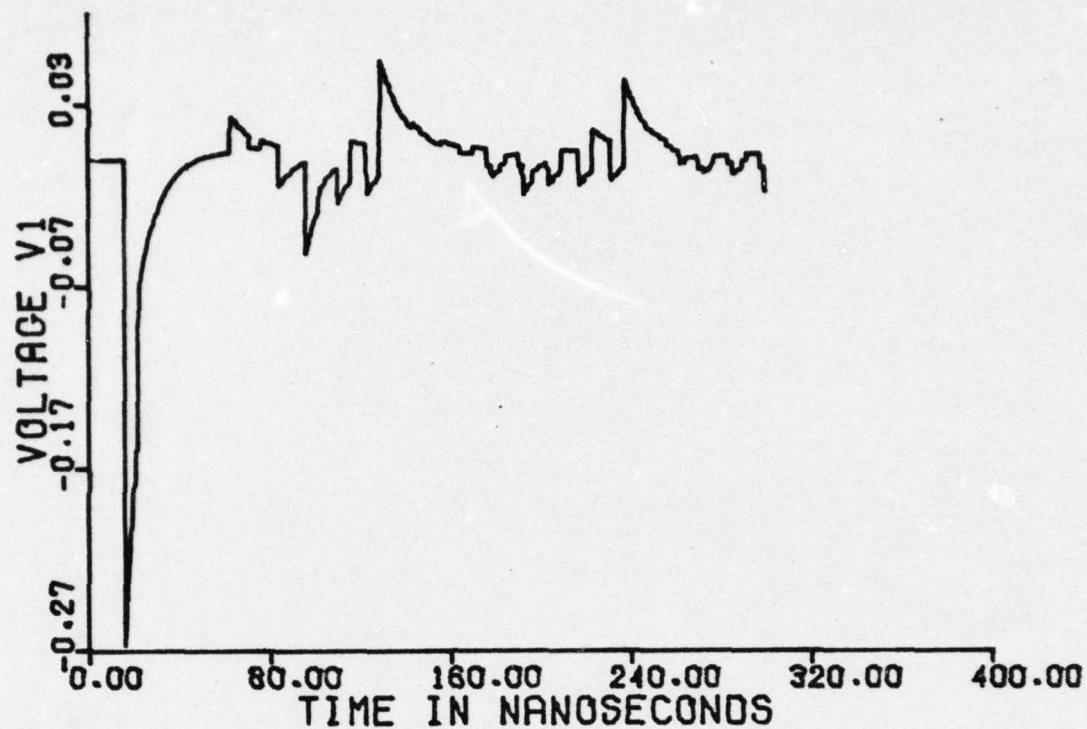
Fig. 14. Voltage waveforms on a 2-conductor line: moderate mismatch.

42

With such a matched termination on the right-hand side, the resulting voltages take the shape as shown in Fig. 15. The first arrival of the odd and even mode is similar to the previous situation in Figure 14. Also, the next four pulses are similar to those from Figure 14, but after that there are no more waves left on the line.

Another extreme situation occurs when there is no attenuation , because the terminations consist of open-circuits or short circuits. In Figure 16, the following terminations have been selected

$$R_{aL} = R_{aR} = 1k\Omega, \quad R_{bL} = R_{bR} = 0.1\Omega \quad R_{cL} = R_{cR} = 0.01 \ \Omega$$

There is little attenuation of the voltage waveshapes in the first 300 ns, and the multiple bouncing on the transmission line continues for a long time.

The computer program evaluates the individual pulse arrivals in the close analogy with the time-table from Figure 7. If the MTL can support N different modes, each of those produces N other reflected modes at each bounce. Very soon the storage requirements become prohibitive. For a 2-conductor line of the total length 12 m as in Figure 10, there are 510 pulse arrivals within 300 ns. If the number of conductors is increased to three, there are 9840 arrivals which are to be stored before sorting them in chronological order. It is obvious that this procedure is practical only for computing the early time responses.

An example of the three conductor parallel-plate MTL is shown in Figure 17. The voltages on the individual conductors are denoted by V_1, V_2, and V_3.

43
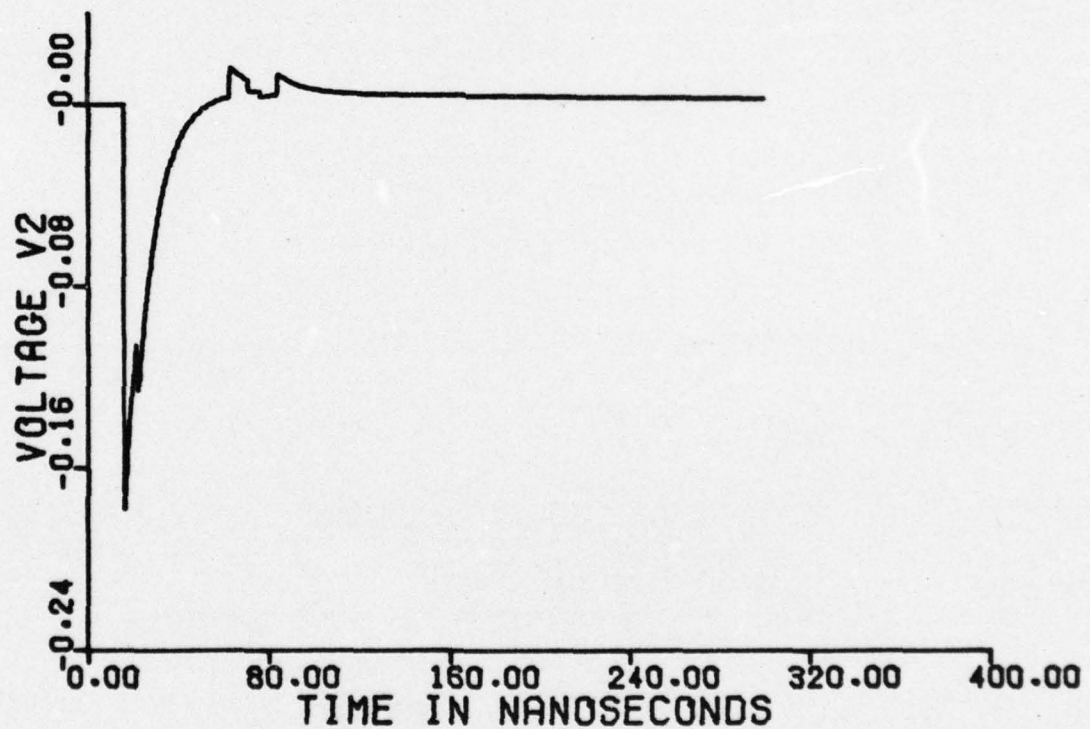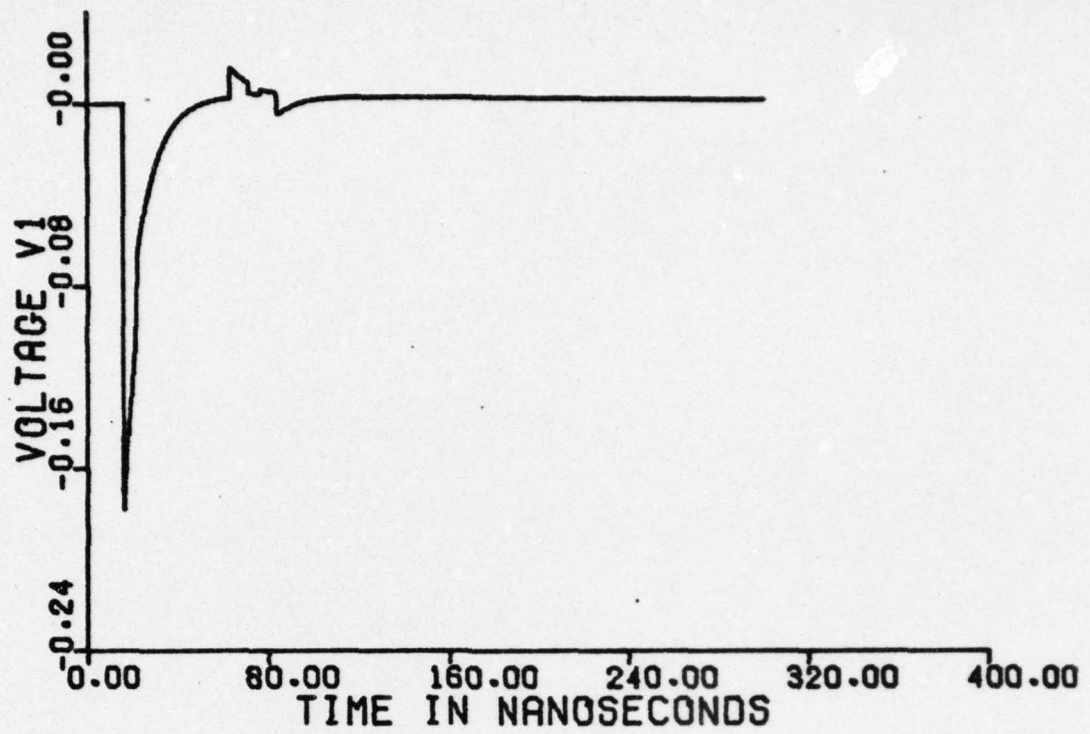
Fig. 15. Voltage waveforms on a 2-conductor line: matched load at left-hand
terminals.

44
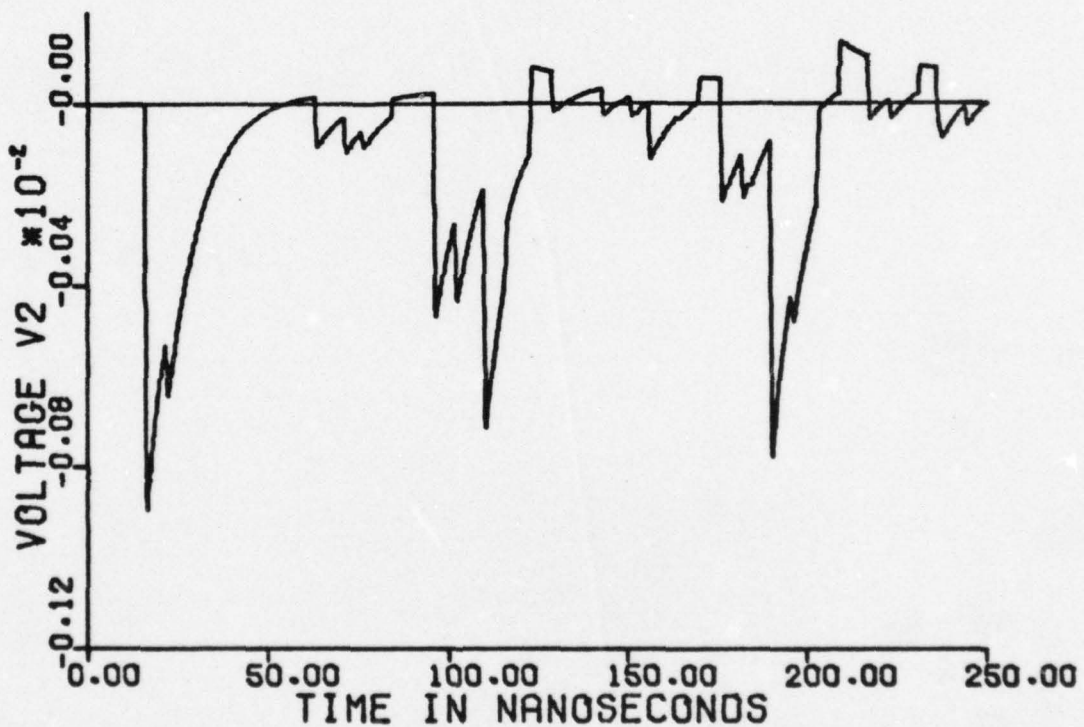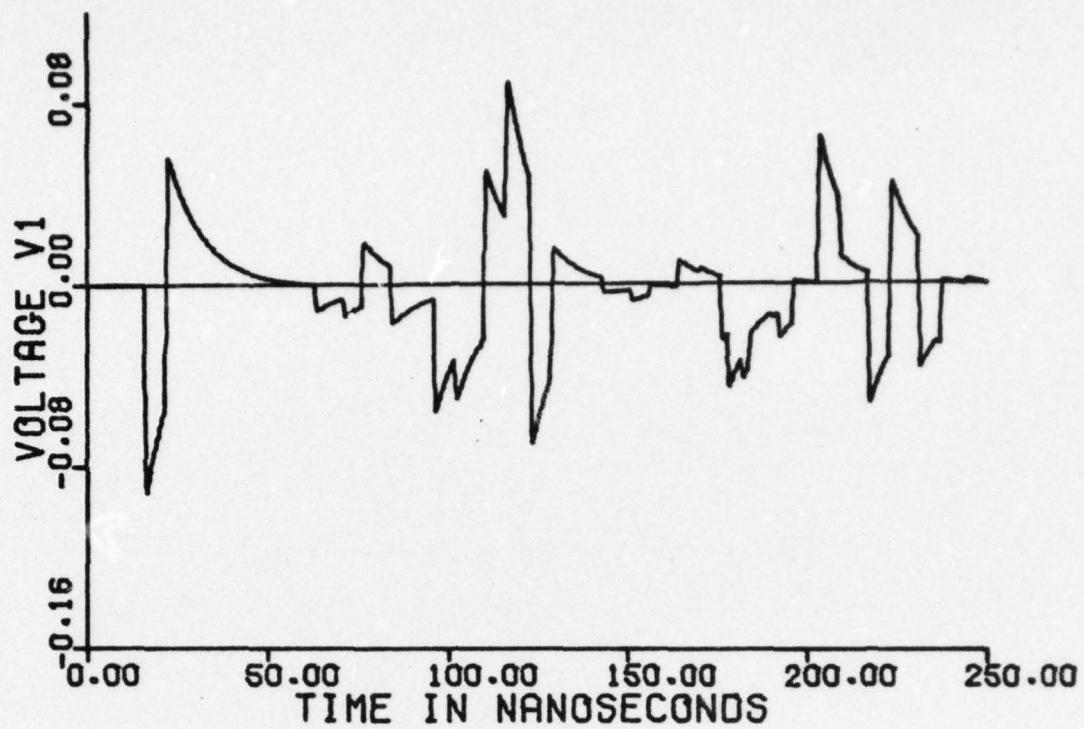
Fig. 16. Voltage waveforms on a 2-conductor line: large mismatch at both ends.

45
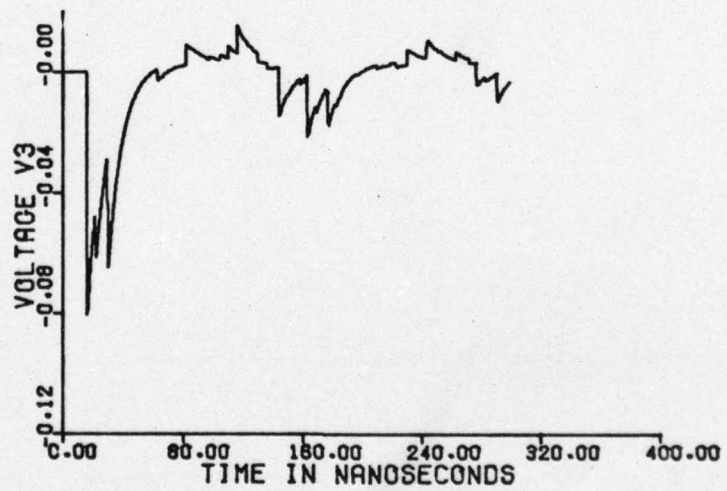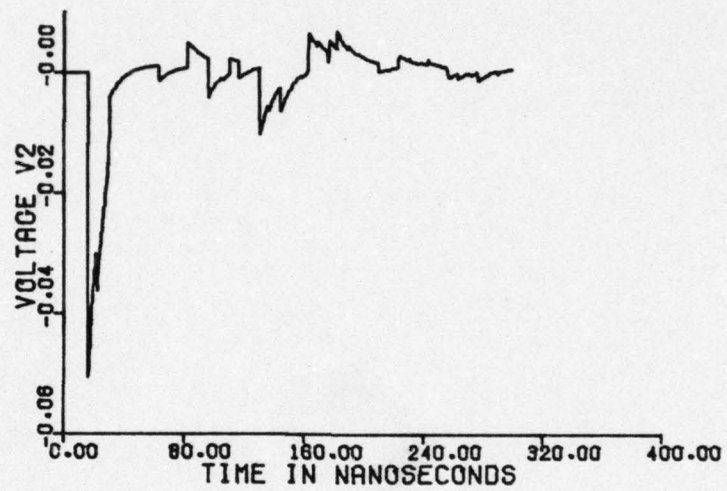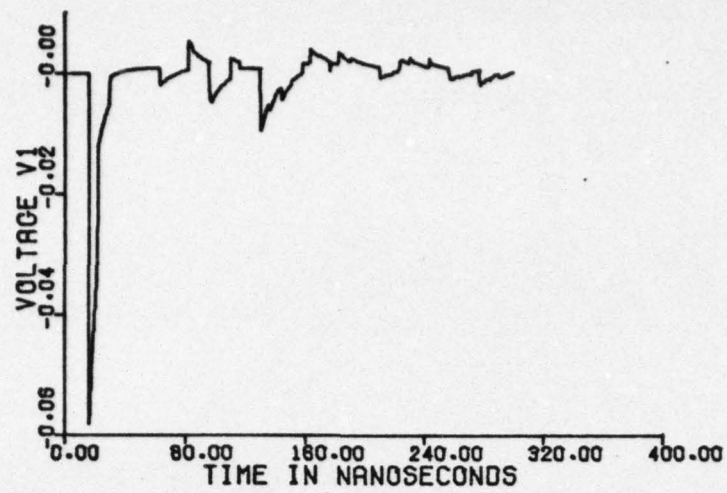
Fig. 17. Voltage waveforms on a 3-conductor line: moderate mismatch.

46

All the examples computed in this Section utilize a parallel-plate model of the MTL with inhomogeneous dielectric, because of the availability of simple formulas for the evaluation of induction coefficient matrix $\underline{K}$ and of the normalized modal functions $e_y(x_0,0)$ and $h_x(x_0,0)$. However, the same procedure of computing the voltage waveforms may be applied to any other set of data for $\underline{K}$, e_y and h_x which may be obtained by a numerical solution of the arbitrary shapes of conductors. Several numerical procedures for computation of the induction coefficient matrix $\underline{K}$ have appeared in the recent literature (see [16] to [18]). If these methods are supplemented by computation of $e_y(x_0,0)$ and $h_x(x_0,0)$ at the aperture center, the rest of the computations of voltage waveforms described in this Section is applicable to arbitrary conductor shapes and sizes.

16. W. T. Weeks, "Calculation of Coefficients of Capacitance of Multiconductor Transmission Lines in the Presence of Dielectric Interface," IEEE Transactions Microwave Theory Techn. Vol. MTT-18, pp. 35-43, Jan. 1970.

17. J. C. Clements, C. R. Paul, A. T. Adams, "Computation of the Capacitance Matrix for Systems of Dielectric-Coated Cylindrical Conductors," IEEE Transactions on Electromag. Compat. Vol. EMC-17, No. 4, pp. 238-248, Nov. 1975. Also see Correction in EMC-18 No. 2, pp. 88-89, May 1976.

18. C. R. Paul, "Computation of the Transmission Line Inductance and Capacitance Matrices from the Generalized Capacitance Matrix," IEEE Transactions Electromag. Compat., Vol. EMC-18. No. 4, pp. 175-183, Nov. 1976.

SECTION V

FIRST-ORDER EQUIVALENT CIRCUIT OF THE SMALL APERTURE

In Fig. 13 , a set of incident waves coming from the left is described by $|a_L>$. The aperture region is located between two planes denoted L and R. There is no incident wave coming from the right, $|b_R> = 0$. The waves $|a_L>$ excite the pair of dipoles c_{ey} and c_{mx}. The excitation field produced by the j-th incident mode is

$$H_{xsj}^{int} = a_{Lj} h_{xj}(x_0, 0) \tag{77}$$

$$E_{ysj}^{int} = a_{Lj} e_{yj}(x_0, 0) \tag{78}$$

This is an internal field, according to Fig. 2. From (8) and (9), the dipole moments produced by the j-th mode are

$$c_{mxj} = j\omega\mu\alpha_m h_{xj}(x_0, 0) a_{Lj} \tag{79}$$

$$c_{eyj} = -j\omega\varepsilon\alpha_e e_{yj}(x_0, 0) a_{Lj} \tag{80}$$

Summed over all the incident modes:

$$c_{mx} = j\omega\mu\alpha_m \sum_{j=1}^{N} h_{xj} a_{Lj} \quad , \tag{81}$$

$$c_{ey} = -j\omega\varepsilon\alpha_e \sum_{j=1}^{N} e_{yj} a_{Lj} \quad , \tag{82}$$

where argument $(x_0, 0)$ has been ommitted for brevity.

These dipoles produce the outgoing waves. Their i-th component is, according to (13) and (14):

48
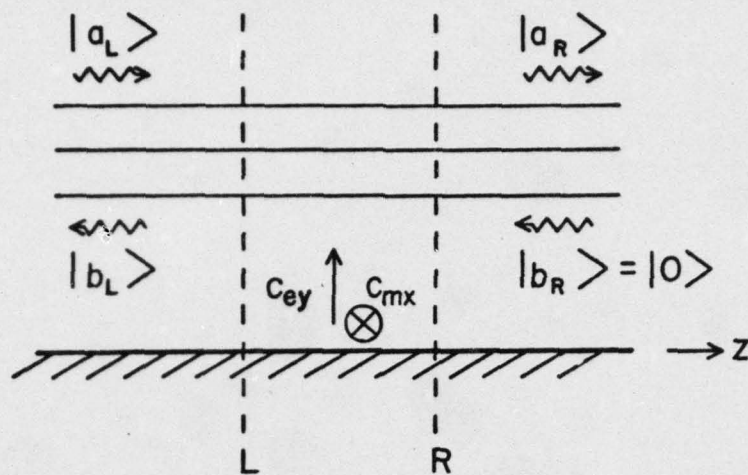
Fig. 18. Aperture junction with sources.
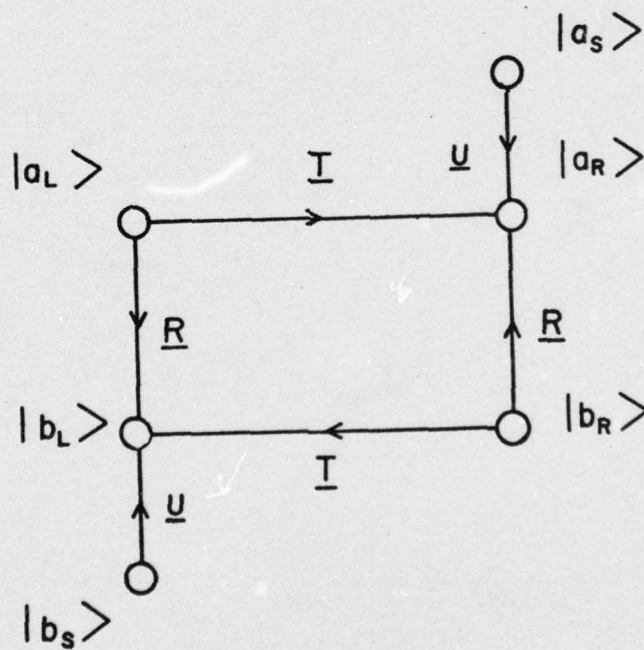
Fig. 19. Signal flow graph of the aperture junction with sources.

49

$$a_{Ri} = \frac{1}{2}[-c_{mx}h_{xi}(x_0,0) - c_{ey}e_{yi}(x_0,0)] + a_{Li} \quad , \tag{83}$$

$$b_{Li} = \frac{1}{2}[c_{mx}h_{xi}(x_0,0) - c_{ey}e_{yi}(x_0,0)] \quad . \tag{84}$$

In what follows, argument $(x_0,0)$ will be ommitted for brevity. In (83) the i-th mode outgoing wave at the right-hand plane in Fig. 18 consists of the (unattenuated) incident wave a_{Li} and the wave originated by the dipole. Using (81) and (82)

$$a_{Ri} = a_{Li} + \frac{1}{2}[-j\omega\mu\alpha_m h_{xi} \sum_{j=1}^{N} h_{xj}a_{Lj} + j\omega\epsilon\mu\alpha_e \sum_{j=1}^{N} e_{yj}a_{Lj}] \quad , \tag{85}$$

$$b_{Li} = \frac{1}{2}[j\omega\mu\alpha_m h_{xi} \sum_{j=1}^{N} h_{xj}a_{Lj} + j\omega\epsilon\mu\alpha_e \sum_{j=1}^{N} e_{yj}a_{Lj}] \quad . \tag{86}$$

This can be written as

$$|a_R> = (\underline{U} - j\,\underline{H} + j\,\underline{E})|a_L> \quad , \tag{87}$$

$$|b_L> = \qquad (j\,\underline{H} + j\,\underline{E})|a_L> \quad , \tag{88}$$

where the real, symmetric matrices $\underline{H}$ and $\underline{E}$ are defined by

$$[\underline{H}]_{ij} = \frac{1}{2}\omega\mu\alpha_m h_{xi}h_{xj} \quad , \tag{89}$$

$$[\underline{E}]_{ij} = \frac{1}{2}\omega\epsilon\alpha_e e_{yi}e_{yj} \quad . \tag{90}$$

Thus, the scattering matrix of the aperture junction, in partitioned form is

$$\begin{pmatrix} |b_L> \\ |a_R> \end{pmatrix} = \begin{pmatrix} \underline{R} & \underline{T} \\ \underline{T} & \underline{R} \end{pmatrix} \begin{pmatrix} |a_L> \\ |b_R> \end{pmatrix} \tag{91}$$

50

where

$$\underline{R} = j\,\underline{H} + j\,\underline{E} \ , \tag{92}$$

$$\underline{T} = \underline{U} - j\,\underline{H} + j\,\underline{E} \ . \tag{93}$$

The signal flow graph [16] is in Fig. 19. Also shown are sources $|a_S\rangle$ and $|b_S\rangle$ from the zeroth-order equivalent circuit. Figure 19 is a complete first-order equivalent circuit for scattering representation. The corresponding immittance representation will be derived next.

Fig. 20 shows a small parallel perturbation on a MTL. The perturbation is described by

$$|V_L\rangle = |V_R\rangle \ , \tag{94}$$

and

$$|I_2\rangle = \underline{Y}\,|V_L\rangle \ . \tag{95}$$

Kirchhoff current law requires

$$|I_L\rangle = |I_2\rangle + |I_R\rangle \ . \tag{96}$$

Change variables $|V\rangle$ and $|I\rangle$ into $|a\rangle$ and $|b\rangle$ according to (35) and (36). Then, (94) and (96) become:

$$\underline{M}_V(|a_L\rangle + |b_L\rangle) = \underline{M}_V(|a_R\rangle + |b_R\rangle) \ ,$$

$$\underline{M}_I(|a_L\rangle - |b_L\rangle) = \underline{Y}\,\underline{M}_V(|a_L\rangle + |b_L\rangle) + \underline{M}_I(|a_R\rangle - |b_R\rangle) \ .$$

Multiply the first equation from the left by $\underline{M}_V^{-1}$ and the second equation by $\underline{M}_I^{-1}$. Use (C-46) and (C-47) to obtain

51
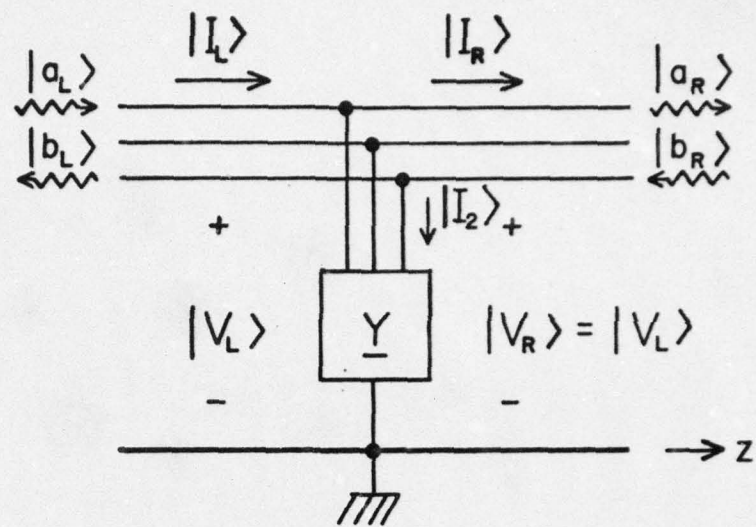
Fig. 20. Small parallel admittance perturbation on MTL.
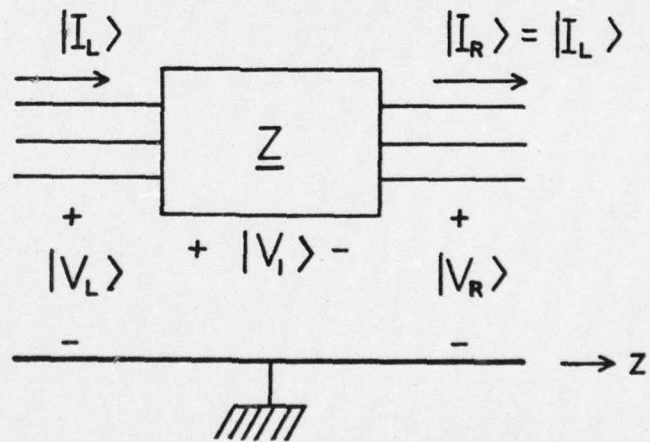
Fig. 21. Small series impedance perturbation on MTL.

52

$$|a_L> + |b_L> = |a_R> + |b_R> \quad ,$$

$$|a_L> - |b_L> = \underline{y}|a_L> + \underline{y}|b_L> + |a_R> - |b_R> \quad ,$$

where the normalized admittance matrix is introduced as

$$\underline{y} = \underline{M}_V^{\dagger} \, \underline{Y} \, \underline{M}_V \quad . \tag{97}$$

By subtracting the above two equations one obtains

$$|b_L> = -(2\underline{U}+\underline{y})^{-1}\underline{y}|a_L> + 2(2\underline{U}+\underline{y})^{-1}|b_R> \quad . \tag{98}$$

When the normalized admittance matrix is "small"[19] it is possible to use the first two terms from Neumann's series:

$$(2\underline{U} + \underline{y})^{-1} \simeq \tfrac{1}{2}(\underline{U} - \tfrac{1}{2}\underline{y}) \quad .$$

Retaining only the linear terms in $\underline{y}$, (98) is approximately given by

$$|b_L> \simeq -\tfrac{1}{2}\underline{y}\,|a_L> + (\underline{U} + \tfrac{1}{2}\underline{y})|b_R> \quad . \tag{99}$$

Next, consider a small series perturbation in Fig. 21, described by

$$|I_L> = |I_R> \quad , \tag{100}$$

$$|V_1> = \underline{Z}|I_L> \quad , \tag{101}$$

and

$$|V_L> = |V_1> + |V_R> \quad . \tag{102}$$

Expressed by scattering variables

$$\underline{M}_I(|a_L> - |b_L>) = \underline{M}_I(|a_R> - |b_R>) \quad ,$$

$$\underline{M}_V(|a_L> + |b_L>) = \underline{Z}\,\underline{M}_I(|a_L> - |b_L>) + \underline{M}_V(|a_R> + |b_R>) \quad .$$

53

Introduce the normalized impedance matrix

$$\underline{z} = \underline{M}_I^\dagger \, \underline{Z} \underline{M}_I \quad .$$

(103)

Using the same approximations as in (99) one obtains

$$|b_L> = \frac{1}{2} \underline{z} \, |a_L> + (\underline{U} - \frac{1}{2} \underline{z})|b_R> \quad .$$

(104)

Now add both series and parallel perturbations as in Fig. 22. The small reflections are simply added as follows

$$|b_L> = \frac{1}{2}(\underline{z} - \underline{y})|a_L> + (\underline{U} - \frac{1}{2} \underline{z} - \frac{1}{2} \underline{y})|b_R> \quad .$$

(105)

Invoking reciprocity and symmetry of the junction

$$\begin{pmatrix} |b_L> \\ |a_R> \end{pmatrix} = \begin{pmatrix} \frac{1}{2} \underline{z} - \frac{1}{2} \underline{y} & \underline{U} - \frac{1}{2} \underline{z} - \frac{1}{2} \underline{y} \\ \underline{U} - \frac{1}{2} \underline{z} - \frac{1}{2} \underline{y} & \frac{1}{2} \underline{z} - \frac{1}{2} \underline{y} \end{pmatrix} \begin{pmatrix} |a_L> \\ |b_R> \end{pmatrix} \quad .$$

(106)

Comparing (106) with (91), one concludes

$$j\underline{H} + j\underline{E} = \frac{1}{2}(\underline{z} - \underline{y}) \quad ,$$

$$-j\underline{H} + j\underline{E} = -\frac{1}{2}(\underline{z} + \underline{y}) \quad .$$

Solving for $\underline{z}$ and $\underline{y}$:

$$\underline{z} = j2\underline{H}$$

(107)

$$\underline{y} = -j2\underline{E}$$

(108)

54
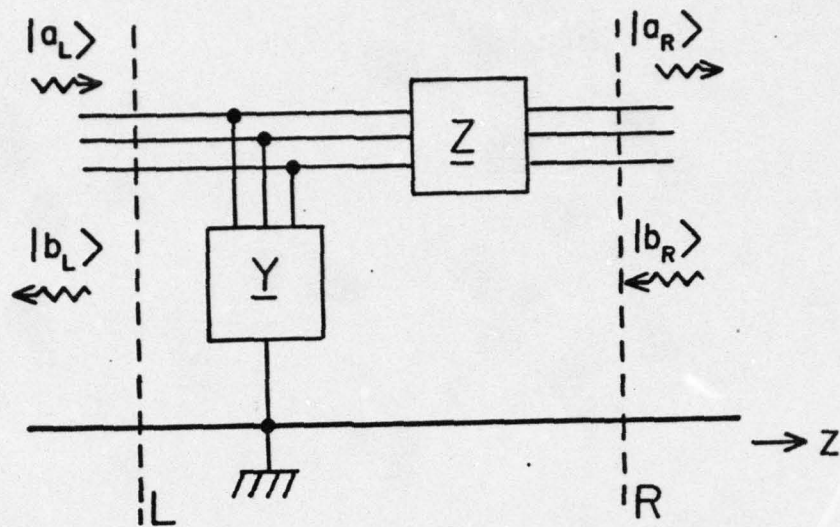
Fig. 22. MTL with both series and parallel perturbations.
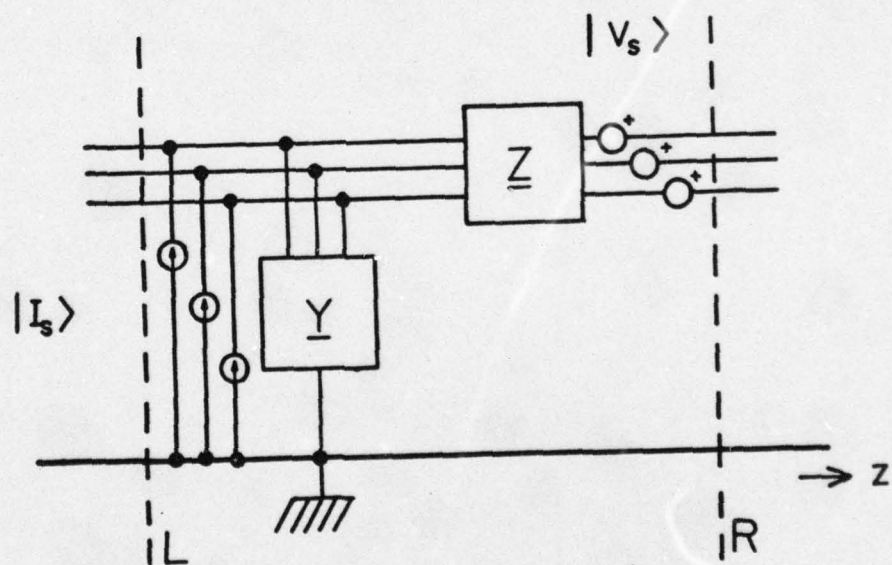
Fig. 23. Equivalent circuit of the aperture junction with sources.

55

From (89) and (90) it can be seen that all the elements of $\underline{H}$ and of $\underline{E}$ are real and proportional to frequency ω. Thus, the elements of $\underline{z}$ are represented by self and mutual normalized inductances

$$\underline{z} = j\omega\underline{\ell} \tag{109}$$

where:

$$\ell_{ij} = \mu\alpha_m h_{xi}(x_0,0)h_{xj}(x_0,0) \quad . \tag{110}$$

These inductances may be positive or negative, depending on the signs of h_{xi} and h_{xj}.

Analogously, the normalized admittance matrix consists of self- and coupling capacitances:

$$\underline{y} = -j \omega \underline{c} \tag{111}$$

where the elements of $\underline{c}$ are

$$c_{ij} = \varepsilon\alpha_e e_{yi}(x_0,0)e_{yj}(x_0,0) \quad . \tag{112}$$

The negative sign signifies that the capacitance is negative if the product $e_{yi}e_{yj}$ comes out to be positive. A note of explanation is necessary on the meaning of the coupling capacitance c_{ij} (when $i \neq j$). Such a circuit element does not exist in lumped-circuit theory. It signifies that the current at the port i is proportional to the rate of change of voltage at the port j, the constant of proportionality being defined as a coupling capacitance.

Finally, to obtain the actual impedance matrix $\underline{Z}$, (103) has to be denormalized as follows

$$\underline{Z} = \underline{M}_V \underline{z} \underline{M}_V^+ = j\omega \underline{M}_V \underline{\ell} \underline{M}_V^{\cdot\cdot} \quad . \tag{113}$$

56

Similarly, the denormalized admittance matrix is

$$\underline{Y} = \underline{M}_I \, \underline{y} \, \underline{M}_I^\dagger = -j\omega \, \underline{M}_I \, \underline{c} \, \underline{M}_I^\dagger \; . \tag{114}$$

Note that all the matrices on the right-hand sides of (113) and (114) are real, thus the equivalent circuit is easy to interpret.

When also the voltage- and current sources from (52) and (55) are included in the circuit, the complete first-order equivalent circuit takes the form shown in Fig. 23.

This representation is valid below the first resonant frequency of the aperture. For a circular aperture of radius a the lowest resonance appears at [20]

$$k\,a = 1.841$$

Thus, the representation is valid for frequencies

$$f \ll \frac{87.9 \cdot 10^6}{a}$$

For an aperture of radius a = 10 cm, the equivalent circuit is valid for f<< 880 MHz. The validity of the equivalent circuit could be further extended in the region close to the aperture resonance by the methods described in [21], which will not be pursued here.

The circuit diagram of matrix $\underline{Z}$ for a 3-conductor system is shown in Fig. 24a. The self inductances are denoted by L_{11}, L_{22}, and L_{23}, and

[20] R. E. Collin, Foundations for Microwave Engineering, New York: McGraw-Hill, 1966, p. 111.

[21] G. L. Matthaei, L. Young, E. M. T. Jones, Microwave Filters, Impedance-Matching Networks, and Coupling Structures, New York: McGraw-Hill, 1964, p. 242.

57
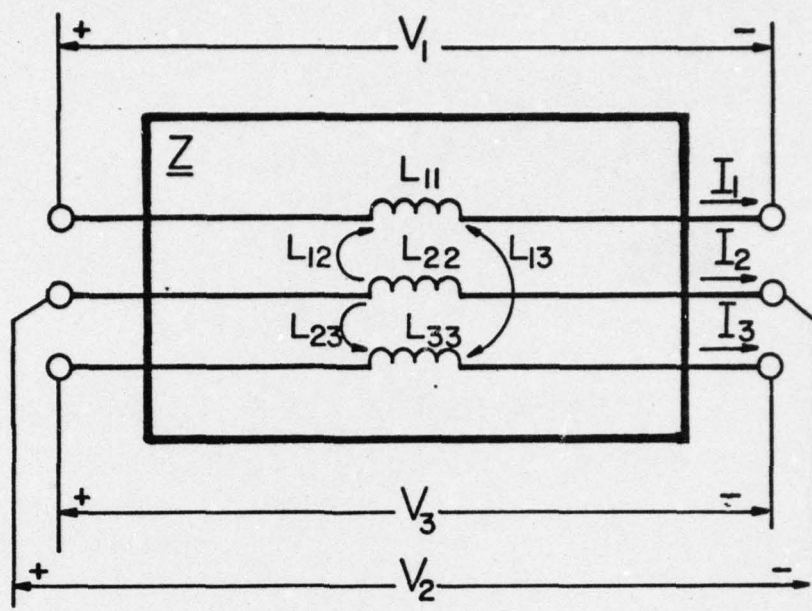
Fig. 24(a).   Impedance perturbation circuit.
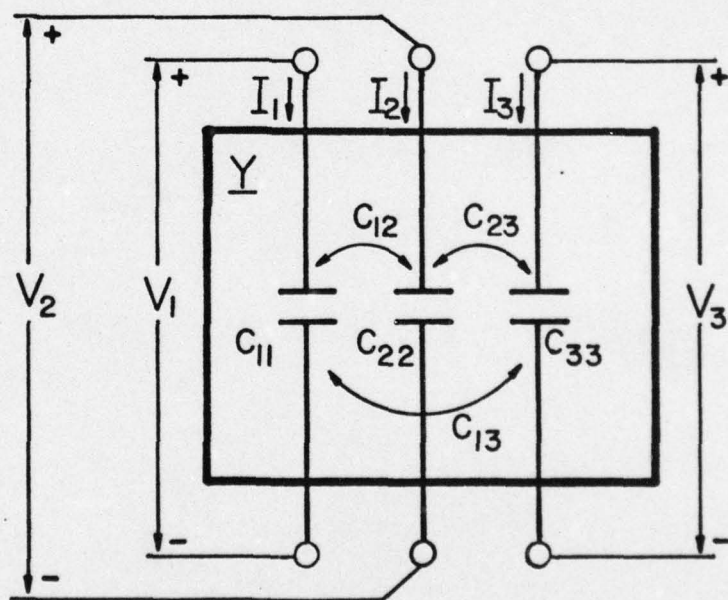
Fig. 24(b).   Admittance perturbation circuit.

58

the mutual inductances are denoted by L_{12}, L_{13}, and L_{23}. The voltage V_1 is then given by

$$V_1 = j\omega(L_{11}V_1 + L_{12}V_2 + L_{13}V_3)$$

Analogous expressions are valid for V_2 and V_3. This circuit is familiar from the conventional circuit theory and it does not require further comments. However, the circuit representation of the matrix $\underline{Y}$ is somewhat unconventional. The self capacitances are denoted by C_{11}, C_{22}, and C_{23}, while the coupling capacitances are denoted by C_{12}, C_{23}, and C_{13}. The current I_1 is given by

$$I_1 = -j\omega(C_{11}V_1 + C_{12}V_2 + C_{13}V_3)$$

and similar expressions may be written for I_2 and I_3. The negative sign signifies that all these capacitances are negative, as compared with the conventional capacitances. From the point of view of energy balance, the negative capacitance is an active element, capable of supplying the energy to the rest of the network. This may be considered as an inconsistency of the equivalent circuit of the aperture, but it will be shown that these negative capacitances are extremely small. Furthermore, the negative capacitance can be thought of as the element which represents missing capacitances on a uniform transmission line which is perturbed by the aperture.

The values of the elements in the equivalent circuit from Fig. 24 will be next computed for a 2-conductor parallel-plate MTL described in Section IV. For a circular aperture of diameter $d = 2$ cm the electric modal functions are computed from (68)

59

$$e_{y1}(x_0,0) = -\frac{-6.1358}{1.10^{-2}} = 613.58$$

$$e_{y2}(x_0,0) = \frac{2.3690}{1.10^{-2}} = -236.90$$

The values of the magnetic modal functions at the position of the aperture are found from (69)

$$h_{x1}(x_0,0) = -0.81491 \qquad h_{x2}(x_0,0) = 0.42212$$

From (110) and (10) the normalized inductances are obtained as

$$\ell_{11} = 1.1127 \cdot 10^{-12}, \; \ell_{22} = 2.9855 \cdot 10^{-13}, \; \ell_{12} = -5.7636 \cdot 10^{-13}$$

For the frequency 1 GHz, the normalized reactances are

$$\omega\ell_{11} = 6.9913 \cdot 10^{-3}, \; \omega\ell_{22} = 1.8758 \cdot 10^{-3}, \; \omega\ell_{12} = -3.6214 \cdot 10^{-3}$$

Similarly the normalized susceptances in parallel with the MTL are found from (112) and (10)

$$\omega c_{11} = 1.3963 \cdot 10^{-2}, \; \omega c_{12} = -5.3909 \cdot 10^{-3}, \; \omega c_{22} = 2.0814 \cdot 10^{-3}$$

Therefore, even at the highest frequency of interest for EMP calculations, the normalized reactances and susceptances are small numbers. Thus it is expected that they do not cause appreciable reflections when a wave is propagating along the MTL.

60

Consider that an incident wave $|a_L\rangle$ is coming from the left toward the equivalent circuit of the aperture in Fig. 22. Assuming that the right-hand side of the equivalent circuit is terminated in an infinitely long MTL, it is of interest to find $|b_L\rangle$ in terms of $|a_L\rangle$. Since for an infinitely long MTL the vector $|b_R\rangle$ vanishes, the equation (106) gives

$$|b_L\rangle = \tfrac{1}{2}(\underline{z}-\underline{y})\ |a_L\rangle$$

Therefore, the reflections due to the presence of the equivalent circuit on a uniform MTL are determined by reflection matrix $\underline{\Gamma}$

$$\underline{\Gamma} = \tfrac{1}{2}(\underline{z}-\underline{y}) = \frac{j}{2}\begin{pmatrix} \omega\ell_{11} + \omega c_{11} & \omega\ell_{12} + \omega c_{12} \\ \omega\ell_{12} + \omega c_{12} & \omega\ell_{22} + \omega c_{22} \end{pmatrix}$$

For the case under consideration, the reflection matrix is

$$\underline{\Gamma} = j\begin{pmatrix} 1.0478 \cdot 10^{-2} & -9.0123 \cdot 10^{-3} \\ -9.0123 \cdot 10^{-3} & 3.9572 \cdot 10^{-3} \end{pmatrix}$$

It can be seen that the reflected amplitude of the first mode is only 1.05% of the incident amplitude for the same mode. The other reflections are even smaller than 1%. At lower frequencies all coefficients of the reflection matrix are proportionally reduced. This fact justifies the procedure from Section IV of computing the voltage waveforms by entirely neglecting the presence of inductances and capacitances in the equivalent circuit.

61

It is of interest to investigate the equivalent circuit of the aperture on a single-conductor transmission line. The geometry of the problem is such as specified by Fig. 3: a round wire of radius r is placed in parallel with the ground plane, so that the center of the wire is elevated above the ground plane for distance d. The circular aperture of radius a is located at $x = x_0$, $y = 0$, $z = 0$.

When $N = 1$, it follows from formulas in the Appendix C that matrices $\underline{M}_I$ and $\underline{M}_V$ reduce to simple scalars:

$$M_I = \sqrt[4]{\frac{C'}{L'}} \quad , \quad M_V = \sqrt[4]{\frac{L'}{C'}}$$

where C' and L' are the distributed capacitance and inductance of the single-wire transmission line. When the subscripts i and j are omitted, the normalized inductance from (110) becomes

$$\ell = \mu \alpha_m h_x^2(x_0, 0)$$

and the normalized negative capacitance from (112) becomes

$$c = \varepsilon \alpha_e e_y^2(x_0, 0)$$

The normalized modal functions h_x and e_y for the TEM mode of a single wire above the ground plane have been derived in [13] as follows

[13] D. Kajfez, "Excitation of a Terminated TEM Transmission Line Through a Small Aperture," Interaction Note 215, July 1974.

$$h_x = \frac{h}{\pi\sqrt{Z_0}\,(x_0^2 + h^2)}$$

$$e_y = -\frac{\eta h}{\pi\sqrt{Z_0}\,(x_0^2 + h^2)}$$

where h denotes the reduced height of the wire:

$$h = \sqrt{d^2 - r^2}$$

In order to obtain the actual values of the equivalent inductance and capacitance, the values are to be denormalized according to (113) and (114):

$$Z = j\omega L = j\omega M_V^2 z$$

$$Y = -j\omega C = -j\omega M_I^2 y$$

The values of L and C are, therefore

$$L = \mu\alpha_e \frac{h^2}{\pi^2(x_0^2 + h^2)^2} \tag{115}$$

$$C = \varepsilon\alpha_e \frac{\eta^2 h^2}{Z_0^2(x_0^2 + h^2)^2} \tag{116}$$

where

63

$$Z_0 = 60 \cos h^{-1} \left(\frac{d}{r}\right)$$

The similar formulas have been derived by Lee and Yang [22]. Their formulas (20.a) reduce to (115) and (116) in the case of a thin wire ($r \ll d$, $h \approx d$). For thick wires it is believed that (115) and (116) are more accurate, because the exact TEM modal functions have been used in the derivation.

[22] K. S. H. Lee, F. C. Yang, "A Wire Passing by a Circular Aperture in an Infinite Ground Plane," Dikewood Corporation, February 1977.

64

SECTION VI

INTERACTION BETWEEN AN APERTURE AND A SINGLE WIRE

In this section we examine the validity of the assumption that the dipole moments in the aperture can be determined from the plane wave exciting the aperture ignoring the presence of the MTL. This assumption has been used to derive the model for aperture coupling to the lines in the preceding sections. For simplicity, we treat only a single wire line over a ground plane. It is possible, in principle, to extend the analysis to treat a MTL backscattering into the aperture by superimposing the backscatter from the individual lines, accounting for the mutual interaction of the various conductors. The general situation is too difficult to treat here, however. As an additional simplification, we assume the conducting line is bare.

Referring to Figs. 2 and 3, in addition to the plane wave fields $\vec{E}_s^{ext}$ and $\vec{H}_s^{ext}$ exciting the aperture, we must now consider aperture fields $\vec{E}_s^{int}$ and $\vec{H}_s^{int}$ which are the fields reradiated from the transmission line. These fields are linearly related to the dipole moments in the aperture and we show in the following that they can be written as

$$H_{xs}^{int} = t_m c_{mx} \tag{117}$$

$$E_{ys}^{int} = t_e c_{ey} \tag{118}$$

where $t_m(t_e)$ is the $x(y)$ component of the short circuit magnetic (electric) field at the aperture reradiated from the line due to the appropriately directed unit magnetic (electric) current moment in the aperture. In the absence of any other sources in the interior region, Eqs. (8) and (9) become with (117) and (118),

$$c_{mx} = \frac{-j\omega\mu\alpha_m \, H_{xs}^{ext}}{(1-j\omega\mu\alpha_m t_m)} \tag{119}$$

65

$$c_{ey} = \frac{j\omega\varepsilon\alpha_e \; E_{ys}^{ext}}{1+j\omega\varepsilon\alpha_e t_e}$$

It is easily seen that the coupling from the line to the apert
be neglected if it can be shown that

$$\omega\mu \; \alpha_m t_m \; \ll 1,$$

$$\omega\varepsilon \; \alpha_e t_e \; \ll 1.$$

In the following we determine t_e and t_m, the aperture fields s
the wires due to unit electric and magnetic dipoles in the ape

Beginning with the dipole sources $\vec{c}_e$ and $\vec{c}_m$ (see, e. g.,
and a single wire in the internal region, the ground plane is
that the dipole and wires are imaged as in Fig. 25. Note that
doubles the current moments of the dipole sources. Transverse
nates $\vec{\rho} = (\rho,\phi)$ and $\vec{\rho}_i = (\rho_i,\phi_i)$ measured from the wire axis a
wire axis, respectively, are also introduced in Fig. 25. The
establishes the location of the aperture with respect to the w

The fields due to the dipoles in the absence of the condu
determined from free space magnetic and electric vector potent

$$A_{ey} = \frac{\mu \; c_{ey} \; e^{-jk|\vec{r}-x_0\vec{a}_x|}}{2\pi|\vec{r} - \vec{\rho}_0|}$$

$$F_{mx} = \frac{\varepsilon \; c_{mx} \; e^{-jk|\vec{r}-x_0\vec{a}_x|}}{2\pi \; |\vec{r}-\vec{\rho}_0|}$$

respectively, where

$$\vec{r} = x\vec{a}_x + y\vec{a}_y + z\vec{a}_z$$

66
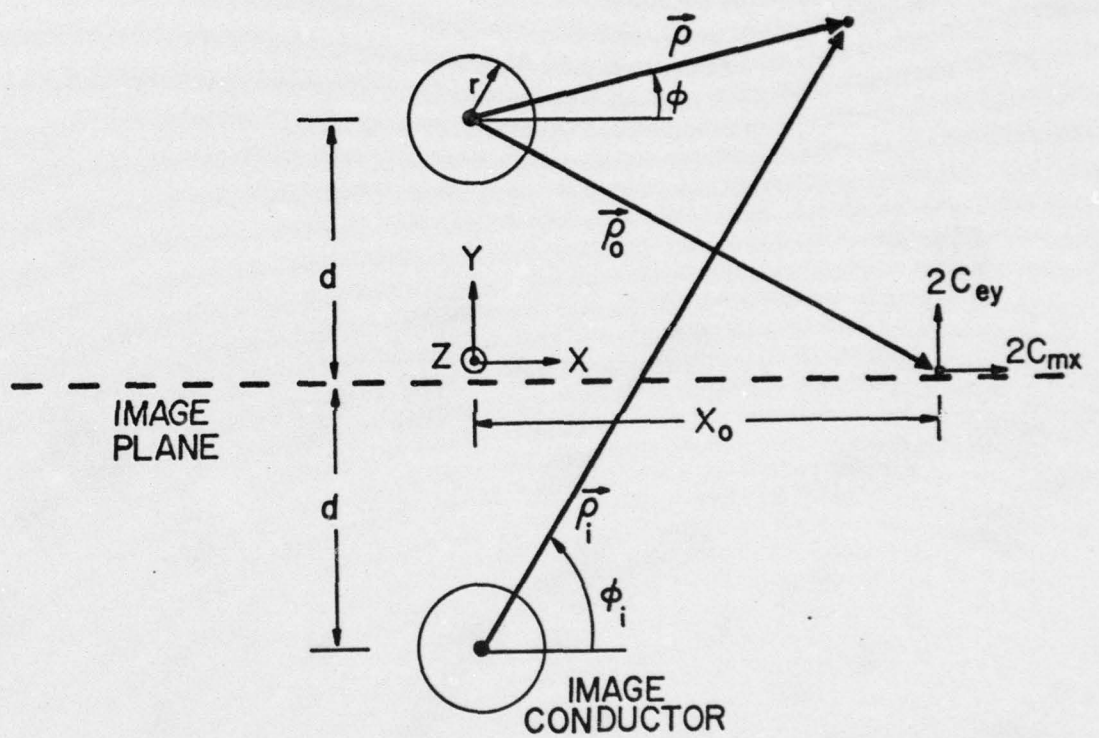
Fig. 25. Geometry of wire over a ground screen with equivalent dipole moment representing an aperture.

The currents on the wire and its image are assumed to be entirely z-di
but in opposite directions. Hence they determine a magnetic vector po
A_z which can in turn be used to determine all field quantities. Bound
conditions require the z-component of electric field to vanish at the
of the upper wire in Fig. 25; however, it must vanish everywhere inter
the wire as well and if we restrict our observation to the wire axis,
only the total or average current $I(z)$ from the upper wire contributes
the vector potential there. This choice of the observation point thus
out of the problem any circumferential variation in the current on the
wire; the circumferentially varying currents on the image wire do, how
contribute to the vector potential at $\vec{\rho} = \vec{0}$. But if the wire is thin a
sufficiently far from the ground plane in terms of the wire radius, i.

$$kr \ll 1,$$

$$r \ll d,$$

then the image wire may essentially be replaced by a line source along
image wire axis which carries a current $I(z)$ directed opposite to that
upper wire. In other words, under conditions (125) and (126), if the
wire is replaced by multipole line sources located at $\vec{\rho}_i = \vec{0}$, the contr
of the dipole, quadrupole and higher order multipole terms can be neg
compared to that of the monopole current filament $I(z)$. Thus the magn
vector potential along the upper wire axis due to the wire and image c
is approximately

$$A_z \Big|_{\vec{\rho}=\vec{0}} = \frac{\mu}{4\pi} \int_{-\infty}^{\infty} I(z') \left[\frac{e^{-jk\sqrt{r^2+(z-z')^2}}}{\sqrt{r^2+(z-z')^2}} - \frac{e^{-jk\sqrt{4d^2+(}}}{\sqrt{4d^2+(z-}} \right.$$

Along the axis of the upper wire E_z must vanish, that is

68

$$\vec{a}_z \cdot \left[\frac{1}{j\omega\mu\epsilon} (k^2 + \nabla\nabla\cdot)(\vec{a}_y A_{ey} + \vec{a}_z A_z) - \frac{1}{\epsilon}\nabla\times(\vec{a}_x F_{mx}) \right]_{\vec{\rho} = \vec{0}} = 0 \qquad (128)$$

or writing out the desired components,

$$\frac{1}{j\omega\mu\epsilon} \left(\frac{\partial^2}{\partial z^2} + k^2 \right) A_z \bigg|_{\vec{\rho} = \vec{0}} = - \frac{1}{j\omega\mu\epsilon} \frac{\partial^2 A_{ey}}{\partial z \partial y} \bigg|_{\vec{\rho} = \vec{0}} - \frac{1}{\epsilon} \frac{\partial F_{mx}}{\partial y} \bigg|_{\vec{\rho} = \vec{0}} \quad .$$

$$(129)$$

Eq. (129) with (123), (124), and (127), is an integro-differential equation for the current $I(z)$ induced on the transmission line by current moments c_{ey} and c_{mx} in the aperture. In order to determine the current we introduce the Fourier transform pair

$$\psi(z) = \frac{1}{\sqrt{2\pi}} \int_{-\infty}^{\infty} \tilde{\psi}(k_z) e^{-jk_z z} \, dk_z \qquad (130)$$

$$\tilde{\psi}(k_z) = \frac{1}{\sqrt{2\pi}} \int_{-\infty}^{\infty} \psi(z) \, e^{+jk_z z} \, dz \qquad (131)$$

where the wavy line indicates Fourier transformed quantities. Writing the current in (127) as an inverse transform and making use of the identity

$$\frac{e^{-jk\sqrt{\rho^2 + (z-z')^2}}}{\sqrt{\rho^2 + (z-z')^2}} = \frac{1}{2j} \int_{-\infty}^{\infty} H_0^{(2)}(k_\rho \rho) e^{-jk_z(z-z')} \, dk_z \qquad (132)$$

69

where $k_\rho = \sqrt{k^2 - k_z^2}$, $\mathrm{Re}\, k_e > 0$, $\mathrm{Im}\, k\rho < 0$, (127) becomes

$$A_z \Big|_{\vec{\rho}=\vec{0}} = \frac{\mu}{4j(2\pi)^{3/2}} \int_{-\infty}^{\infty} \int_{-\infty}^{\infty} \int_{-\infty}^{\infty} \tilde{I}(k_z)[H_0^{(2)}(k_\rho' r) - H_0^{(2)}(2k_\rho' d)]\, e^{-j(k_z - k_z')z'}$$

(133)

$$\times\, e^{-jk_z' z}\, dk_z\, dk_z'\, dz' \quad .$$

Noting that

$$\int_{-\infty}^{\infty} e^{-j(k_z - k_z')z'}\, dz' = 2\pi\delta(k_z - k_z')$$

(134)

(133) simplifies to the transform representation

$$A_z \Big|_{\vec{\rho}=\vec{0}} = \frac{\mu}{4j\sqrt{2\pi}} \int_{-\infty}^{\infty} \tilde{I}(k_z)[H_0^{(2)}(k_\rho r) - H_0^{(2)}(2k_\rho d)]e^{-jk_z z}\, dk_z$$

(135)

Similarly, we express the right hand side of (129) in transform representation:

$$\frac{\partial^2 A_{ey}}{\partial z \partial y} \Big|_{\vec{\rho}=\vec{0}} = \frac{\partial^2}{\partial z \partial y} \left[\frac{\mu\, c_{ey}\, e^{-jk|\vec{r}-\vec{\rho}_0|}}{2\pi\, |\vec{r}-\vec{\rho}_0|} \right]_{\vec{\rho}=\vec{0}}$$

$$= \frac{\mu\, c_{ey}}{4j\pi} \frac{\partial^2}{\partial z \partial y} \int_{-\infty}^{\infty} H_0^{(2)}(k_\rho |\vec{\rho}-\vec{\rho}_0|)e^{-jk_z z}\, dk_z \Big|_{\vec{\rho}=\vec{0}}$$

$$= \frac{\mu\, c_{ey}\, d}{4\pi\sqrt{x_0^2+d^2}} \int_{-\infty}^{\infty} k_z k_\rho H_1^{(2)}(k_\rho \sqrt{x_0^2+d^2})e^{-jk_z z}\, dk_z$$

70

(136)

and

$$\frac{\partial F_{mx}}{\partial y}\Bigg|_{\vec{\rho}=\vec{0}} = \frac{\partial}{\partial y}\left[\frac{\varepsilon\, c_{mx}\, e^{-jk|\vec{r}-\vec{\rho}_0|}}{2\pi|\vec{r}-\vec{\rho}_0|}\right]_{\vec{\rho}=\vec{0}}$$

$$= \frac{\varepsilon\, c_{mx}}{4j\pi}\,\frac{\partial}{\partial y}\int_{-\infty}^{\infty} H_0^{(2)}(k_\rho|\vec{\rho}-\vec{\rho}_0|)e^{-jk_z z}\, dk_z\Bigg|_{\vec{\rho}=\vec{0}}$$

$$= \frac{j\varepsilon\, c_{mx}\, d}{4\pi\sqrt{x_0^2+d^2}}\int_{-\infty}^{\infty} k_\rho H_1^{(2)}\left(k_\rho\sqrt{x_0^2+d^2}\right)e^{-jk_z z}dk_z$$

$$\tag{137}$$

Substituting (135), (136) and (137) into (129) and taking the Fourier inverse of the resulting equation yields finally the transform of the current,

$$\tilde{I}(k_z) = \frac{j\sqrt{2/\pi}\; d}{k\rho\sqrt{x_0^2+d^2}}\,\frac{H_1^{(2)}\left(k_\rho\sqrt{x_0^2+d^2}\right)}{H_0^{(2)}(k_\rho r)-H_0^{(2)}(2k_\rho d)}\left(\frac{k c_{mx}}{\eta}-k_z c_{ey}\right)$$

$$= \tilde{I}_m(k_z) + \tilde{I}_e(k_z)\tag{138}$$

where $\tilde{I}_m(k_z)$ and $\tilde{I}_e(k_z)$ are identified as the partial currents arising from the corresponding source terms c_{mx} and c_{ey}, respectively. Note that $\tilde{I}_m$ is an even function whereas $\tilde{I}_e$ is an odd function of the variable k_z.

71

The total line current can be obtained by taking the Fourier inverse of (138). Our interest, however, is in obtaining the fields that the wire and image currents scatter into the aperture and these can be found most easily from the vector potential expressed in terms of the current transform. The vector potential at an arbitrary point is obtained by again treating both the line and its image as current filaments at $\vec{\rho}=\vec{0}$ and $\vec{\rho}_i=\vec{0}$, respectively:

$$
A_z = \frac{\mu}{4\pi} \int_{-\infty}^{\infty} I(z') \left[\frac{e^{-jk|\vec{\rho}+\vec{a}_z(z-z')|}}{|\vec{\rho}+\vec{a}_z(z-z')|} - \frac{e^{-jk|\vec{\rho}_i+\vec{a}_z(z-z')|}}{|\vec{\rho}_i+\vec{a}_z(z-z')|} \right] dz'
$$

$$
= \frac{\mu}{4j\sqrt{2\pi}} \int_{-\infty}^{\infty} \tilde{I}(k_z) [H_0^{(2)}(k_\rho|\vec{\rho}|) - H_0^{(2)}(k_\rho|\vec{\rho}_i|)] e^{-jk_z z} dk_z \tag{139}
$$

where again (132) and (134) have been used. The desired field quantities in the aperture are

$$
E_{ys}^{int} = \frac{1}{j\omega\mu\epsilon} \frac{\partial^2 A_z}{\partial y \partial z} \Bigg|_{\substack{x=x_0, \\ y=z=0}}
$$

$$
= \frac{jd}{2\sqrt{2\pi}\omega\epsilon\sqrt{x_0^2 + d^2}} \int_{-\infty}^{\infty} \tilde{I}(k_z) k_z k_\rho H_1^{(2)} \left[k_\rho\sqrt{x_0^2 + d^2} \right] dk_z
$$

$$
= \frac{jd}{2\sqrt{2\pi}\omega\epsilon\sqrt{x_0^2 + d^2}} \int_{-\infty}^{\infty} \tilde{I}_e(k_z) k_z k_\rho H_1^{(2)} \left[k_\rho\sqrt{x_0^2 + d^2} \right] dk_z
$$

$$
= \frac{c_{ey}\eta}{2\pi k} \left(\frac{d^2}{x_0^2 + d^2} \right) \int_{-\infty}^{\infty} \frac{k_z^2 \left[H_1^{(2)} \left[k_\rho\sqrt{x_0^2+d^2} \right] \right]^2 dk}{H_0^{(2)}(k_\rho r) - H_0^{(2)}(2k_\rho d)} = t_e c_{ey} \tag{140}
$$

72

and

$$H_{xs}^{int} = \frac{1}{\mu} \left. \frac{\partial A_z}{\partial y} \right|_{\substack{x=x_0 \\ y=z=0}}$$

$$= \frac{d}{2j\sqrt{2\pi}\,\sqrt{x_0^2+d^2}} \int_{-\infty}^{\infty} \tilde{I}(k_z) k_\rho H_1^{(2)}\left[k_\rho\sqrt{x_0^2+d^2}\right] dk_z$$

$$= \frac{d}{2j\sqrt{2\pi}\,\sqrt{x_0^2+d^2}} \int_{-\infty}^{\infty} \tilde{I}_m(k_z) k_\rho H_1^{(2)}\left[k_\rho\sqrt{x_0^2+d^2}\right] dk_z$$

$$= \frac{c_{mx}k}{2\pi\eta}\left(\frac{d^2}{x_0^2+d^2}\right) \int_{-\infty}^{\infty} \frac{\left[H_1^{(2)}\left[k_\rho\sqrt{x_0^2+d^2}\right]\right]^2 dk_z}{H_0^{(2)}(k_\rho r) - H_0^{(2)}(2k_\rho d)}$$

$$= t_m c_{mx} \tag{141}$$

where we have used the even and odd properties of $\tilde{I}_m$ and $\tilde{I}_e$ to appropriately simplify the integrals (140) and (141).

Returning to the examination of conditions (121) and (122), we first note that the four parameters k, x_0, d, and r in the integrals can be reduced to three parameters if all distances are measured in terms of wavelengths. Thus, we examine

$$\omega\mu\alpha_m t_m = \frac{(SF)_m (k\ell)^3 (kd)^2 \tilde{t}_m (kx_0,\ kd,\ kr)}{(kx_0)^2 + (kd)^2} \tag{142}$$

73

$$\omega \varepsilon \alpha_e t_e = \frac{(SF)_e (k\ell)^3 (kd)^2 \tilde{t}_e (kx_0, \ kd, \ kr)}{(kx_0)^2 + (kd)^2} \tag{143}$$

where we have introduced the aperture shape factors defined as

$$(SF)_m = \frac{\alpha_m}{\ell^3} \tag{144}$$

$$(SF)_e = \frac{\alpha_e}{\ell^3} \tag{145}$$

where α_m and α_e are the aperture polarizabilities and ℓ is the largest aperture dimension. The shape factors have been determined for a variety of aperture shapes by numerical and experimental means [11-12] and are typically somewhat smaller than unity. The normalized functions $\tilde{t}_m$ and $\tilde{t}_e$ are defined as

$$\tilde{t}_m (kx_0, \ kd, \ kr) = \frac{\eta (x_0^2 + d^2)}{k^2 d^2} \ t_m$$

$$= \frac{1}{2\pi} \int_{-\infty}^{\infty} \frac{H_1^{(2)} \left[\sqrt{(1-\alpha^2)[(kx_0)^2 + (kd)^2]} \right]^2 d\alpha}{H_0^{(2)} \left[\sqrt{1-\alpha^2} \ kr \right] - H_0^{(2)} \left[\sqrt{1-\alpha^2} \ kd \right]} \tag{146}$$

[11] S.B. Cohn, "Determination of Aperture Parameters by Electrolytic-Tank Measurements", Proc. I.R.E., Vol. 39, pp. 1416-1421, November 1951.

[12] S.B. Cohn, "The Electric Polarizability of Apertures of Arbitrary Shape," Proc. I.R.E., Vol. 40, pp. 1069-1071, September 1952.

$$\tilde{t}_e(kx_0, kd, kr) = \frac{x_0^2 + d^2}{k^2 d^2 \eta} \, t_e$$

$$= \frac{1}{2\pi} \int_{-\infty}^{\infty} \frac{\alpha^2 \left[H_1^{(2)} \left[\sqrt{(1-\alpha^2)\left[(kx_0)^2 + (kd)^2\right]} \right] \right]^2 \, d\alpha}{H_0^{(2)}\left(\sqrt{1-\alpha^2}\, kr\right) - H_0^{(2)}\left(\sqrt{1-\alpha^2}\, kd\right)}$$

(147)

Since our assumption that the aperture may be replaced by current moments $\vec{c}_e$ and $\vec{c}_m$ requires that the aperture be small, say less than a tenth of a wavelength, then $(k\ell)^3 < .25$ and since

$$(SF)_{e,m} < 1 \tag{148}$$

$$\frac{kd^2}{(kx_0)^2 + (kd)^2} \leq 1 \tag{149}$$

we need only demonstrate that

$$|\tilde{t}_m| \ll 1, \tag{150}$$

$$|\tilde{t}_e| \ll 1, \tag{151}$$

to show that the wire does not sufficiently excite the aperture that its effect needs to be accounted for in computing the aperture dipole moments.

The integrals (146) and (147) are numerically evaluated by (1) noting the symmetry of the integrals about $\alpha = 0$; (2) integrating numerically using Gauss-Legendre integration on the interval $0 \leq \alpha \leq 2$, with a singularity of the form $1/(\alpha-1)$ removed; (3) adding a contribution from the branch point at $\alpha = 1$; and (4) integrating numerically on the interval $2 \leq \alpha \leq \infty$ using

75

Gauss-Laguerre integration which assumes an exponentially decaying integrand. The appropriate rate of exponential decay in the integrand can be determined from the large argument approximations to the Hankel functions appearing in (146) and (147).

From the numerical calculations, Figs. 26-33 show that over a wide range of parameters kx_0, kd, and kr, Eqs. (150) and (151) are indeed satisfied. However, when the wire is directly above and close to the aperture ($kx_0 = 0$ and kd small), (150) and (151) are not satisfied. If the wire is close to the aperture, however, the aperture must be small in order for the dipole moment representation to remain valid. Calculations by Lee and Yang [22] indicate that the dipole moment representation of a circular aperture (without considering backscattering from the wire) is accurate to about 10% only if $2k\ell \leq kd$ and it seems reasonable that this upper bound on the maximum aperture dimension would hold for other aperture shapes as well. Using this as an upper bound on $k\ell$ and noting that $\tilde{t}_m$ and $\tilde{t}_e$ are largest when $kx_0 \neq 0$, it is sufficient to show that

$$\left(\frac{kd}{2}\right)^3 \left|\tilde{t}_m(0,kd,kr)\right| \ll 1 \qquad (152)$$

$$\left(\frac{kd}{2}\right)^3 \left|\tilde{t}_m(0,kd,kr)\right| \ll 1 \qquad (153)$$

in order to exclude consideration of wire-to-aperture coupling. These quantities are plotted in Figs. 34-35. The figures show that the effect of the wire on the aperture dipole moment is negligible whenever the representation of the aperture by dipole moments is valid.

This completes the task set for this section, but it is interesting and instructive to return to the current transform (138) and use it to find the current on the line by inverse transforming:

---

[22] K. S. H. Lee, F. C. Yang, "A Wire Passing by a Circular Aperture in an Infinite Ground Plane," Dikewood Corporation, February, 1977.

Fig. 26. Magnitude of t_m for a wire of radius kr = 0.1.

KR= 0.1000

KD= 0.2000
KD= 0.3000
KD= 0.4000
KD= 0.5000
KD= 0.6000
KD= 0.7000
KD= 0.8000
KD= 0.9000
KD= 1.0000

$|t_e|$

KX

Fig. 27. Magnitude of t_e for a wire of radius kr = 0.1.

78
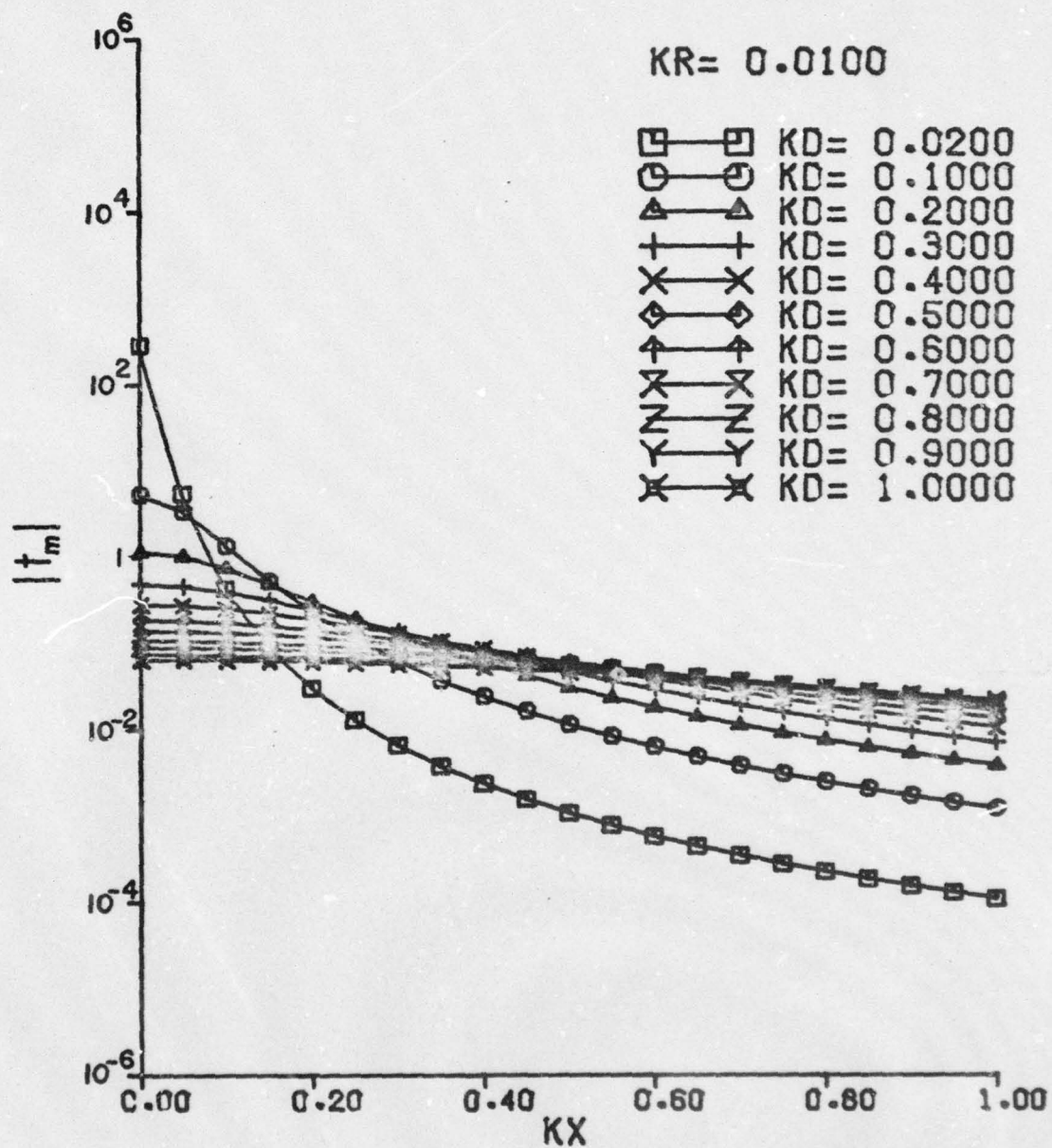
Fig. 28. Magnitude of t_m for a wire of radius $kr = 0.01$.

Fig. 29. Magnitude of t_e for a wire of radius kr

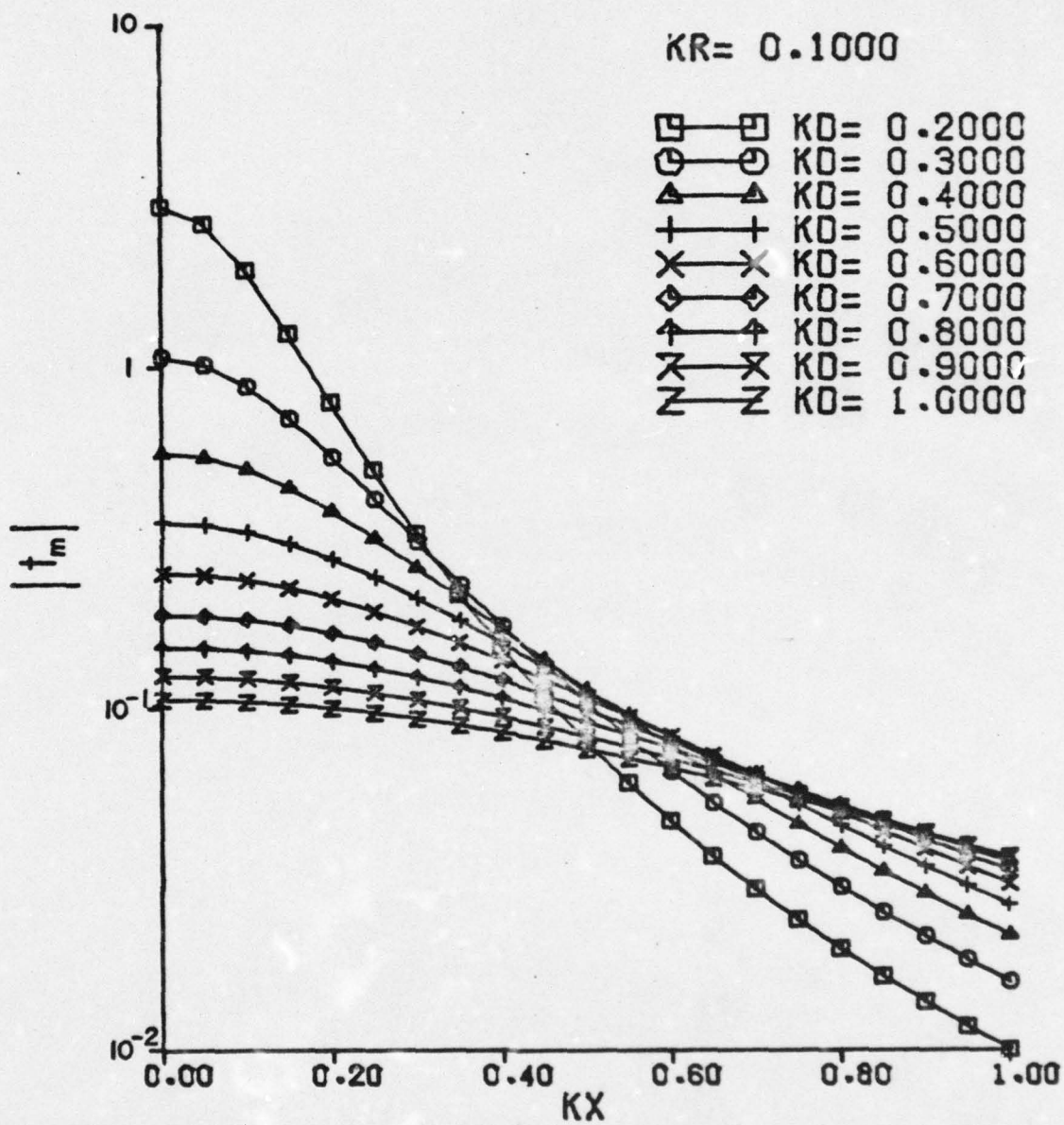Fig. 30. Magnitude of t_m for a wire of radius
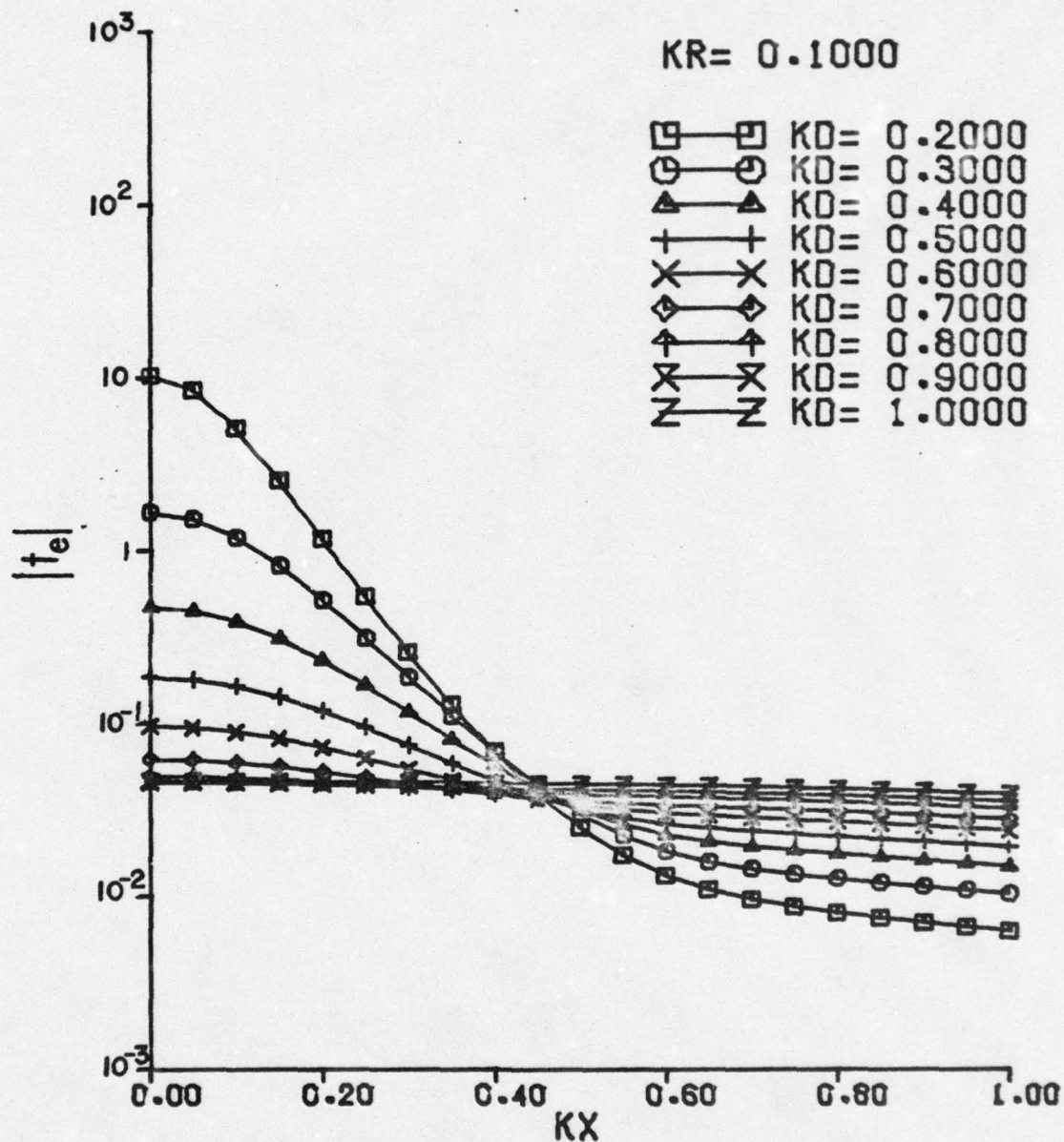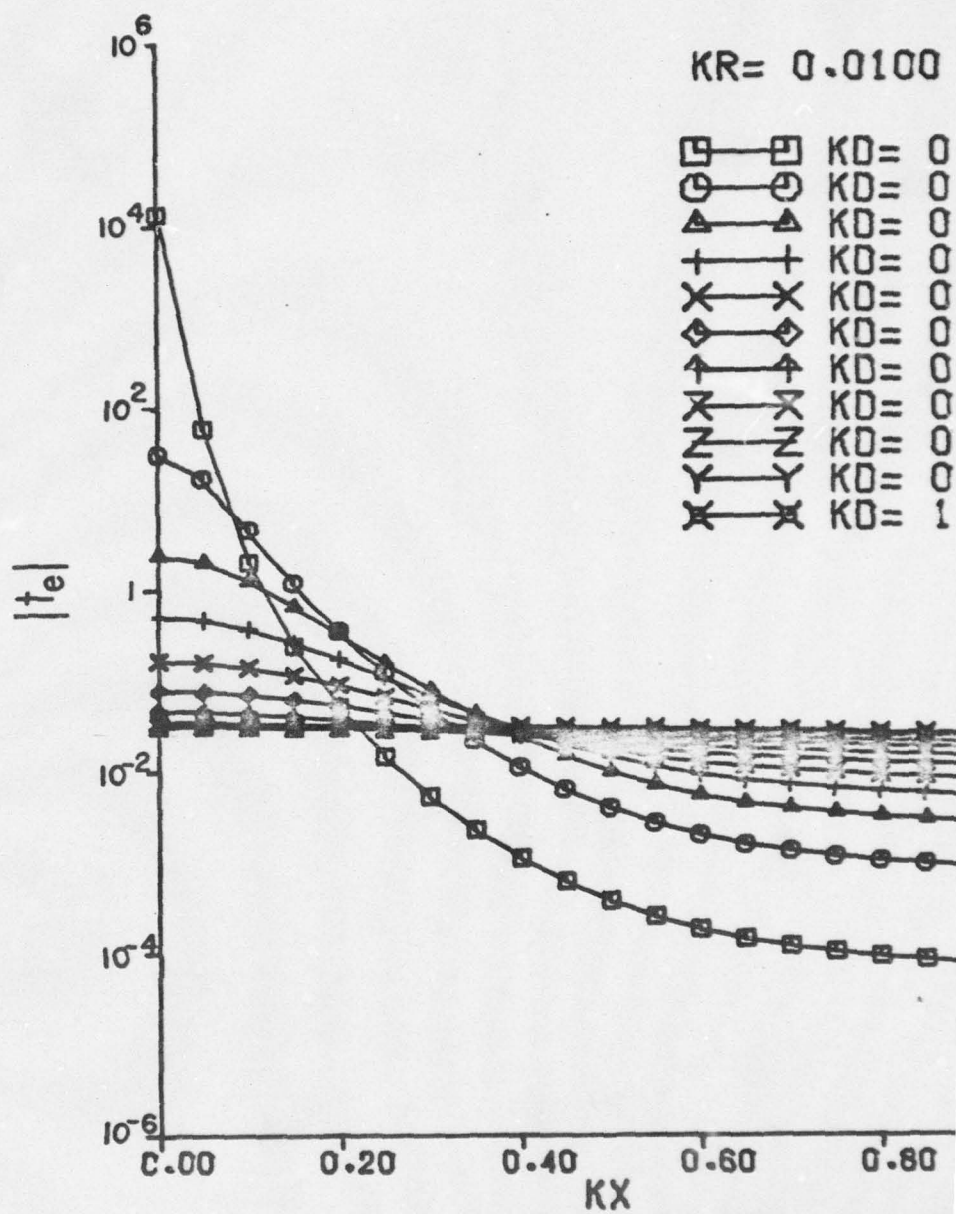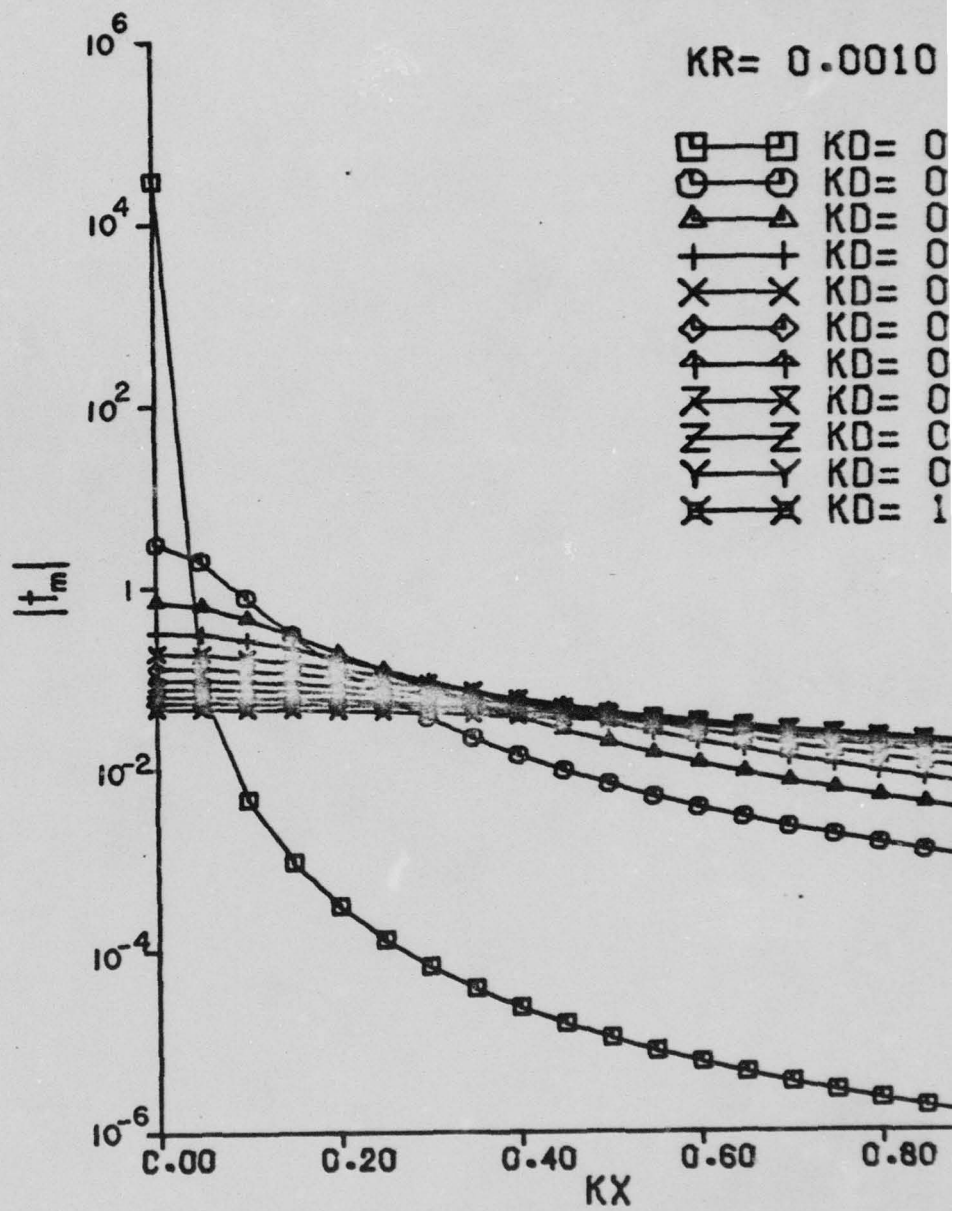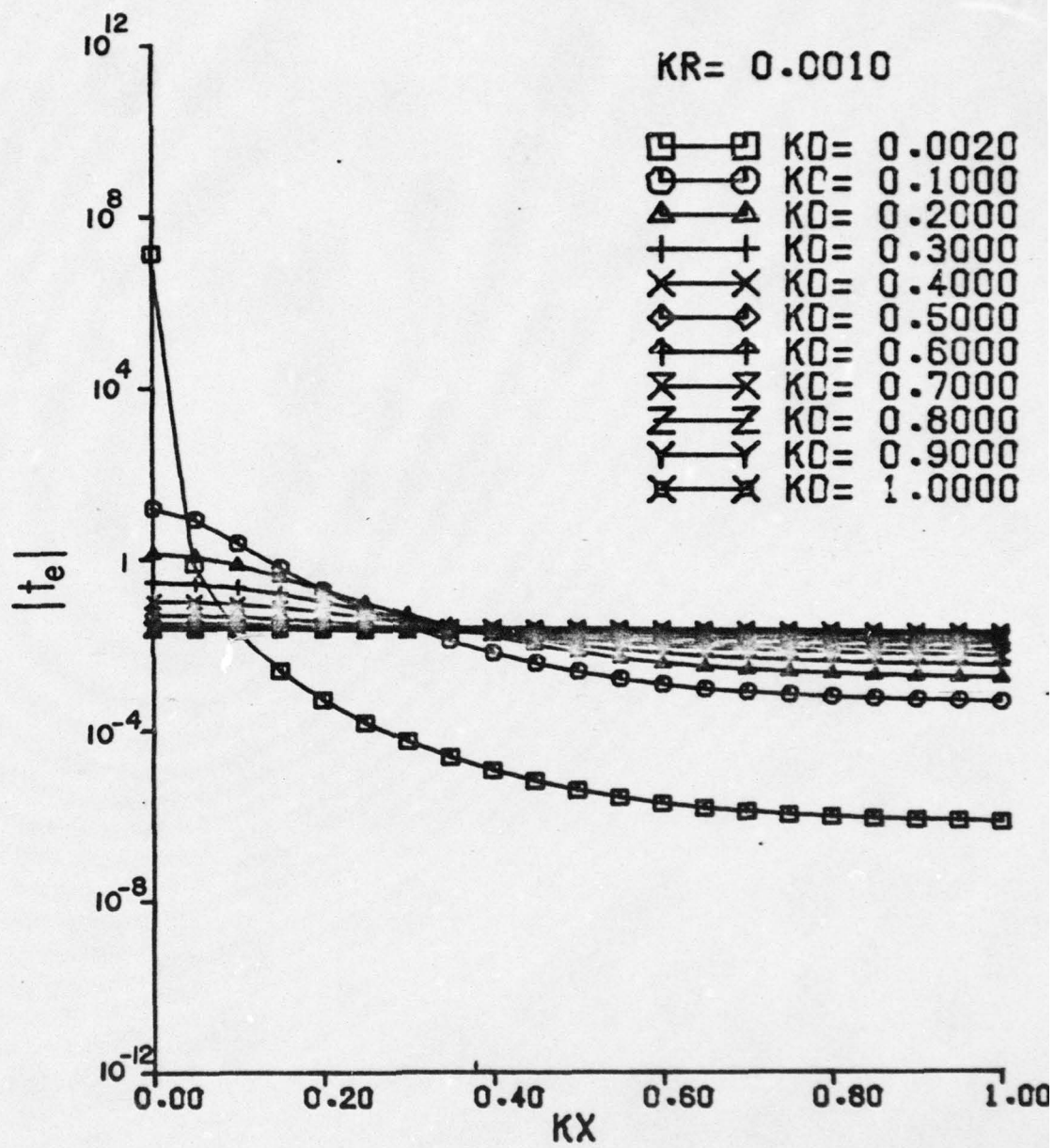
Fig. 31. Magnitude of t_e for a wire of radius kr = 0.001.

82
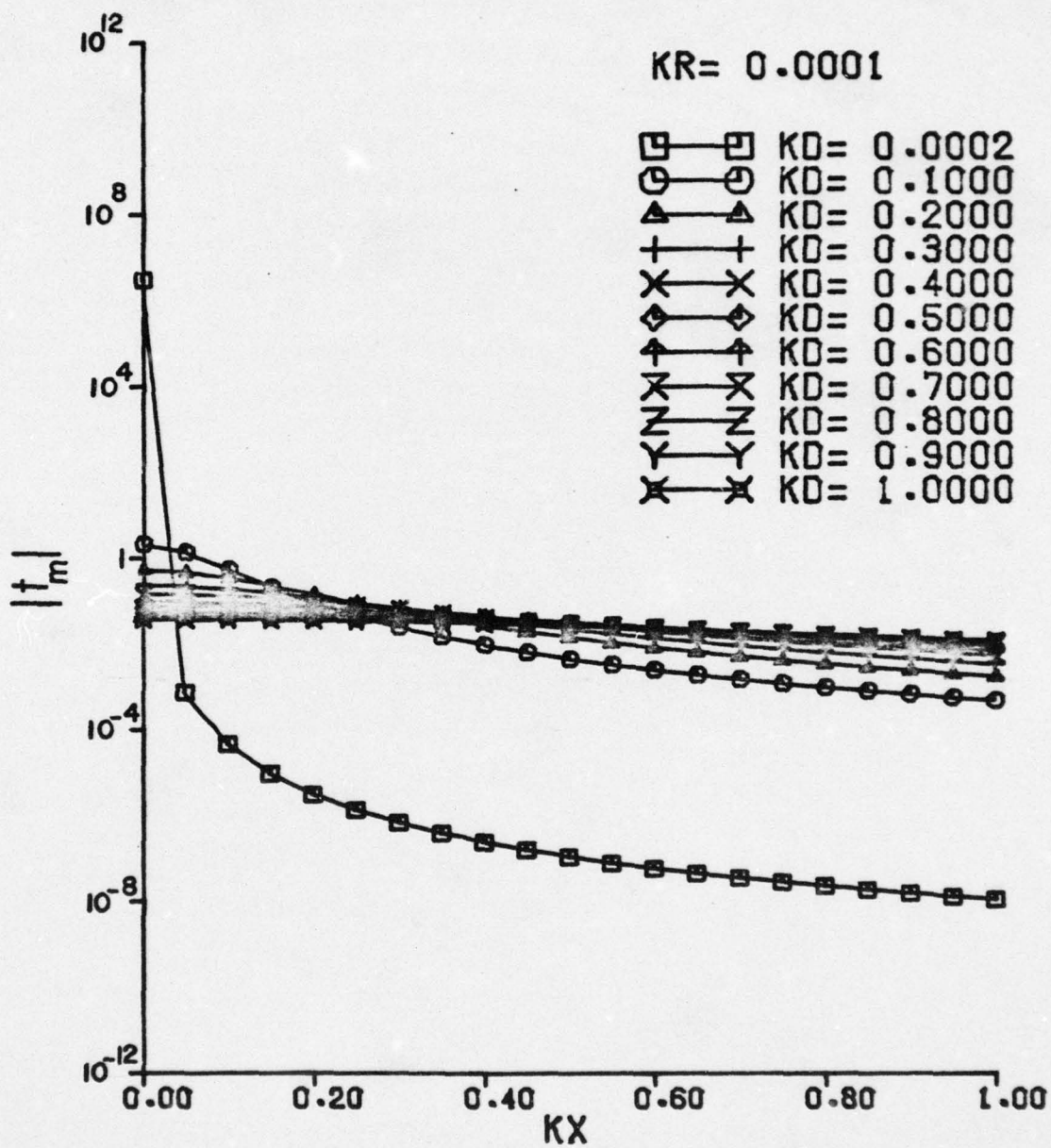
Fig. 32. Magnitude of t_m for a wire of radius kr = 0.0001.
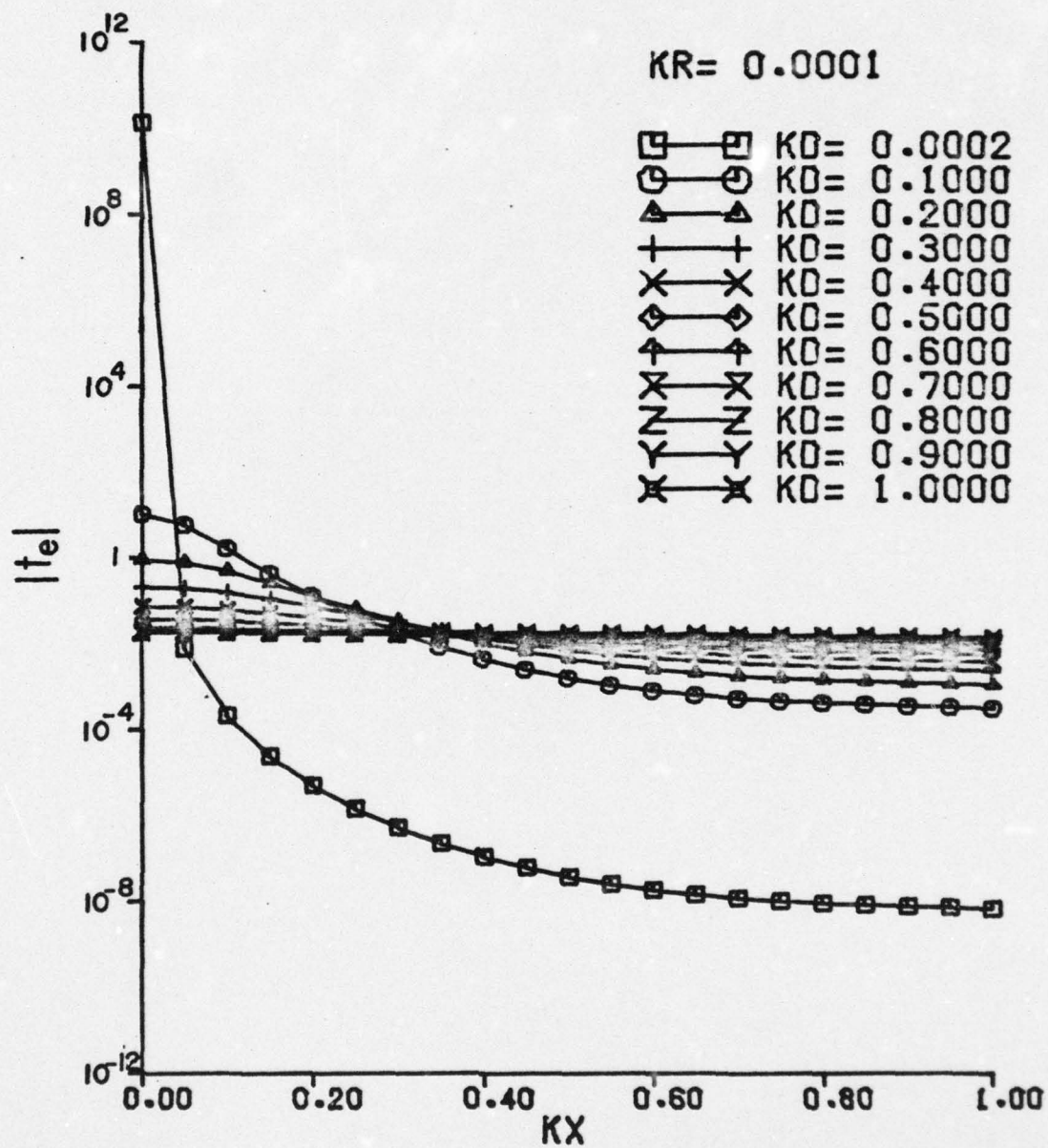
Fig. 33. Magnitude of t_e for a wire of radius kr = 0.0001.
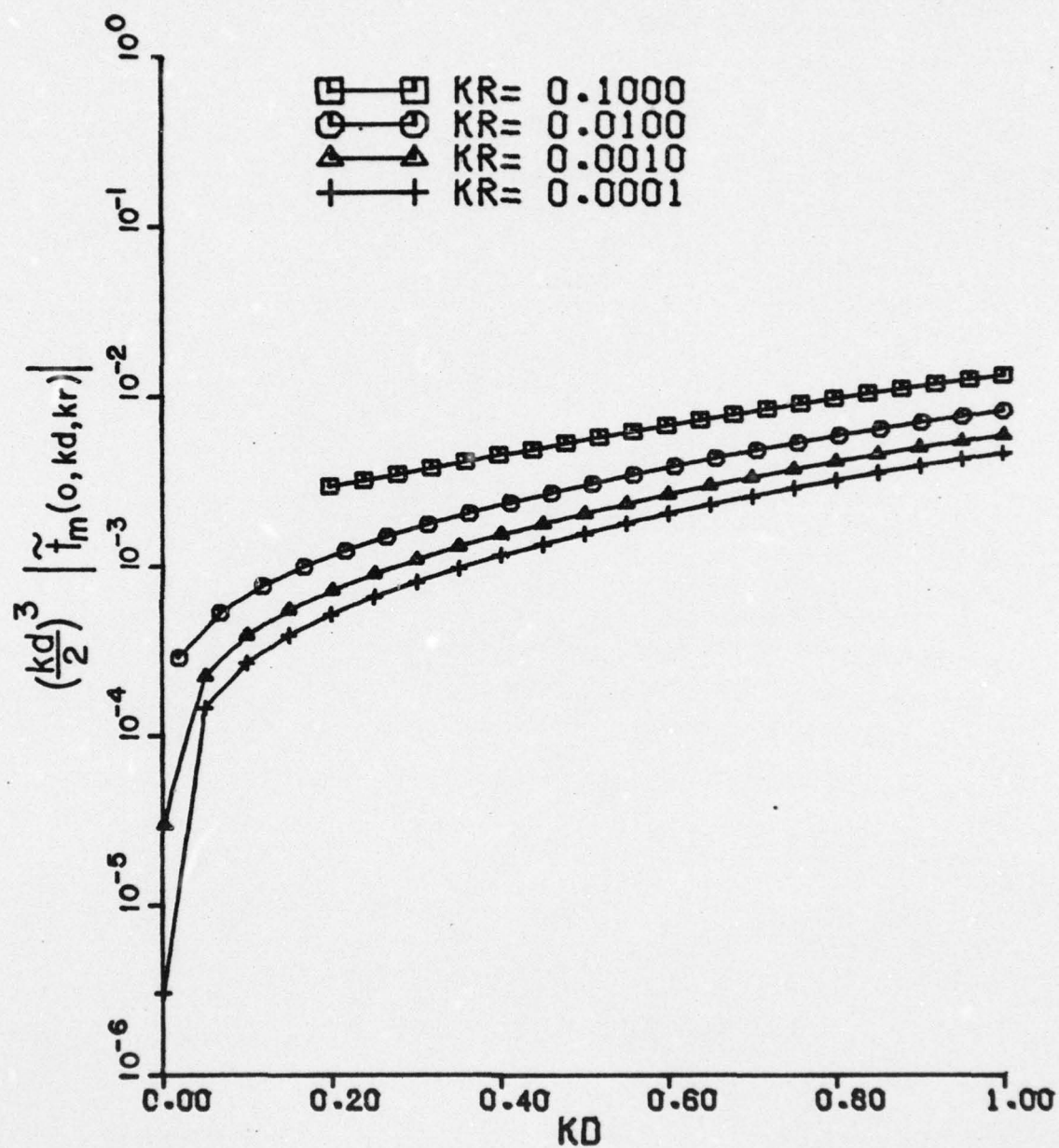
Fig. 34. Magnitude of $(kd/2)^3 \, \tilde{t}_m(0, kd, kr)$.

85
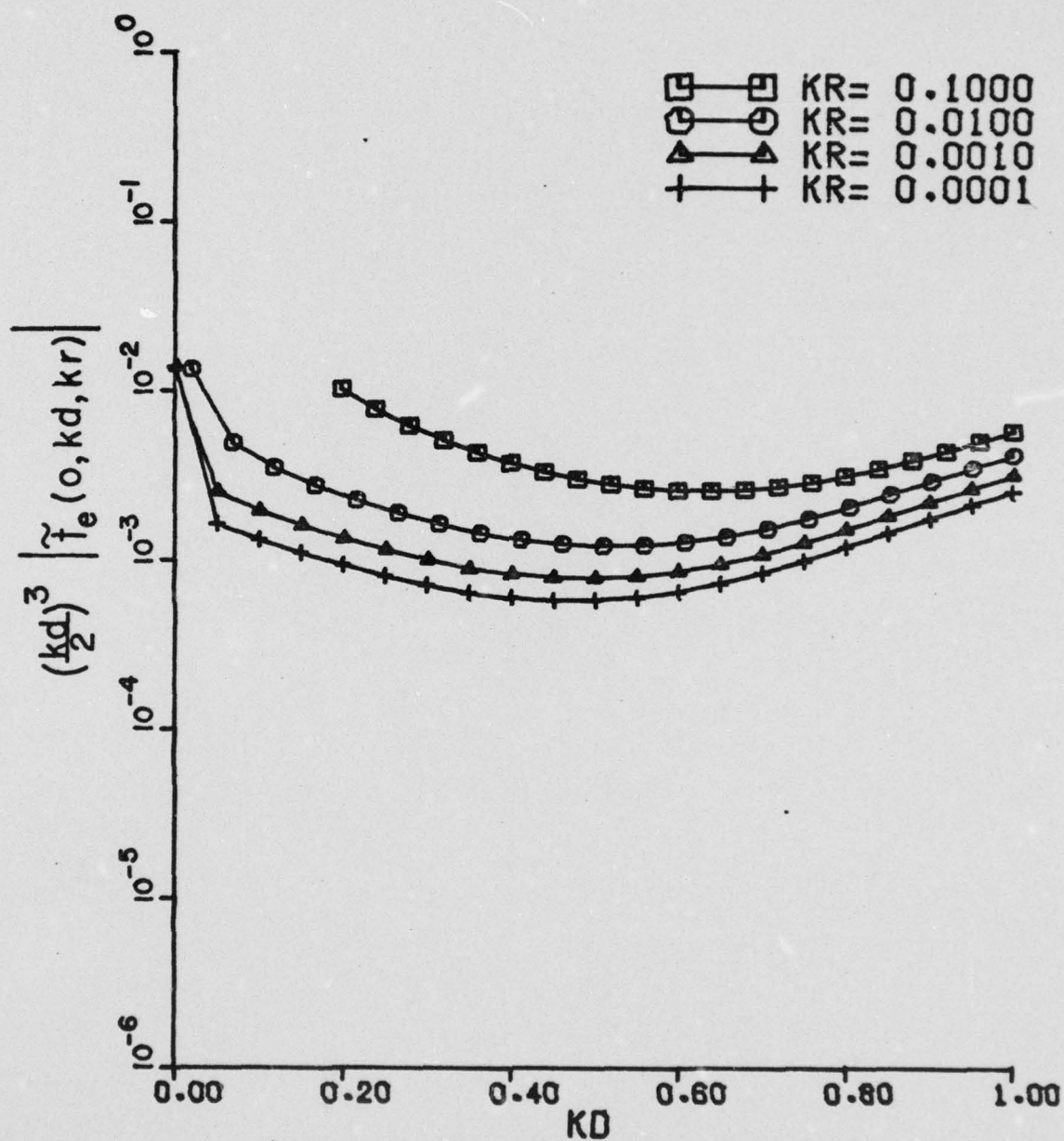
Fig. 35. Magnitude of $(kd/2)^3 \tilde{t}_e(0, kd, kr)$.

86

$$I(z) = \frac{1}{\sqrt{2\pi}} \int_{-\infty}^{\infty} \tilde{I}(k_z) e^{-jk_z z} \, dk_z$$

$$= \frac{jd}{\pi\sqrt{x_0^2+d^2}} \int_{-\infty}^{\infty} \frac{H_1^{(2)}\left[k_\rho\sqrt{x_0^2+d^2}\right]}{k_\rho\left[H_0^{(2)}(k_\rho r) - H_0^{(2)}(2k_\rho d)\right]} \left(\frac{kc_{mx}}{\eta} - k_z c_{ey}\right)$$

$$\times \; e^{-jk_z z} \, dk_z \qquad (154)$$

The contour of integration in (154) is shown in Fig. 36 which assumes that the medium is very slightly lossy so that k is complex. Branch cuts in the k_z plane are chosen along the loci $\text{Im}\,k_\rho = 0$ and k_z is assumed to be in the sheet $\text{Im}\,k_\rho < 0$ so that the radiation condition is satisfied for each component cylindrical wave in the integral representation (154). If z is positive, the contour then may be deformed around the branch cut as shown in Fig. 37 (where k has also been allowed to become real) and the integral becomes

$$I(z) = I_e(z) + I_m(z) \qquad (155)$$

where

$$I_e(z) = \frac{c_{ey} d \, e^{-jkz}}{(x_0^2+d^2)\log\frac{2d}{a}}$$

$$+ \frac{2c_{ey}d}{\pi\sqrt{x_0^2+d^2}} \int_0^k \text{Im}\left\{\frac{H_1^{(2)}\left[\sqrt{(k^2-\beta^2)(x_0^2+d^2)}\right]}{H_0^{(2)}\left[\sqrt{k^2-\beta^2}\,r\right] - H_0^{(2)}\left[2\sqrt{k^2-\beta^2}\,d\right]}\right\} \frac{\beta e^{-j\beta z} d\beta}{\sqrt{k^2-\beta^2}}$$

$$+ \frac{2c_{ey}d}{\pi\sqrt{x_0^2+d^2}} \int_0^\infty \text{Im}\left\{\frac{H_1^{(2)}\left[\sqrt{(k^2+\alpha^2)(x_0^2+d^2)}\right]}{H_0^{(2)}\left[\sqrt{k^2+\alpha^2}\,r\right] - H_0^{(2)}\left[2\sqrt{k^2+\alpha^2}\,d\right]}\right\} \frac{\alpha e^{-\alpha z} d\alpha}{\sqrt{k^2+\alpha^2}}$$

87
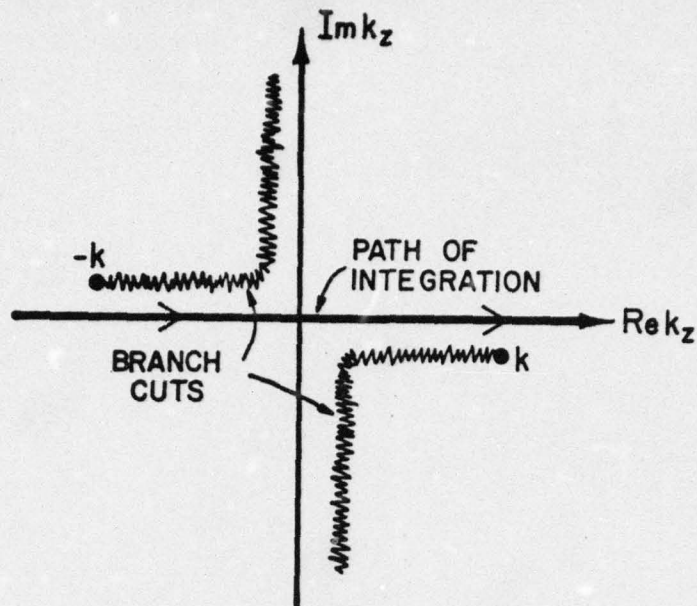
Fig. 36. Branch cuts and contour of integration in the k_z plane.
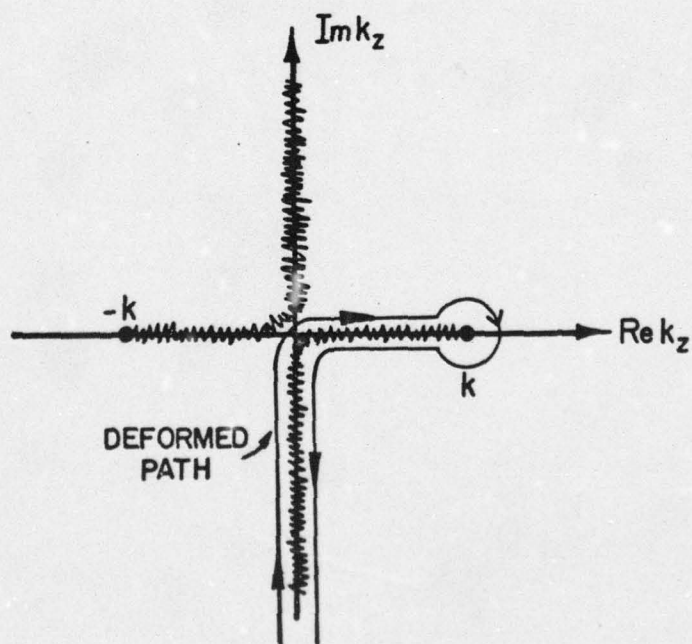
Fig. 37. Deformation of the contour around the branch cut.

88

$$= -I_e(-z), \quad z > 0 \tag{156}$$

$$I_m(z) = \frac{-c_{mx} d e^{-jkz}}{\eta(x_0^2 + d^2)\log\frac{2d}{a}}$$

$$- \frac{2c_{mx} kd}{\eta\pi\sqrt{x_0^2 + d^2}} \int_0^k \text{Im}\left\{\frac{H_1^{(2)}\sqrt{(k^2 - \beta^2)(x_0^2 + d^2)}}{H_0^{(2)}\left[\sqrt{k^2 - \beta^2}\, r\right] - H_0^{(2)}\left[2\sqrt{k^2 - \beta^2}\, d\right]}\right\} \frac{e^{-j\beta z} d\beta}{\sqrt{k^2 - \beta^2}}$$

$$- j\, \frac{2c_{mx} kd}{\eta\pi\sqrt{x_0^2 + d^2}} \int_0^\infty \text{Im}\left\{\frac{H_1^{(2)}\left[\sqrt{(k^2 + \alpha^2)(x_0^2 + d^2)}\right]}{H_0^{(2)}\left[\sqrt{k^2 + \alpha^2}\, r\right] - H_0^{(2)}\left[2\sqrt{k^2 + \alpha^2}\, d\right]}\right\} \frac{e^{-\alpha z} d\alpha}{\sqrt{k^2 + \alpha^2}}$$

$$= I_m(-z), \quad z > 0 \tag{157}$$

The first two terms on the RHS of (156) and (157) represent the TEM modes excited by the electric and magnetic dipoles, respectively, and arise from the branch point contribution from the deformed path in Fig. 37. The remaining two integrals in each expression represent the current due to the propagating and the evanescent spectrum, in that order. Noting that the integrands for the evanescent fields are bounded by some number C, say, we can bound those integrals by the integral

$$\int_0^\infty C e^{-\alpha z} d\alpha = \frac{C}{z} = \mathcal{O}(1/z). \tag{158}$$

The integrands for the propagating fields are of bounded variation and hence, by the Riemann-Lesbegue lemma [23] are $\mathcal{O}(1/z)$ as well. Hence, for large z,

---

[23] E. T. Whittaker, G. N. Watson, A Course of Modern Analysis, New York: Cambridge Press, 1973, p. 172.

$$I(z) \sim \left(c_{ey} - \frac{c_{mx}}{\eta} \right) \frac{de^{-jkz}}{(x_0^2 + d^2) \log \frac{2d}{a}} + \mathcal{O}(1/z) \tag{159}$$

which shows that at large distances from the aperture, only the TEM wave is significant.

APPENDIX A

LUMPED ELEMENT TRAVELING WAVE SOURCE

In many network computations it is convenient to use scattering parameters, defined in (ref. A1), (ref. A2)

$$a_k = \frac{1}{2\sqrt{R_{0k}}} (V_k + Z_{0k}I_k) \qquad (A1)$$

$$b_k = \frac{1}{2\sqrt{R_{0k}}} (V_k - Z_{0k}^* I_k) \qquad (A2)$$

In the above, V_k and I_k are the actual (not normalized) voltage and current at port k of an N-port, while $Z_{0k} = R_{0k} + jX_{0k}$ is the normalization impedance at port k. The asterisk denotes a complex-conjugate number. When scattering representation of networks is used, it is convenient to replace the voltage and current sources with corresponding traveling-wave sources. It seems that no convenient circuit elements have been found for that purpose. Penfield and Rafuse (ref. A3) have used a symbol reminiscent of a voltage source in combination with a directional coupler, such as in Figure A1. However, this symbol represents a pure traveling-wave source only in the limiting case when the coupling tends to zero and the voltage source tends to infinity. For any finite value of the coupling, a fraction of the energy from the main guide will be unavoidably absorbed in the matched termination.

A1. D. C. Youla, "On Scattering Matrices Normalized to Complex Port Numbers," Proc. I.R.E. Vol. 49, p. 1221, July 1961.

A2. M. T. Carlin, A. B. Giordano, Network Theory, an Introduction to Reciprocal and Nonreciprocal Circuits, Englewood Cliffs: Prentice Hall, 1964, pp. 326 and 144.

A3. P. Penfield, Jr., R. P. Rafuse, Varactor Applications, Cambridge: M.I.T. Press, 1962, p. 26.

A convenient source of the traveling-wave to be proposed here is a combination of the voltage source and the current source such as shown in Figure A2(a). To verify this, write the Kirchhoff laws for this circuit:

$$I_1 + I_2 + I_s = 0 \qquad (A3)$$

$$V_1 - V_2 + V_s = 0 \qquad (A4)$$

Take the normalization impedance for the port 1 to be Z_{01} and for the port 2 to be Z_{02}. Then using (1) and (2) obtain the following:

$$
\begin{bmatrix} b_1 \\ b_2 \end{bmatrix}
=
\begin{bmatrix}
\dfrac{Z_{02}-Z_{01}^*}{Z_{02}+Z_{01}} & \sqrt{\dfrac{R_{01}}{R_{02}}} \cdot \dfrac{Z_{02}+Z_{02}^*}{Z_{02}+Z_{01}} \\[3mm]
\sqrt{\dfrac{R_{01}}{R_{02}}} \cdot \dfrac{Z_{01}+Z_{01}^*}{Z_{01}+Z_{02}} & \dfrac{Z_{01}-Z_{02}^*}{Z_{01}+Z_{02}}
\end{bmatrix}
\cdot
\begin{bmatrix} a_1 \\ a_2 \end{bmatrix}
+
\begin{bmatrix}
\sqrt{R_{02}} \; \dfrac{Z_{01}I_s - V_s}{Z_{01}+Z_{02}} \\[3mm]
\sqrt{R_{01}} \; \dfrac{Z_{02}I_s + V_s}{Z_{01}+Z_{02}}
\end{bmatrix}
\qquad (A5)
$$

A convenient choice of the normalization impedance, is as follows:

$$Z_{01} = Z_{02}^* = Z_0 = R_0 + jX_0 \qquad (A6)$$

When such a choice is made the diagonal terms in (A5) become zero and the two port in Figure A2(a) becomes an allpass:

$$
\begin{bmatrix} b_1 \\ b_2 \end{bmatrix}
=
\begin{bmatrix} 0 & 1 \\ 1 & 0 \end{bmatrix}
\begin{bmatrix} a_1 \\ a_2 \end{bmatrix}
+
\frac{1}{2\sqrt{R_0}}
\begin{bmatrix} Z_0 I_s - V_s \\ Z_0^* I_s + V_s \end{bmatrix}
\qquad (A7)
$$

Furthermore, the source of the outgoing wave at port 1 can be made equal to zero by choosing

$$I_s = \frac{V_s}{Z_0} \qquad (A8)$$

92
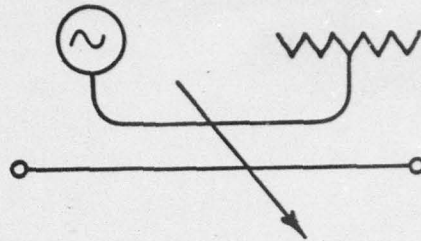
Fig. A1. Conventional symbol for traveling-wave source.
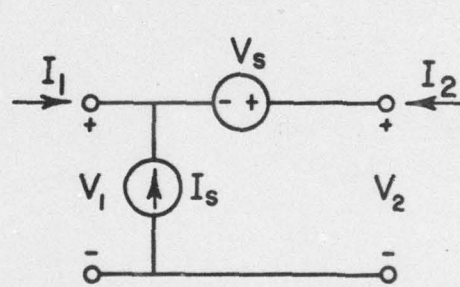
(a)
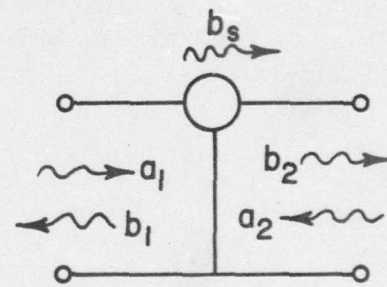
(b)

Fig. A2(a). Combination of voltage and current sources.

Fig. A2(b). Proposed symbol for traveling-wave source.

93
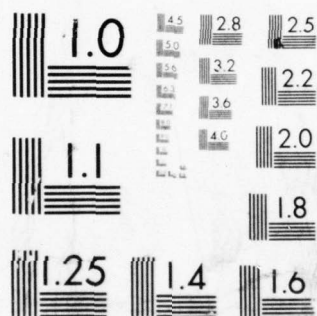
MICROCOPY RESOLUTION TEST CHART
NATIONAL BUREAU OF STANDARDS-1963-A

Therefore, under constraints (A6) and (A8), the circuit in Figure A2(a) becomes a true source of an outgoing wave emerging from port 2. Matrix equation (A5) reduces to

$$b_1 = a_2 \qquad\qquad (A9)$$

$$b_2 = a_1 + b_{2s} \qquad\qquad (A10)$$

where the outgoing-wave source b_{2s} is

$$b_{2s} = \frac{V_s}{2\sqrt{R_0}} \left(1 + \frac{Z_0^*}{Z_0} \right) \qquad\qquad (A11)$$

Very often, one chooses a real normalization:

$$Z_{01} = Z_{02} = R_0 \qquad\qquad (A12)$$

so that the corresponding outgoing-wave source becomes

$$b_{2s} = \frac{V_s}{\sqrt{R_0}} \qquad\qquad (A13)$$

From (A9) it is apparent that any wave a_2 impinging upon port 2, passes through the circuit in Figure A2(a) unaffected, and emerges at port 1 as an outgoing wave b_1. On the other hand, it follows from (A10) that wave a_1, incident at port 1, passes unaffected through the circuit and emerges at port 2. In addition to a_1, a source wave b_{2s} also emerges at port 2. This source wave is independent of b_1 or b_2. Hence, it has been shown that a source of a traveling wave is a twoport consisting of a voltage source and a current source such as in Figure A2(a). These two sources must be related by (A8) and the normalization impedances must be selected according to (A6) for the complex normalization, or according to (A12) for the real normalization.

94

To simplify the circuit diagrams, the traveling-wave source between ports 1 and 2 could be represented by a single symbol such as in Figure A2(b). Note that the symbol represents a two port which is a three-terminal device. The value of the source b_{2s} is given by (A11) for complex normalization and by (A13) for real normalization.

APPENDIX B

MATRIX ALGEBRA IN DIRAC'S NOTATION

The presented material is an abridgement from (ref. B1) and (ref. B2). A column vector in an N-dimensional space is denoted by

$$|x> = \begin{pmatrix} x_1 \\ x_2 \\ \cdot \\ \cdot \\ \cdot \\ x_N \end{pmatrix}$$

A square matrix in an N-dimensional space is denoted by

$$\underline{A} = \begin{pmatrix} a_{11} & a_{12} & \cdots & a_{1N} \\ a_{21} & a_{22} & \cdots & a_{2N} \\ \vdots & \vdots & & \vdots \\ a_{N1} & a_{N2} & & a_{NN} \end{pmatrix}$$

Matrix $\underline{A}$ is an operator. When it operates on vector $|x>$, the result is a new vector $|v>$

$$|v> = \underline{A}|x> \tag{B1}$$

Using the rule for matrix multiplication, one finds that the kth component of the vector $|v>$ is

$$v_k = \sum_{j=1}^{N} A_{kj}x_j \tag{B2}$$

B1. B. Friedman, Principles and Techniques of Applied Mathematics, New York: Wiley, 1956, pp. 1-33.

B2. A. Messiah, Quantum Mechanics, Vol I, Amsterdam: North Holland, 1965, pp. 162-179.

The transpose conjugate of column vector $|x\rangle$ is denoted by $\langle x|$, and it represents a row vector as follows

$$\langle x| = (x_1^* \ x_2^* \ \cdots \ x_N^*) \ , \tag{B3}$$

where * denotes a complex-conjugate value. The transpose conjugate of a square matrix $\underline{A}$ is denoted $\underline{A}^+$

$$\underline{A}^+ = \begin{pmatrix} a_{11}^* & \cdots & a_{N1}^* \\ a_{12}^* & \cdots & a_{N2}^* \\ \cdot & & \cdot \\ \cdot & & \cdot \\ \cdot & & \cdot \\ a_{1N}^* & \cdots & a_{NN}^* \end{pmatrix}$$

The transpose conjugate of a product of several matrices is obtained by reversing the order of multiplication and by taking the transpose conjugate of each individual matrix in the product:

$$(\underline{A} \ \underline{B} \ \underline{C})^+ = \underline{C}^+ \ \underline{B}^+ \ \underline{A}^+$$

The same rule applies if one of the matrices is a vector ($=N \times 1$ matrix):

$$(\underline{A} \ \underline{B} \ |x\rangle)^+ = \langle x|\underline{A}^+ \ \underline{B}^+ \tag{B4}$$

The result of the above operation is a row vector. A matrix which is equal to its own transpose conjugate:

$$\underline{A}^+ = \underline{A}$$

is said to be Hermitian. Instead of N^2 distinct elements, such a matrix contains only $\frac{1}{2} N(N+1)$ distinct elements. The elements located symmetrically across the main diagonal are complex conjugates of each other. Also, the elements on the main diagonal are

97

all real.

Frequently, a product of a row vector and a column vector is to be computed as follows

$$\langle x|y \rangle = (x_1^* \; x_2^* \cdots x_N^*) \begin{pmatrix} y_1 \\ y_2 \\ \cdot \\ \cdot \\ \cdot \\ y_N \end{pmatrix} = \sum_{j=1}^{N} x_j^* y_j \qquad (B5)$$

The result of this operation is a scalar (= a complex number), and (B5) is called scalar product. The same two vectors $|x\rangle$ and $|y\rangle$ can be used to form a scalar product in the reverse order:

$$\langle y|x \rangle = (y_1^* \; y_2^* \cdots y_N^*) \begin{pmatrix} x_1 \\ x_2 \\ \cdot \\ \cdot \\ \cdot \\ x_N \end{pmatrix} = \sum_{j=1}^{N} y_j^* x_j \quad .$$

The result is equal to the complex conjugate of (B5). Thus,

$$\langle x|y \rangle = \langle y|x \rangle^* \quad .$$

If one of the vectors in a scalar product has been obtained by the linear transformation such as in (B1) above, the scalar product takes the following form

$$\langle v|y \rangle = \langle x|\underline{A}^+|y \rangle \qquad (B6)$$

Again, the result of this operation is a scalar. The right-hand side in (B6) may be interpreted as a scalar product of the row vector $\langle x|\underline{A}^+$ with the column vector $|y\rangle$. Alternatively, (B6)

98

may be interpreted as a scalar product of the row vector $\langle x|$ with the column vector $\underline{A}^{+}|y\rangle$. Computing the product in either way gives identical results, because a matrix multiplication is associative:

$$\underline{A}\,(\underline{B}\,\underline{C}) = (\underline{A}\,\underline{B})\,\underline{C}\ .$$

When the order of multiplication in (B5) is such that a column vector multiplies a row vector:

$$|y\rangle\langle x| = \begin{pmatrix} y_1 \\ y_2 \\ \cdot \\ \cdot \\ \cdot \\ y_N \end{pmatrix} (x_1^* \ x_2^* \ \cdots \ x_N^*) \quad ,$$

the result is a square matrix:

$$|y\rangle\langle x| = \begin{pmatrix} y_1 x_1^* & y_1 x_2^* & \cdots & y_1 x_N^* \\ \cdots\cdots\cdots\cdots\cdots\cdots\cdots \\ y_N x_1^* & y_N x_2^* & \cdots & y_N x_N^* \end{pmatrix} \tag{B7}$$

This is a special class of a square matrix, defined by only 2 N distinct numbers (y_1 through y_N and x_1 through x_N).

One of the advantages of writing the matrix equations in Dirac's notation is that the notation itself clearly indicates what type of the result one should expect. For example, the expressions like

$$\langle x|\underline{A}|x\rangle \ , \ \beta\langle c|x\rangle \ , \ \langle x|\underline{A}^{+}\underline{B}|y\rangle$$

represent   scalars. Another class of expressions which looks like

99

$$\underline{A}|x> \quad , \quad |x><y|c> \quad , \quad \sum_{n=1}^{N} \alpha_n |x_n>$$

represent   vectors. Finally, the operations like

$$\underline{A} \ \underline{B} \ \underline{C}^{+} \quad \text{or} \quad \underline{A}|x><b|\underline{B}|y><c|$$

will each result in a square matrix. For the sake of clarity,
one should specify the following was assumed:

$\beta, \ \alpha_n \cdot \cdot \cdot$ are scalars,

$|x_n>, \ |x>, \ |y>, \ |b>, \ |c> \ \cdot \cdot \cdot$ are vectors,

$\underline{A}, \ \underline{B}, \ \underline{C} \cdot \cdot \cdot$ are square matrices.

APPENDIX C

MULTICONDUCTOR-LINE FORMULATION BY SIMULTANEOUS
DIAGONALIZATION OF TWO MATRICES

Multiconductor transmission line (abbrev. MTL) consists of N
conductors   and   a reference, or a "ground" conductor. The
voltages of each conductor with respect to reference are arranged in
voltage vector $|V>$

$$|V> = \begin{pmatrix} V_1 \\ \vdots \\ V_N \end{pmatrix}$$

and the currents are similarly arranged in current vector $|I>$. The
length coordinate of the MTL is z, while the cross-section coordinates
are x and y. The reference directions of the currents and voltages on
any of the conductors are such that real, positive values of V_i and I_i
result in a power flow in the positive z direction (see Fig. C1). On
the lossless MTL, the sinusoidal steady-state voltages and currents are
related through the following equations (see e.g. references [C1] through
[C8])

$$\frac{d}{dz} |V> = -j\omega \underline{L}|I> \quad , \tag{C1}$$

$$\frac{d}{dz} |I> = -j\omega \underline{K}|V> \quad . \tag{C2}$$

$\underline{L}$ is the inductance matrix, and $\underline{K}$ is the electric induction
coefficient matrix. Often a symbol $\underline{C}$ is used to denote the induction
coefficient matrix. Unfortunately, some recent publications associate
the erroneous term "capacitance matrix" with the symbol $\underline{C}$ (see [C8] and
[C9], although the proper term should be "electric induction coefficient
matrix" [C10]. To avoid the possible confusion, symbol $\underline{K}$ has been used here.

101
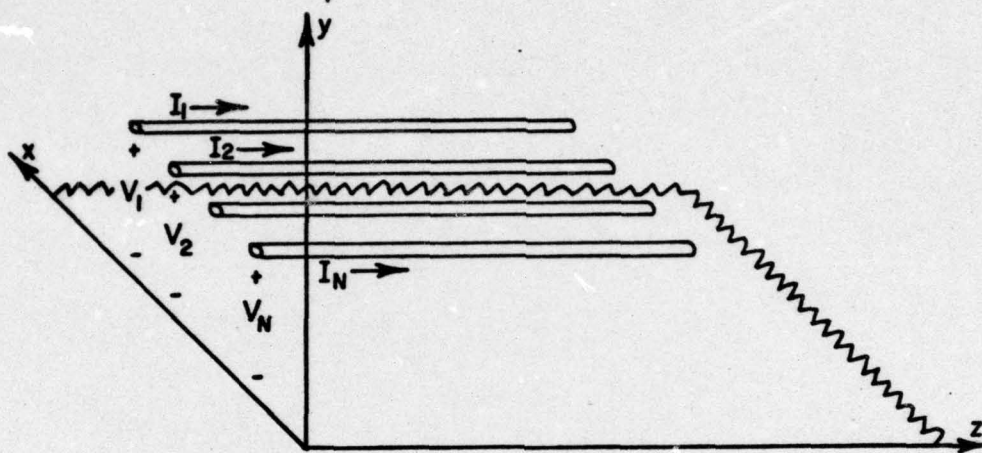
Fig. C1. Voltages and currents on MTL.

Only the lossless lines without magnetic materials and with iso-tropic dilectrics will be considered here. When the dielectric is homogeneous, the well-known TEM propagation occurs, in which all the waves propagate with the velocity of light. Such MTL are commonly treated in terms of impedance parameters [C11], [C8], image parameters scattering matrix parameters [C13], and chain parameters [C14].

When the dielectric between conductors is not homogeneous, the waves on MTL are HEM [C15], i.e. both the electric and the magnetic vectors acquire a longitudinal component. However, the dominant HEM modes do not have a cutoff frequency, and at very low frequencies, their longi-tudinal field components are negligibly small. For this reason these dominant HEM waves are called "quasi-TEM" waves, which are the subject of the present report.

The formulation of voltages and currents on MTL in terms of voltage and current eigenvectors, as introduced by Amemiya [C6] and Marx [C7], is well suited to the treatment of transients as well as steady state waveforms. Their analysis starts from the decoupled equations, which are obtained from (C1) and (C2):

$$\frac{d^2}{dz^2}|V> = -\omega^2 \underline{L}\,\underline{K}\,|V> \tag{C3}$$

$$\frac{d^2}{dz^2}|I> = -\omega^2 \underline{K}\,\underline{L}\,|I> \tag{C4}$$

In the present report, the eigenvector formulation of Amemiya and Marx will be extended by using a simultaneous diagonalization of two matrices [C8], [C16], [C17]. For this purpose, it is convenient to rewrite (C3) and (C4) as follows:

103

$$\underline{L}^{-1} \frac{d^2}{dz^2} |V\rangle = -\omega^2 \underline{K} |V\rangle \ , \tag{C5}$$

$$\underline{K}^{-1} \frac{d^2}{dz^2} |I\rangle = -\omega^2 \underline{L} |I\rangle \ . \tag{C6}$$

The method of simultaneous diagonalization of two real, symmetric matrices [C16] presents a convenient way of solving these two equations. The method can be applied only when one of the two matrices is positive definite. Since both $\underline{L}$ and $\underline{K}$ matrices represent the stored energy of a passive multiconductor network, they are both positive definite and thus qualify.

The first step in the method is to find the eigenvectors $|x_i\rangle$ and eigenvalues λ_i of the matrix $\underline{L}^{-1}$:

$$\underline{L}^{-1} |x_i\rangle = \lambda_i |x_i\rangle \ . \tag{C7}$$

The corresponding eigenvalue equation is

$$\det(\underline{L}^{-1} - \lambda \underline{U}) = 0 \ , \tag{C8}$$

where $\underline{U}$ is the identity matrix. It is convenient to make eigenvectors orthonormal:

$$\langle x_i | x_j \rangle = \delta_{ij} \ \text{(Kroneker delta)}. \tag{C9}$$

Next, a square matrix $\underline{G}$ is formed, having eigenvectors $|x_i\rangle$ for its columns

$$\underline{G} = (|x_i\rangle \ldots \ldots |x_N\rangle) \ . \tag{C10}$$

$\underline{G}$ is orthogonal real matrix which diagonalizes $\underline{L}^{-1}$ as follows

$$\underline{G}^+ \underline{L}^{-1} \underline{G} = \begin{pmatrix} \lambda_1 & & 0 \\ & \ddots & \\ 0 & & \lambda_N \end{pmatrix} = \underline{\Lambda} \ , \tag{C11}$$

104

where superscript + denotes a transpose conjugate. Since $\underline{L}^{-1}$ is positive definite, λ_i's are positive real. Therefore, it is meaningful to define a square-root matrix $\underline{\Lambda}^{\frac{1}{2}}$

$$\underline{\Lambda}^{\frac{1}{2}} = \begin{pmatrix} \sqrt{\lambda_1} & & 0 \\ & \ddots & \\ 0 & & \sqrt{\lambda_N} \end{pmatrix} \tag{C12}$$

such that

$$\underline{\Lambda}^{-\frac{1}{2}}\underline{\Lambda}\,\underline{\Lambda}^{-\frac{1}{2}} = \underline{U} \quad,$$

with $\underline{U}$ being an identity matrix.

Next, a new variable, $|y\rangle$, is defined in terms of $|V\rangle$:

$$|V\rangle = \underline{G}\,\underline{\Lambda}^{-\frac{1}{2}}|y\rangle \quad. \tag{C13}$$

When this change of variables is introduced in (C5), the following equation is obtained

$$\frac{d^2}{dz^2}|y\rangle = -\omega^2\,\underline{B}|y\rangle \quad, \tag{C14}$$

where $\underline{B}$ is a symmetric real matrix

$$\underline{B} = \underline{\Lambda}^{-\frac{1}{2}}\underline{G}^{+}\,\underline{K}\,\underline{G}\,\underline{\Lambda}^{-\frac{1}{2}} \quad, \tag{C15}$$

where (C11) has been used to eliminate matrix $\underline{L}$.

Thus, $\underline{B}$ can be diagonalized by an orthogonal transformation matrix, which will be here denoted by $\underline{Q}$. The eigenvalues of $\underline{B}$ are all real positive. It comes out that they have a dimension of inverse velocity squared:

$$\underline{B}|t_i\rangle = \frac{1}{v_i^2}\,|t_i\rangle \tag{C16}$$

where $|t_i\rangle$ are eigenvectors of $\underline{B}$. Transformation matrix $\underline{Q}$ consists of

orthonormal eigenvectors $|t_i\rangle$ as its columns:

$$\underline{Q} = (|t_1\rangle \ldots \ldots |t_N\rangle) \ . \tag{C17}$$

$\underline{Q}$ diagonalizes $\underline{B}$ as follows

$$\underline{Q}^+ \underline{B} \, \underline{Q} = \begin{pmatrix} \dfrac{1}{v_1^2} & & 0 \\ & \ddots & \\ 0 & & \dfrac{1}{v_N^2} \end{pmatrix} \tag{C18}$$

(C14) can be thus diagonalized by the following change of variables

$$|y\rangle = \underline{Q} \, |\xi\rangle \ . \tag{C19}$$

Using (C19) in (C14) one obtains the diagonal equation

$$\frac{d^2}{dz^2} |\xi\rangle = -\begin{pmatrix} \beta_1^2 & & 0 \\ & \ddots & \\ 0 & & \beta_N^2 \end{pmatrix} |\xi\rangle \tag{C20}$$

where

$$\beta_i^2 = \frac{\omega^2}{v_i^2} \quad \text{for} \quad i = 1,2,\ldots N \ . \tag{C21}$$

(C20) is a decoupled system of differential equations

$$\frac{d^2}{dz^2} \xi_i = -\beta_i^2 \xi_i \quad \text{for} \quad i = 1,2,\ldots,N \ , \tag{C22}$$

which has exponential solutions

$$\xi_i = \xi_i^+ e^{-j\beta_i z} + \xi_i^- e^{j\beta_i z} \ . \tag{C23}$$

These are the normal modes (or fundamental modes) of the multiconductor transmission line, each of them propagating with its own propagation constant β_i in the positive or negative z direction. The total vector

106

$|\xi>$ is then

$$|\xi> = \sum_{i=1}^{N} (\xi_i^+ e^{-j\beta_i z} + \xi_i^- e^{j\beta_i z})|u_i> , \qquad (C24)$$

where $|u_i>$ denotes a unit column vector having all zero components except the i-th:

$$|u_i> = \begin{pmatrix} 0 \\ 0 \\ \vdots \\ 1 \\ \vdots \\ 0 \end{pmatrix} \longleftarrow \text{i-th row} \qquad . \qquad (C25)$$

Vector $|\xi>$ thus represents the state of the multiconductor transmission line in terms of individual modes, the component ξ_i describes the magnitude of the i-th mode at some position z along the line. Each mode has in turn certain magnitude of voltage and current on each of the conductors of the multiconductor transmission line. The voltages on individual conductors can be now determined by transforming the coordinates $|\xi>$ back into $|V>$, where the transformation is specified by (C13) and (C19)

$$|V> = \underline{G} \, \underline{\Lambda}^{-\frac{1}{2}} \, \underline{Q} \, |\xi> \qquad (C26)$$

The voltages on individual conductors are now

$$|V> = \sum_{i=1}^{N} (\xi_i^+ e^{-j\beta_i z} + \xi_i^- e^{j\beta_i z}) \, \underline{G} \, \underline{\Lambda}^{-\frac{1}{2}}|t_i> . \qquad (C27)$$

In the above (C17) was used to write $\underline{Q}|u_i> = |t_i>$. The current vector may be now obtained from $|V>$ by using (C1):

$$|I> = \sum_{i=1}^{N} \frac{\beta_i}{\omega} (\xi_i^+ e^{-j\beta_i z} - \xi_i^- e^{j\beta_i z}) \underline{L}^{-1} \underline{G} \, \underline{\Lambda}^{-\frac{1}{2}}|t_i> . \qquad (C28)$$

107

The power carried along the multiconductor transmission line is

$$P = \frac{1}{2} \, \text{Re} \, \langle V | I \rangle \qquad (C29)$$

where $\langle V |$ denotes a transpose conjugate of $|V\rangle$, and Re denotes the real part. For simplicity, consider only the waves propagating in positive z direction ($\xi_i^- = 0$ for all i). Then, (C29) gives the following simple expression for the power transmitted in the positive z direction:

$$P^+ = \frac{1}{2} \sum_{i=1}^{N} \frac{1}{v_i} |\xi_i^+|^2 \, . \qquad (C30)$$

The i-th mode carries the power $\frac{1}{2} |\xi^+|^2 / v_i$. In analogy with the two-wire transmission lines (which e.g. consist of a single conductor and a shield), the forward-wave scattering amplitude of the i-th mode will be denoted by a_i, and the reverse-wave amplitude with b_i:

$$a_i = \frac{\xi_i^+}{\sqrt{v_i}} \qquad , \qquad b_i = \frac{\xi_i^-}{\sqrt{v_i}} \qquad , \qquad (C31)$$

so that the forward-traveling wave carries the power $\frac{1}{2}|a_i|^2$, and the reverse-traveling wave the power $\frac{1}{2}|b_i|^2$. In terms of scattering amplitudes, (C27) becomes

$$|V\rangle = \sum_{i=1}^{N} (a_i e^{-j\beta_i z} + b_i e^{j\beta_i z}) |\phi_i\rangle \qquad (C32)$$

where the voltage eigenvector $|\phi_i\rangle$ is defined as

$$|\phi_i\rangle = \sqrt{v_i} \, \underline{G} \, \underline{\Lambda}^{-\frac{1}{2}} |t_i\rangle \, . \qquad (C33)$$

The current vector $|I\rangle$ from (C28) may be expressed in terms of the same voltage eigenvectors $|\phi_i\rangle$ as follows:

108

$$|I\rangle = \sum_{i=1}^{N} (a_i e^{-j\beta_i z} - b_i e^{j\beta_i z}) \frac{1}{v_i} \underline{L}^{-1} |\phi_i\rangle \qquad (C34)$$

Alternately, one can introduce the current eigenvectors $|\psi_i\rangle$ as follows:

$$|\psi_i\rangle = \frac{1}{v_i} \underline{L}^{-1} |\phi_i\rangle \quad , \qquad (C35)$$

and represent the current vector as

$$|I\rangle = \sum_{i=1}^{N} (a_i e^{-j\beta_i z} - b_i e^{j\beta_i z}) |\psi_i\rangle \ . \qquad (C36)$$

If (C36) is substituted in (C2), an alternative expression for $|V\rangle$ is obtained

$$|V\rangle = \sum_{i=1}^{N} (a_i e^{-j\beta_i z} + b_i e^{j\beta_i z}) \frac{1}{v_i} \underline{K}^{-1} |\psi_i\rangle \ .$$

Comparison with (C32) yields

$$|\phi_i\rangle = \frac{1}{v_i} \underline{K}^{-1} |\psi_i\rangle \ . \qquad (C37)$$

Normalized voltage eigenvectors $|\phi_i\rangle$, defined by (C33), are also eigenvectors of the matrix $\underline{L}\,\underline{K}$

$$\underline{L}\,\underline{K} |\phi_i\rangle = \frac{1}{v_i^2} |\phi_i\rangle \ , \qquad (C38)$$

what can be verified by using (C33) and (C16). Similarly, $|\psi_j\rangle$ is the eigenvector of the matrix $\underline{K}\,\underline{L}$

$$\underline{K}\,\underline{L} |\psi_j\rangle = \frac{1}{v_j^2} |\psi_j\rangle \ . \qquad (C39)$$

Voltage and current eigenvectors form the bi-orthonormal set

$$\langle \phi_i | \psi_j \rangle = \delta_{ij} \ . \qquad (C40)$$

109

From (C37) and (C11) the explicit expression for current eigenvector is obtained

$$|\psi_i\rangle = \frac{1}{\sqrt{v_i}} \, \underline{G} \, \underline{\Lambda}^{\frac{1}{2}} \, |t_i\rangle \, . \tag{C41}$$

Following the notation from [C6] and [C7], define $\underline{M}_V$ as a matrix which contains the voltage eigenvectors as its columns:

$$\underline{M}_V = (|\phi_1\rangle \, \ldots \, |\phi_N\rangle) \, . \tag{C42}$$

Similarly $\underline{M}_I$ is a matrix containing all the current eigenvectors

$$\underline{M}_I = (|\psi_1\rangle \ldots |\psi_N\rangle) \, . \tag{C43}$$

An arbitrary forward traveling wave is, from (C32)

$$|V_f\rangle = \sum_{i=1}^{N} a_i e^{-j\beta_i z} |\phi_i\rangle \tag{C44}$$

Take the scalar product from the left with $\langle \psi_j|$

$$\langle \psi_j|V_f\rangle = \sum_{i=1}^{N} a_i e^{-j\beta_i z} \langle \psi_j|\phi_i\rangle = a_j e^{-j\beta_j z} \, .$$

Thus, the expansion (C44) can be also written as

$$|V_f\rangle = \sum_{i=1}^{N} \langle \psi_i|V_f\rangle \, |\phi_i\rangle$$

Since the bracket is a scalar, one can place it behind $|\phi_i\rangle$

$$|V_f\rangle = \sum_{i=1}^{N} |\phi_i\rangle \langle \psi_i|V_f\rangle \, . \tag{C45}$$

The above is true for arbitrary $|V_f\rangle$, thus the following identity is obtained

$$\sum_{i=1}^{N} |\phi_i\rangle \langle \psi_i| = \underline{U} \, ,$$

110

which can also be written as

$$\underline{M}_I \, \underline{M}_V^+ = \underline{U}$$ (C46)

Similarly, one obtains

$$\underline{M}_V \, \underline{M}_I^+ = \underline{U} \ .$$ (C47)

When the propagation is assumed to be in the forward z direction, as in (C44), the current vector for an arbitrary forward-traveling mixture of modes is

$$|I_f\rangle = \sum_{i=1}^{N} a_i e^{-j\beta iz} |\psi_i\rangle \ .$$ (C48)

By multiplying from the left with $\langle\phi_j|$ one obtains

$$a_j e^{-j\beta_j z} = \langle\phi_j|I_f\rangle \ .$$

Comparison of this equation and (C45) yields

$$|V_f\rangle = \sum_{i=1}^{N} \langle\phi_i|I_f\rangle \, |\phi_i\rangle \ .$$

Again, the bracket is a scalar, thus it may postmultiply $|\phi_i\rangle$:

$$|V_f\rangle = \sum_{i=1}^{N} |\phi_i\rangle \langle\phi_i|I_f\rangle = \underline{Z}_0 |I_f\rangle$$

The matrix relating $|V_f\rangle$ and $|I_f\rangle$ is the characteristic impedance matrix $\underline{Z}_0$:

$$\underline{Z}_0 = \sum_{i=1}^{N} |\phi_i\rangle \langle\phi_i| = |\phi_1\rangle \langle\phi_1| + \ldots + |\phi_N\rangle \langle\phi_N| \ .$$ (C49)

This can be written as

$$\underline{Z}_0 = \underline{M}_V \, \underline{M}_V^+ = \underline{M}_V \, \underline{M}_I^{-1} \ ,$$ (C50)

where also (C46) has been used. Similarly one finds the characteristic admittance matrix as

$$\underline{Y}_0 = \underline{Z}_0^{-1} = \underline{M}_I \ \underline{M}_I^+ = \underline{M}_I \ \underline{M}_V^{-1} \ . \tag{C51}$$

Multiplying (C49) from the right by $|\psi_j>$ and using the biorthogonality property (C40) one obtains

$$|\phi_j> = \underline{Z}_0 \ |\psi_j> \ , \tag{C52}$$

which has the inverse

$$|\psi_j> = \underline{Y}_0 \ |\phi_j> \ . \tag{C53}$$

Characteristic impedance and admittance matrices can be also related through matrices $\underline{L}$ and $\underline{K}$. The relationship can be obtained by substituting (C35) into (C42) and (C43)

$$\underline{M}_V = \underline{L} \ \underline{M}_I \ \underline{\nu} \ , \tag{C54}$$

where the diagonal velocity matrix is defined as

$$\underline{\nu} = \text{diag} \ (v_1, \ v_2, \ldots, v_N) \ . \tag{C55}$$

When (C37) is substituted into (C42) and (C43) it follows

$$\underline{M}_I = \underline{K} \ \underline{M}_V \ \underline{\nu} \ . \tag{C56}$$

If these equations are now substituted in (C51) the following relation is obtained

$$\underline{Y}_0 \ \underline{L} = \underline{K} \ \underline{Z}_0 \ . \tag{C57}$$

For each mode i, there is a fixed ratio of the voltage and current on conductor j. This ratio is also called a characteristic impedance of the conductor j for the mode i, denoted Z_{0i}^j [C18]. These characteristic impedances

112

(scalars) are not to be confused with the elements of the characteristic admittance matrix $\underline{Z}_0$. If the coordinates of the eigenvectors are denoted by superscripts, such as

$$|\phi_i> = \begin{pmatrix} \phi_i^1 \\ \cdot \\ \cdot \\ \cdot \\ \phi_i^N \end{pmatrix} \quad ; \quad |\psi_i> = \begin{pmatrix} \psi_i^1 \\ \cdot \\ \cdot \\ \cdot \\ \psi_i^N \end{pmatrix}$$

then, for the mode i, the characteristic impedance of the j-th conductor is

$$z_{0i}^j = \frac{\phi_i^j}{\psi_i^j} = \frac{<u_j|\underline{Z}_0|\psi_i>}{<u_j|\psi_i>} \quad . \tag{C58}$$

REFERENCES

[1] H.A. Bethe, "Theory of Diffraction by Small Holes", Phys. Rev., Vol. 66, pp. 163-182, October 1944.

[2] S.A. Schelkunoff, Electromagnetic Waves, Princeton: Van Nostrand, 1943, p. 129.

[3] R.F. Harrington, Time-Harmonic Electromagnetic Fields, New York: McGraw-Hill, 1961, p. 78.

[4] W.L. Weeks, Electromagnetic Theory for Engineering Applications, New York: Wiley, 1964, p. 310.

[5] G.L. Matthaei, L. Young, E.M.T. Jones, Microwave Filters, Impedance-Matching Networks and Coupling Structures, New York: McGraw-Hill, 1964, pp. 229-243.

[6] C.E. Baum, K.S.H. Lee, "Application of Modal Analysis to Braided Shield Cables", Interaction Note 132, January 1973.

[7] C.E. Baum, "Some Characteristics of Electric and Magnetic Dipole Antennas for Radiating Transient Pulses", Sensor and Simulation Note 125, January 1971, p. 16.

[8] S.A. Schelkunoff, Electromagnetic Waves, Princeton: Van Nostrand, 1943, p. 162.

[9] R.F. Harrington, Time-Harmonic Electromagnetic Fields, New York: McGraw-Hill, 1961, p. 100.

[10] W.L. Weeks, Electromagnetic Theory for Engineering Applications, New York: Wiley, 1964, p. 565.

[11] S.B. Cohn, "Determination of Aperture Parameters by Electrolytic-Tank Measurements", Proc. I.R.E., Vol 39, pp. 1416-1421 November 1951.

[12] S.B. Cohn, "The Electric Polarizability of Apertures of Arbitrary Shape", Proc. I.R.E., Vol. 40, pp. 1069-1071, September 1952.

[13] D. Kajfez, "Excitation of a Terminated TEM Transmission Line through a Small Aperture," Interaction Note 215, July 1974.

[14] R.E. Collin, Foundations for Microwave Engineering, New York: McGraw-Hill, 1966, p. 146.

[15] M.T. Carlin, A.B. Giordano, Network Theory, an Introduction to Reciprocal and Nonreciprocal Circuits, Englewood Cliffs: Prentice Hall, 1964.

[16] W.T. Weeks, "Calculation of Coefficients of Capacitance of Multi-conductor Transmission Lines in the Presence of Dielectric Interface," IEEE Transactions on Microwave Theory Techn., Vol. MTT-18, pp. 35-43, Jan. 1970.

[17] J.C. Clements, C.R. Paul, A.T. Adams, "Computation of the Capacitance Matrix for Systems of Dielectric-Coated Cylindrical Conductors," IEEE Transactions on Electromag. Compat., Vol. EMC-17, No. 4, pp. 238-248, November 1975. Also see Correction in EMC-18, No. 2, pp. 88-89, May 1976.

[18] C.R. Paul, Computation of the Transmission Line Inductance and Capacitance Matrices from the Generalized Capacitance Matrix," IEEE Transactions Electromag. Compat., Vol. EMC-18, No. 4, pp. 175-183, November 1976.

[19] B. Friedman, Principles and Techniques of Applied Mathematics, New York: Wiley, 1956, p. 34.

[20] R.E. Collin, Foundations for Microwave Engineering, New York: McGraw-Hill, 1966, p. 111.

[21] C.L. Matthaei, L. Young, E.M.T. Jones, Microwave Filters, Impedance-Matching Networks, and Coupling Structures, New York: McGraw-Hill, 1964, p. 242

[22] K.S.H. Lee, F. C. Yang, "A Wire Passing by a Circular Aperture in an Infinite Ground Plane," Dikewood Corporation, February, 1977.

[23] E.T. Whittaker, G.N. Watson, A Course of Modern Analysis, New York: Cambridge Press, 1973, p. 172.

[A1] D. C. Youla, "On Scattering Matrices Normalized to Complex Port Numbers," Proc. I.R.E., Vol 49, p. 1221, July 1961.

[A2] M. T. Carlin, A. B. Giordano, Network Theory, an Introduction to Reciprocal and Nonreciprocal Circuits, Englewood Cliffs: Prentice Hall, 1964, pp. 326 and 144.

[A3] P. Penfield, Jr., R. P. Rafuse, Varactor Applications, Cambridge: M.I.T. Press, 1962, p. 26.

[B1] B. Friedman, Principles and Techniques of Applied Mathematics, New York: Wiley, 1956, pp. 1-33.

[B2] A. Messiah, Quantum Mechanics, Vol. I, Amsterdam: North Holland, 1965, pp. 162-179.

[C1] J.R. Carson, R.S. Hoyt, "Propagation of Periodic Currents Over a System of Parallel Wires", Bell Syst. Tech. Jour., Vol. 6, pp. 495-545, July 1927.

[C2] L.A. Pipes, "Matrix Theory of Multiconductor Transmission Lines", Phil. Mag., Vol. 24, pp. 97-113, July 1937.

[C3] L.V. Bewley, Traveling Waves on Transmission Systems, New York: Dover, 1963.

[C4] S.A. Schelkunoff, "Generalized Telegraphist's Equations for Wave-guides", Bell Syst. Tech. Jour., Vol. 31, pp. 784-801, July 1952.

[C5] S. Frankel, Cable and Multiconductor Transmission Line Analysis, Springfield, VA: Nat'l Tech. Info. Service, AD-A000848, June 1974.

[C6] H. Amemiya, "Time-domain Analysis of Multiple Parallel Transmission Lines", RCA Rev., Vol. 28, pp. 241-276, June 1967.

[C7] K.D. Marx, "Propagation Modes, Equivalent Circuits, and Characteristic Termination For Multiconductor Transmission Lines with Inhomogeneous Dielectrics", IEEE Trans. Microwave Theory Tech., Vol. MTT-21, pp. 456-457, July 1973.

[C8] C.R. Paul, "Efficient Numerical Computation of the Frequency Response of Cables Illuminated by an Electromagnetic Field", IEEE Trans. Microw. Theory Tech., Vol. MTT-22, pp. 454-457, April 1974.

[C9] R.A. Speciale, "Even- and Odd-Mode Waves for Nonsymmetrical Coupled Lines in Nonhomogeneous Media", IEEE Trans. Microw. Theory Tech., Vol. MTT-23, pp. 897-908, November 1975.

[C10] S. Ramo, J.R. Whinnery, T. Van Duzer, Fields and Waves in Communication Electronics, New York: Wiley, 1965, p. 314.

[C11] A. Matsumoto (ed.), Microwave Filters and Circuits, New York: Acad. Press, 1970, Ch. 8.

[C12] T. Nishide, A. Matsumoto, "Multiport Image Parameter Theory", Monogr. No. 18, Research Institute of Applied Electricity, Hokkaido Univ., 1970.

[C13] D. Kajfez, "Multiconductor Transmission Lines", Interaction Note 151, June 1972.

[C14] C.R. Paul, "Useful Matrix Chain Parameters Identities of Multiconductor Transmission Lines", IEEE Trans. Microw. Theory Tech., Vol. MTT-23, pp. 756-760, Sep. 1975.

[C15]   IRE Standards on Antennas and Waveguides: Definitions of Terms, 1953, Proc. I.R.E, pp. 1721-1728, December 1953.

[C16]   B. Friedman, Principles and Techniques of Applied Mathematics, New York: John Wiley, 1956, pp. 107-110.

[C17]   D. Kajfez, "Distributed Circuit Approach to the Curved Multi-conductor Transmission Lines", Jour. Mississippi Acad. Sci., Vol. 13, pp. 75-83, 1967.

[C18]   G.L. Matthaei, L. Young, E.M.T. Jones, Microwave Filters, Impedance-Matching Networks, and Coupling Structures, New York: McGraw-Hill, 1964, p. 193.